CONSTRUCTING A GIS-BASED 3D URBAN MODEL USING LiDAR AND AERIAL PHOTOGRAPHS

A Thesis

by

WEI-MING LIN

Submitted to the Office of Graduate Studies of
Texas A&M University
in partial fulfillment of the requirements for the degree of

MASTER OF SCIENCE

December 2004

Major Subject: Geography

CONSTRUCTING A GIS-BASED 3D URBAN MODEL USING

LiDAR AND AERIAL PHOTOGRAPHS

A Thesis

by

WEI-MING LIN

Submitted to Texas A&M University
in partial fulfillment of the requirements
for the degree of

MASTER OF SCIENCE

Approved as to style and content by:

Hongxing Liu (Chair of Committee)	Daniel Z. Sui (Member)
Robert S. Bednarz (Member)	Christopher D. Ellis (Member)

Douglas J. Sherman
(Head of Department)

December 2004

Major Subject: Geography

ABSTRACT

Constructing a GIS-based 3D Urban Model Using

LiDAR and Aerial Photographs. (December 2004)

Wei-Ming Lin, B.S., Fu-Jen Catholic University, Taiwan

Chair of Advisory Committee: Dr. Hongxing Liu

Due to the increasing availability of high-resolution remotely sensed imagery and detailed terrain surface elevation models, urban planners and municipal managers can now model and visualize the urban space in three dimensions. The traditional approach to the representation of urban space is 2D planimetric maps with building footprints, facilities and road networks. Recently, a number of methods have been developed to represent true 3D urban models. Those include panoramic imaging, Virtual Reality Modeling Language (VRML), and Computer-aided Design (CAD). These methods focus on aesthetic representation, but they do not have sufficient spatial query and analytical capabilities.

This research evaluates the conventional approaches to 3D urban models, and identifies their advantages and limitations; GIS functionalities have been combined with 3D urban visualization techniques to develop a GIS-based urban modeling method; The algorithms and techniques have been explored to derive urban objects and their attributes from airborne LiDAR and high-resolution

imagery for constructing and visualizing 3D urban models; and 3D urban models for the Texas A&M University (TAMU) campus and downtown Houston have been implemented using the algorithms and techniques developed in this research. By adding close-range camera images and high-resolution aerial photographs as the texture of urban objects, effect of photorealism visualization has been achieved for walk-through and fly-through animations.

The Texas A&M University campus model and the downtown Houston model have been implemented to offer proof-of-concept, namely, to demonstrate the advantages of the GIS-based approach. These two prototype applications show that the GIS-based 3D urban modeling method, by coupling ArcGIS and MultiGen-Paradigm Site Builder 3D software, can realize the desired functionalities in georeferencing, geographical measurements, spatial query, spatial analysis, and numerical modeling in 3D visual environment.

DEDICATION

This thesis is dedicated to my parents, Jenn-Yeu and Lyu-Shih, who have shaped me into the person that I am today, and to my wife, Meng-Fang, whose love and support has helped make this goal a reality.

ACKNOWLEDGMENTS

I would like to express my greatest gratitude to Dr. Hongxing Liu who led me into the fascinating world of GIS and remote sensing; his patient guidance and constant encouragement were instrumental to the completion of this project.

Special thanks should be given to Dr. Robert Bednarz, Dr. Daniel Sui, and Dr. Christopher Ellis for serving on my thesis committee and giving me their advice.

My appreciation is also extended to Lei Wang, Jaehyung Yu, Cesar Arias, Jose Gavinha, Matthew Clemonds, Wei Tu, Bing Lu, Zengwang Xu, Laura Laurencio, Masaki Watabe, Jiahui Peng, Luohan Peng, Brad Hollas, Treye Rice, and Steven Hsieh for their generous support and the wonderful time we spent together during the past two years.

Last, but not least, I would like to share this day with my lovely wife, Meng-Fang Lu, for her love, patience and support during my life in the United States.

TABLE OF CONTENTS

CHAPTER Page

Page

LIST OF FIGURES

FIGURE Page

FIGURE Page

FIGURE Page

LIST OF TABLES

CHAPTER I

INTRODUCTION

1.1 Research Background

3D technology offers fast and effective methods for simulating and visualizing the urban environment. The recent decade has seen a tremendous increase in demand for 3D urban information. 3D urban models provide a better visual representation of urban space and urban features than 2D maps (Ranzinger and Gleixner 1995). The importance of 3D urban models with multiple levels of detail has been evidenced by a wide range of applications, such as urban planning, architecture, navigation, public safety studies, transmitter placement for telecommunication, and flight simulation (Weidner 1996; Rau and Chen 2001; Shiode 2001; Zhou et al. 2004). The 3D urban modeling technique enables urban residents to visualize future urban construction and development. It also supports standard activities of urban design and city planning and allows urban planners to explain proposed projects to the public. In addition, urban models can be utilized in engineering, infrastructure planning, and scenario simulation with movable and hypothetic buildings, military combat simulations, and telecommunications (Batty et al. 2000).

This thesis follows the style of *Photogrammetric Engineering & Remote Sensing*.

Just one generation ago, one of the main tasks for urban planners was to manually produce paper drawings for representing existing urban features and plan blueprints. With the advance of computer technology, various digital urban models have been created to assist the urban design and planning work. The early digital urban models commonly represented urban space in a two-dimensional format, in which man-made structures, such as buildings and roads, were abstracted into simple geometric shapes like rectangles, polygons, and lines. Although the 2D urban models can accurately represent planimetric information about the footprints or floor plans of buildings and central lines or edge lines of roads, they are unable to render a realistic view of urban space and urban features.

The recent decade has witnessed enormous progress by researchers and software vendors in the development of 3D urban modeling techniques. Three major modeling methods have been used for constructing and visualize 3D urban models: panoramic imaging, virtual reality modeling language (VRML), and computer-aided design (CAD) (Batty 2000). These methods provide urban planners an effective means to design urban landscape, manage urban space and infrastructure, and preserve historical buildings and districts. Despite their obvious advantages over 2D representations, shortcomings and limitations can be identified for each method.

The panoramic imaging method allows the user to look around an urban scene with a full 360° view. However, the user is unable to roam inside the scene or manipulate individual features in the scene (Naimark 1998).

Virtual reality modeling language (VRML) is a computer language that can be used as a framework to create a virtual 3D view for a small urban scene. With this technique, the walk-through or fly-by views of urban space can be simulated, and an interactive query about the properties of urban features is also possible (Pesce 1996). Nevertheless, the urban scene created with VRML commonly has a low level of details. This is because the requirement for fast data retrieval and display with the browser interface restricts the 3D data to a small volume (Evans and Hudson-Smith 2001).

The computer-aided design (CAD) technique is a very sophisticated and powerful tool. CAD technique has strong capabilities in storing and managing large amounts of geometric information about urban objects, and it is an efficient tool for designing and creating urban objects (Sinning-Meister et al 1996). The contemporary CAD systems also offer full 3D rendering capability to visualize urban objects and the urban scene. However, the CAD technique is only suitable for constructing 3D models for a small urban community due to its high demand for geometric detail. For a large urban area, CAD technology is not an efficient approach for the construction of 3D urban models. Furthermore, CAD technology lacks spatial analytical functionalities. It does not support

spatial queries about properties of urban features or geographical analysis on the spatial relationships between the urban features.

The lack of spatial analytical functions and the deficiency in handling a large urban area are the primary limitations of the above three methods. Geographical Information Systems (GIS) technology was developed from the need to handle and manipulate a large volume of geographically referenced spatial data. The great ability of GIS to integrate diverse geographical information has been widely recognized. In the inception stage, the major functionality of GIS lied in the storage, retrieval, manipulation and display of geographic data. Since the late 1980s, substantial spatial analytical and modeling capabilities have been developed and included in GIS. Therefore, the combination of GIS and 3D urban visualization technology offers the potential to overcome the limitations of the conventional 3D urban modeling methods.

The prerequisite for constructing and visualizing 3D urban models is the collection of planimetric and vertical information for urban objects, including natural features (trees, lawns, lakes, streams, hills, and depressions) and man-made structures (buildings, roads, bridges, poles). Currently, accurate geometric information is only available for a few of cities. For most cities, lack of accurate and reliable geometric information represents the biggest constraint for applying 3D technology to model, simulate, and visualize the urban landscape.

Traditionally, the planimetric information for urban objects were acquired by using the following three techniques: 1) digitizing archival urban planning documents and maps; 2) directly measuring urban features using survey instruments; and 3) manually tracing aerial photographs. The vertical information about the height of urban objects is even scarcer, compared with the planimetric information. The conventional methods for vertical data acquisition include ground survey and photogrammetric analysis of stereo pairs of aerial photographs. These techniques are time-consuming and labor-intensive, and hence, impractical for application in a large and complex metropolitan area (Hu 2003, Palmer and Shan 2002).

The rapid development of remote sensing technology and digital image processing techniques has made it possible to efficiently derive both planimetric and vertical information about urban objects from a variety of remotely sensed data. The emergence of high-resolution satellite sensors (like IKONOS and Quickbird) and airborne digital sensors has produced the repetitive, accurate and low-cost data over urban areas. Orthorectified high-resolution imagery contains the planimetric information about building footprints, pole locations, and the position and shape of tree canopy and lawns (Lin and Nevatia 1998). In addition, airborne LiDAR (Light Detection and Ranging) technology has been emerging in recent years as a cost-effective alternative for the acquisition of highly detailed surface topographic information. By integrating Differential

Global Positioning Systems (DGPS) and Inertial Navigation Systems (INS) to track precise airplane position and orientation, airborne LiDAR systems can acquire surface height information at a vertical accuracy of 15 to 50 cm with a data density of 3-4 points per meter along the flight line. Dense high-rise buildings characterize downtowns and central business districts (CBD) of most cities and limit the use of aerial photographs for geometric data acquisition. The severe solar shadows and occlusions induced by tall buildings prohibit a complete delineation of the footprints of urban objects from a single aerial photograph and also hamper the extraction of height information from stereo pairs of aerial photographs. Airborne LiDAR technology can effectively overcome these problems and are, therefore, particularly valuable for deriving both planimetric and vertical measurements in an urban area with densely distributed tall buildings.

Now, there is a consensus that the high-resolution imagery and airborne LiDAR data have become the most important data sources for creating, updating, and maintaining the 3D urban database. However, algorithms and data processing techniques for transferring image and raw LiDAR data into explicit geometric information are still in its infancy. A greater effort needs to be directed to ward the exploration and development of automated algorithms and techniques for efficiently extracting urban objects and their geometric and

thematic attributes from remotely sensed data, which can be readily used to construct and visualize the 3D urban model.

1.2 Problem Statement

Panoramic imaging, VRML, and CAD are the major methods currently used for 3D urban model construction and visualization. Each method has unique advantages. The panoramic imaging method can be used to create a realistic and aesthetically pleasing view of the urban scene, which displays subtle features such as street features and small landmarks. VRML can be used to produce interactive virtual reality animations to simulate a walk-through and fly-by of the urban scene, which can be disseminated among the users via the internet. CAD technology has great capabilities in creating urban objects and managing geometric attributes for urban objects. It is widely used in architectural design and urban landscape planning and management.

Despite their unique advantages, it is quite clear from the previous discussion that these methods suffer from their inadequacies in handling large urban areas and their lack of functionality in regard to performing spatial manipulation, query, and analysis. These are essential for many practical applications of 3D urban models, such as 3D urban navigation systems, telecommunication planning, and military combat simulations. To address the limitations of these methods, this research intends to develop a GIS-based 3D

urban modeling method by coupling GIS technology with 3D visualization techniques.

Application of 3D urban modeling technology requires a large volume of accurate planimetric and vertical information for urban areas. In reality, such data are largely unavailable for most cities. With the advance of remote sensing technology, an increasing volume of high-resolution imagery and LiDAR data have become available for many urban areas. But, how to efficiently and accurately convert raw imagery and LiDAR data into explicit 3D geometric information for urban objects is still an unanswered question. This research will also explore and develop algorithms and techniques for automatically extract urban objects and their geometric attributes from remote sensing data for constructing and visualizing 3D urban models with a GIS based method.

1.3 Research Scope and Objectives

This research will address deficiencies of the current 3D urban modeling methods and the unavailability of urban geometric data. The general goal of this research is to explore GIS-based methodology to construct and visualize 3D urban models based on planimetric and vertical information derived from high-resolution remote sensing data. Specific objectives of this research include:

- Evaluating the conventional approaches to 3D urban models, including panoramic imaging, VRML, and CAD, and identifying their advantages and limitations.
- Combining GIS functionalities with 3D urban visualization techniques to develop a GIS-based 3D urban modeling method.
- Exploring the algorithms and techniques to derive urban objects and their attributes from airborne LiDAR and high-resolution imagery for constructing and visualizing 3D urban models.
- Implementing 3D urban models for the TAMU campus and downtown Houston using the algorithms and techniques developed in this research.

The object-oriented concept will be used to represent and organize urban features. ArcGIS software and MultiGen-Paradigm Site Builder 3D software will be utilized to realize the GIS-based 3D urban modeling method. Coupling the ArcGIS and MultiGen-Paradigm Site Builder 3D software will provide the benefits of georeferencing, spatial query, spatial modeling, and analysis, while keeping the advantages of conventional methods of photorealism, efficient management of geometric data, and virtual touring through walk-through and fly-by simulations. Spatial query and analysis can be conducted interactively within the simultaneous 3D scene of urban objects, and query and analysis results can be displayed with the 3D urban scene as a background.

Automated algorithms and techniques will be explored and developed to extract explicit 3D geometric representations of urban objects. These techniques will be applied to assist the construction of two urban models: Texas A&M University Campus model and downtown Houston model. To construct the Texas A&M University model, an image classification and automated feature delineation method will be applied to high-resolution digital aerial photographs to extract and update the planimetric database for campus objects and the road system. Conventional photogrammetric methods and laser ranging methods will be used to acquire the height information for campus objects. For the downtown Houston model, both airborne LiDAR data and high-resolution digital aerial photographs are utilized as input data sources. Automated data processing algorithms are developed to extract and update the footprints and vertical dimensions of various urban objects.

The texture data for the urban object models are acquired by a digital frame camera and a digital video camera and then processed into texture chips using Photoshop software. The texture chips are linked with individual urban objects in MultiGen-Paradigm Site Builder 3D to achieve a photorealism visual effect. As an application example, the 3D urban model is used to examine the impact of buildings on spatial-temporal variations of solar radiation in downtown Houston.

1.4 Research Structure

This thesis is organized in six chapters. The research background and objectives have been presented in the preceding sections.

Chapter II presents an overview of different conventional 3D urban modeling methods. The strengths and weaknesses of the methods are discussed and evaluated.

Chapter III will describe the conceptual framework for the GIS-based urban modeling method. This chapter proceeds from the discussion of the object-oriented approach to represent and model individual urban objects. Urban features are classified into different classes of objects whose geometric properties and essential thematic attributes are identified. Methods for extracting and representing planimetric and height information for urban objects are reviewed. Then, the techniques for acquiring and processing texture data are presented. The final section of this chapter examines the 3D urban visualization technique with an emphasis on the concept of "level of detail" (LOD).

Chapter IV provides a detailed description of how the GIS-based urban modeling method is used to construct the Texas A&M University Campus model. At the start of the chapter, the input data sources and software tools are introduced. An automated method is presented, which combines a series of image processing algorithms to extract urban objects from classified aerial

photographs. A number of photogrammetric techniques are tested for deriving vertical dimensions for campus buildings, including the relief-displacement method, the shadow method, and the differential parallax method. Using the laser ranging measurements as the ground truth, these techniques are compared and evaluated. By coupling the ArcGIS and MultiGen-Paradigm Site Builder 3D software packages, a GIS-based 3D urban model is established for the Texas A&M University Campus. The resultant model is used to create a virtual touring movie.

Chapter V focuses on the construction of the downtown Houston model with airborne LiDAR data and high-resolution aerial photographs. First, the limitations of aerial photographs are illustrated for modeling the high-rise buildings concentrated in urban area, and the comparative advantages of airborne LiDAR technology are highlighted. Then, algorithms for extracting 3D geometric information from LiDAR data are presented, and their performances are examined. Besides a fly-by movie, the resultant 3D urban model of downtown Houston is used to simulate the impact of buildings on seasonal and spatial variations of solar radiation. The implication of spatio-temporal variation of solar radiation is briefly discussed in the context of formulating a scientific plan for planting various trees, grasses, and flowers in different places and in different seasons.

The final chapter summarizes the research findings and contributions and discusses future research directions for 3D urban model construction and visualization.

CHAPTER II

CONVENTIONAL APPROACHES TO 3D URBAN MODELS

2.1 Overview of Conventional Approaches

The more commonly used methods for 3D urban models include panoramic imaging, VRML, and 3D CAD systems (Batty 2000). Panoramic imaging technique can render a highly realistic visualization of a full field of view around the urban area. VRML method can display a representation of the large city area with full functions of walkthrough and flythrough, which allows users to freely explore a view from any angle on the internet. CAD method is used to create, edit, and display 3D graphics models and model urban scene from its object-oriented database system.

Recently, a new technique known as virtual reality (VR) was developed, which opened up new horizons for 3D visualization. It provides a mean for humans to visualize, manipulate and interact with computers and extremely complex data (Kumaradevan and Kumar 2001). It allows simulating actions and observing reactions similar to the real world.

2.2 Panoramic Imaging Method

Since the dawn of photography in 1839, photographers have tried to represent the world that they see through the camera. The human field of vision

can be expended by rotating the view point. Photographers began to assemble images horizontally in order to represent the entire scene surrounding them.

Any image covering more than 100-degree may technically be called a panorama. A stretched panorama image can totally encircle the viewer, reaching a full 360-degree field of view (Figure 1). Panoramas are regarded as wide-field images and they represent a single point of view in 2-Dimension. Panoramic imagery offers limited navigational interactivity. Viewers can pan and tilt through a panoramic scene, but can not move laterally nor manipulate features in the imagery (Naimark 1998).

Figure 1: Stretched panorama image of Texas A&M University

Rendering techniques attempt to extend the use of image data by warping images to enable production of novel viewpoints of the object. Two main techniques have emerged in this category: those based upon panoramic images, and those based on range images draped with photographic texture.

For these two techniques, they were used 360-degree panoramic images that provide a quick and easy way to portray a sense of location from user's eye view, and make a panoramic video in a virtual environment (Chen 1995; Pintaric et al. 2000; Chen et al. 1998).

In general, stitching and constructing a 360 degrees panoramic image needs 15 to 30 images in average (Chen et al.. 1998). An example of panoramic image for a part of Texas A&M University campus is shown in Figure 1. This panorama image was created by the author using 17 digital images using panoramic software. The software uses markers to indicate stitching points in the overlapping area which was 60 percent of both input images (Figure 2). Cutting off the redundant remaining, and then wrap the remaining images into a cylinder image which was embedded with color adjustment, bright modifications, and image resampling. The 17 captured images of Texas A&M University were shown in Figure 3.

Figure 2: Overlapping areas with the stretched panorama image

Figure 3: Captured images of Texas A&M University

Panoramic images provide a highly realistic visualization from static viewpoints within the study area, and some subtle features like furnatures on the street can be captured. The detail level of the scene is higher than 3D CAD models (Shiode 2001). However, from the unchanging camera position, the

user's view point is fixed to the original location. The user is not able to walkthrough or fly into the scenes in the same way as in other methods. Furthermore, if we stitch together multiple images which are not taken from a solitary point of view, then distortion is inevitable.

2.3 Virtual Reality Modeling Language Models

In 1994, Mark Pesce and Tony Parisi develop an early 3D prototype three-dimensional interface, labyrinth, to the web. After that, Pesce presented the Virtual Reality Modeling Language (VRML) at the first international conference. Since it was approved as a web standard, it has gained popularity for visualization of urban models (Çöltekin 2002).

VRML is a kind of computer languages that provides a framework for space and virtual environments and a file format for portraying interactive 3D objects and worlds on the internet (Pesce 1996). It is also intended to be universal interchangeable format for integrated 3D graphics and multimedia. VRML has been designed to fulfill editing, composing, extending, implementing, performing, and scaling requirements (Çöltekin 2002). It allows for a sample definition of 3D words and objects and is capable of representing static, dynamic 3D animation, and multimedia objects with hyperlinks to movies and textures. A VRML model of Texas A&M University developed by Xiao (1996) was shown in Figure 4.

Figure 4: VRML of Texas A&M University (Xiao, 1996)

Most of the VRML models created pre-designed files which are stored in an ASCII file. A browser is necessary to display this data on the screen. A user can specify parameters for the dynamics of objects in a text file for screen design. The browser provides screen rendering capability and an interface to navigate through and interact with models (Zlatanova 1999b). VRML also provides representation of a large area and allows the user to freely explore a model and view details from any angle with walk-through or fly-through.

Zlatanova (1999a) and Smith et al. (1998) proposed a client-server database for spatial query and analysis (Figure 5). The database can be selected

by filling out a form or selecting an area of interest in a 2D map or by pointing to a 3D map. The user can freely send queries and receive responses from center server which contains the data for 3D world by internet in a short period time.

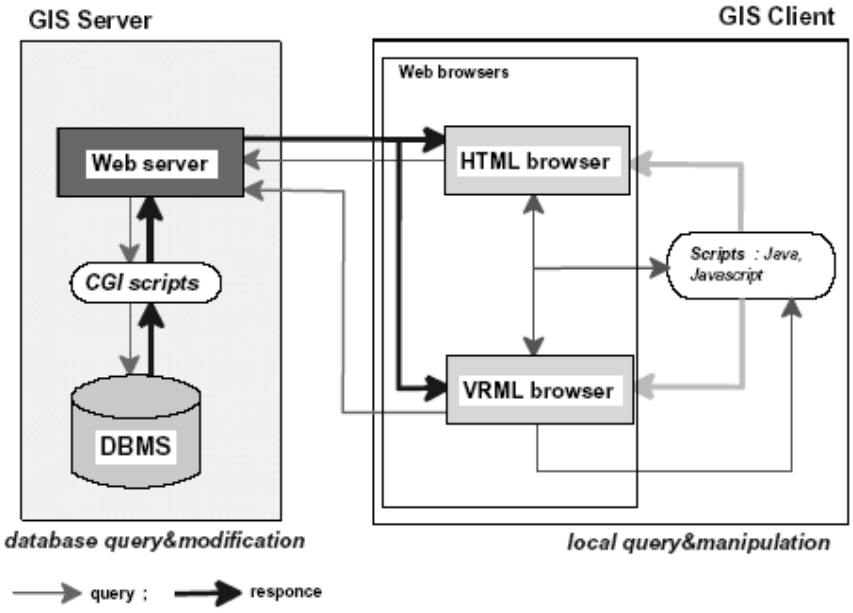

Figure 5: Client-server database (Zlatanova, 1999b)

The advantages of VRML include small files, quick query-response from client-server database system, interactive simulations, many angles of view, and small scale of area for walk into and fly-through. VRML is actually a large language similar to HTML. Different from HTML, for a 3D scene description, thus the user must have the language programming skills. So far, the users also

need a browser for plug-in to use VRML in a standard Internet Explorer or Netscape Navigator browser. In addition, spatial query and analysis features are missing when the user tried to save into small files (Evans and Hudson-Smith 2001). Due to real-time rendering based on a small file, the VRML models commonly have a low level of detail.

2.4 Computer-aided Design Models

Computer-aided design (CAD) systems have been developing and advancing over the past decades. They are showing completely mature and continuing to become more powerful tools from the extended power and efficacy of 3D models and their ability to restore or advance drawings. Since 1980s, CAD became the standard method for producing drawing (Schoonmaker 2003).

Early CAD programs were primarily 2D drawing (edges and surfaces) programs (Schoonmaker 2003). In the 2D sketch, work with the CAD system is based on plannar mathematics and flat representation of spatial data. Although 2D CAD systems have eliminated manual drafting and production of drawings, they still require that the user mentally visualize the solid physical object based on flat views. Figure 6 shows a 2D CAD drawing of Texas A&M University campus developed by Texas A&M University GIS office.

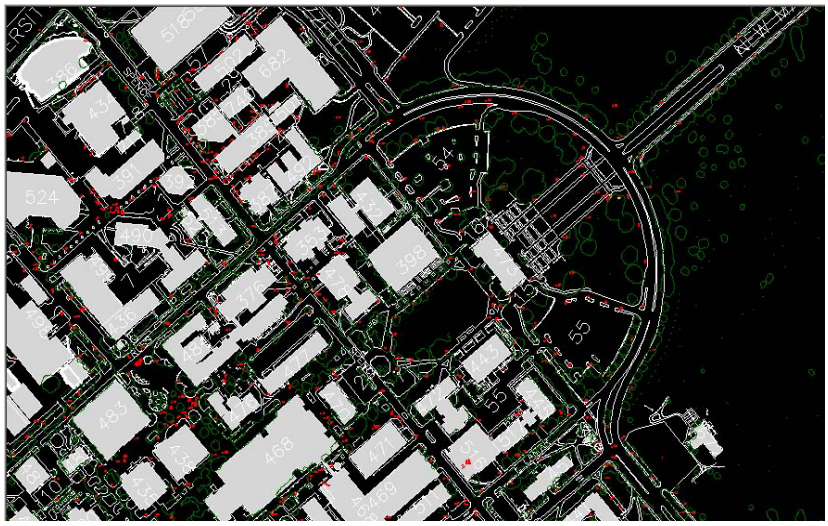

Figure 6: 2D CAD drawings of Texas A&M University (TAMU GIS office)

Modern CAD programs provide additional benefits of maintaining 3D data for analysis and viewing. 2D plan view and 3D perspective view can be converted rapidly. With vertical dimension information, 2D objects cab be rendered as solid 3D models (Sheppard 1989). Moreover, full geometric properties of objects can be queried and analyzed in many ways. Distances in 3D models can be measured in many ways, such as point-to-point, points-to-lines, points-to-edges, or surfaces-to-points. Figure 7 shows a full architectural CAD model, which is developed based on the geometrical information derived from Documenta company website (www.asfound.com/fresnomuseum.htm).

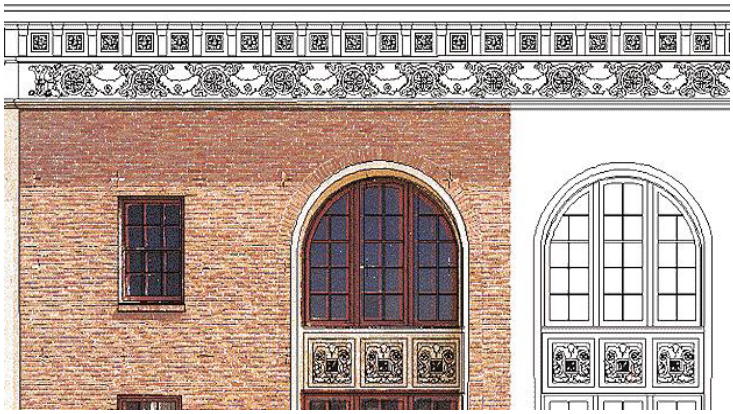

Figure 7: Full architectural CAD model (www.asfound.com/fresnomuseum.htm)

The CAD environment provides greater use of the mathematical models and functions to represent the subjects at a detail level approaching photo-realism. With 3D CAD models, multiple view angles of visualization, realistic rendering, and good visual reality are possible. Brail and Klosterman (2001) also mentioned that two important changes have been occurring in CAD programs. First, most modern programs included the concept of object-oriented model. Second, CAD programs now are providing database tools that allow the association of external data with CAD objects.

Although CAD models are built in computer environment, the geometric information about the models are mainly derived from manual measurements or retrieved from design plans. The creation 3D CAD urban models with high geometric content were and continue to be expensive to produce. New techniques with much less geometric content are being developed. Image-based

rendering techniques and 2.5D image draping are widely used at present (Figure 8). Although CAD technique offers full 3D modeling capabilities, it lacks interoperability. Thus it is difficult to link spatial data in a GIS environment (Sinning-Meister et al. 1996).

Figure 8: 2.5D image of Texas A&M University

Objects in CAD are represented in an arbitrary coordinate system. They are not georeferenced and cannot rapidly link with other geographical data layers. The CAD technique is designed for describing spatial objects in a small area with the detailed geometric information. It is not suitable for portraying a large urban area with such high geometric contents.

2.5 Summary

In this chapter, an overview of conventional models has been outlined and described. The advantages of conventional models can be applied to GIS-based 3D urban models, and their limitations can be improved for this research in the next chapter.

CHAPTER III

THEORETIC FRAMEWORK AND METHODOLOGY

3.1 GIS-based 3D Urban Models

The study of GIS-based 3D urban models is to understand for integrating information about 3D geometry and thematic attribution, spatial relationships, and GIS functionalities. Currently, most of these developments in 3D urban models are with good visual reality, but they have limited GIS functionality.

GIS is a computer-based tool for modeling, collecting, manipulating, storing, displaying, and analyzing geographical data and events in the context of their geographical location. In a typical GIS, information is stored in thematic layers, and the layers are linked by attribute data (Mahoney 1998). For the GIS-based model, it is a combined concept for improving the limitation of conventional models such as panoramic models, VRML models, and CAD models with good GIS functionality and taking their advantages with spatial relationships between them.

In panoramic models, a static point of view is the main weakness for utilizing a full 3D functionality. The user is not able to walk-through or fly into the scenes or virtual worlds. Furthermore, distortion problem can be affected the scene when we stitch together multiple images from little different point of view.

In VRML models, the user have to familiar with a 3D scene description language and need a browser for plug-in to an internet explore software. If we want to save the loading and downloading time, the limited use for the low level detail of scene is unavoidable.

CAD models are largely used for design review in the architectural and urban design domain but lack interoperability in a GIS environment, and are thus difficult to link to spatial data. Moreover, CAD provides an arbitrary coordinate system for a large scale area, and the data is not georefenced.

Coupling with advantages of these techniques and overcoming with their limitations, we can take good visual reality from panoramic imaging and CAD models; spatial query and analysis, multiple angles of view, and small scale of survey area for walkthrough and fly into from VRML models; rich geometric contents and object-oriented concept from CAD models.

For this research, we use high spatial characteristics of the range image within each building footprint from 15 feet resolution LiDAR data and 1 foot high-resolution aerial photographs that can enable the extrusion of the map data to yield significant shapes. After that, MultiGen-Paradigm 3D software packages and Arcview GIS software are utilized to make an aesthetic view of visualization and link spatial data for interoperable GIS environment. Figure 9 is the plan concept and dataflow for the GIS-based 3D urban model.

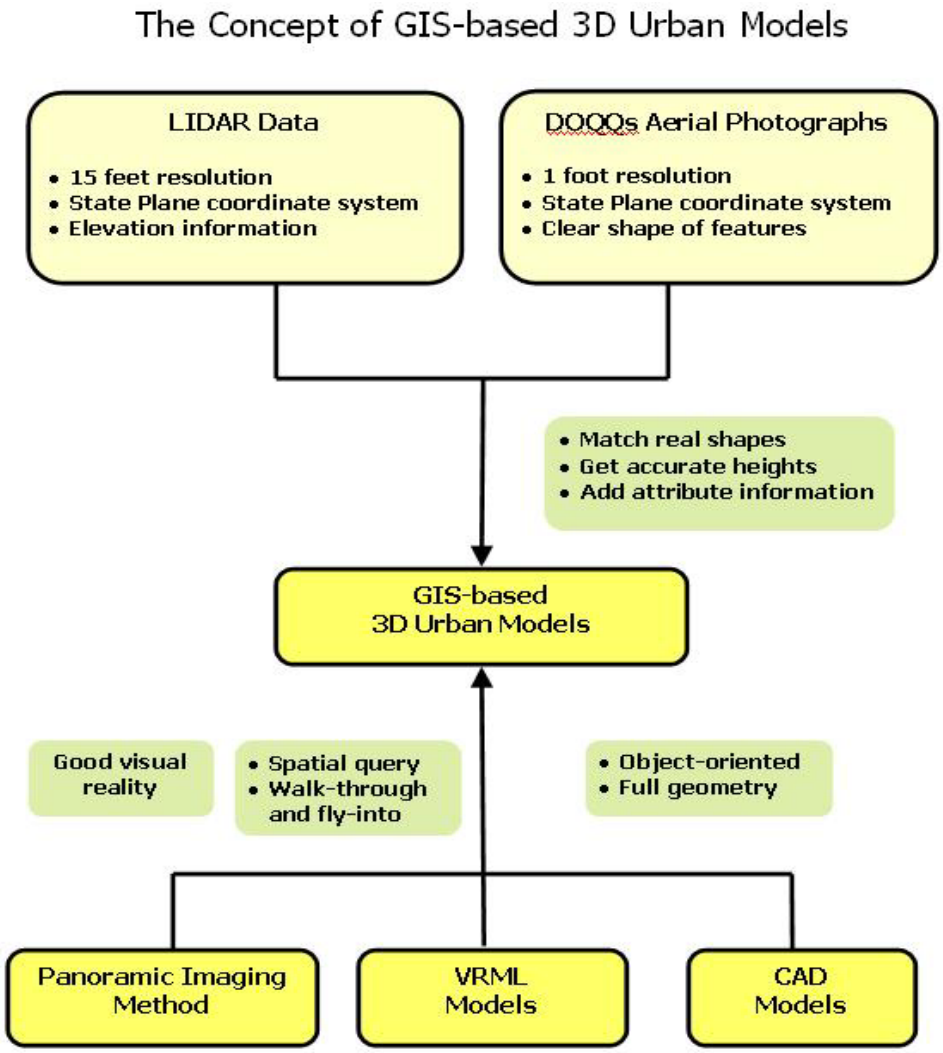

Figure 9: Plan concept of GIS-based 3D urban models

3.2 Object-oriented Models

An object is a self-contained package of information describing the characteristic and capabilities of a geographical entity. Real world geographical features can be modeled as a collection of objects. Zlatanova et al. (2004) presents an overview on object-oriented topological models for detecting spatial

relationships between objects. The advantages and disadvantages of differential models such as 3D formal data structure, object-oriented 3D models, and solid object management system were discussed in their research. The object-oriented 3D model was shown in Figure 10. Each urban object has two main fields in geometric and thematic domains.

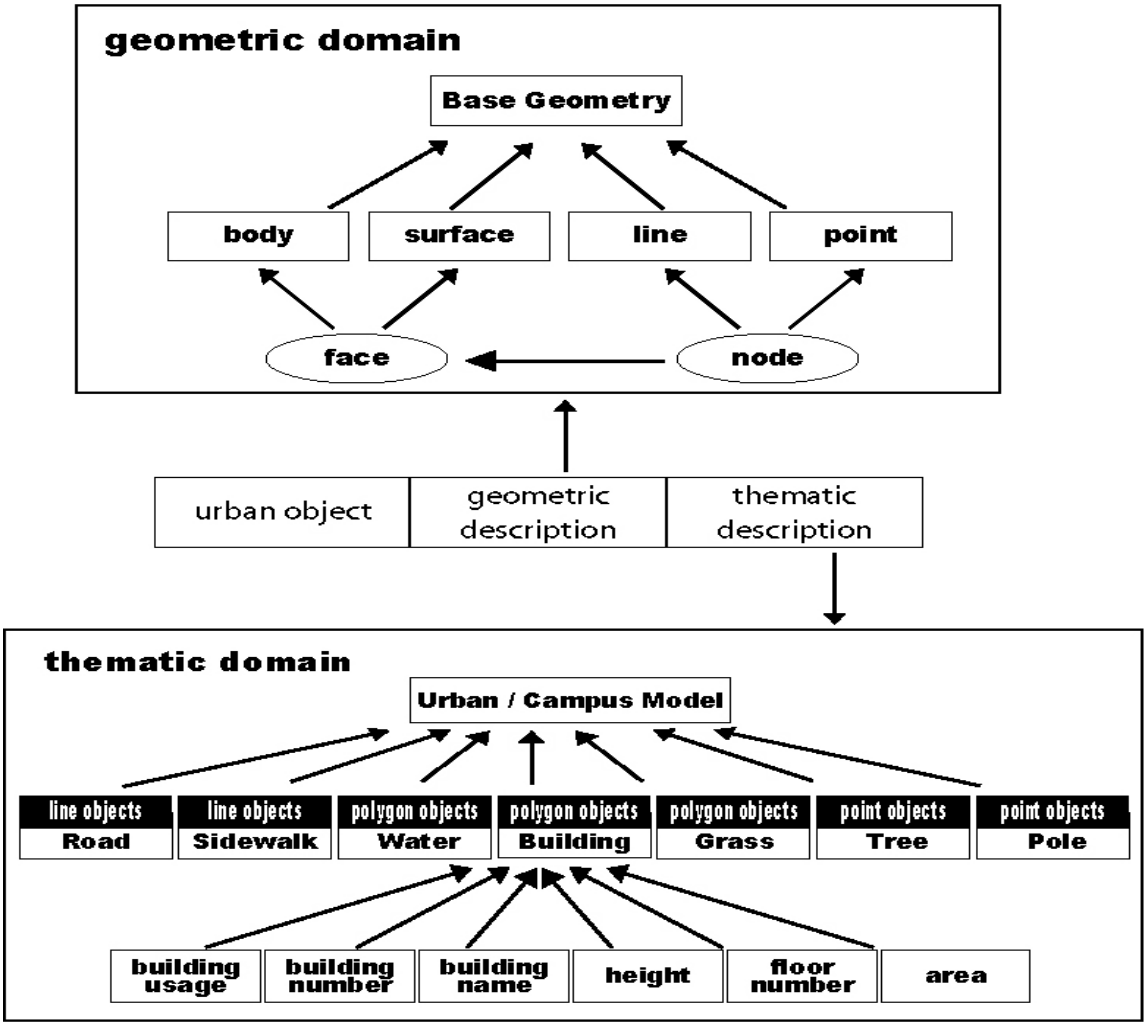

Figure 10: Object-oriented 3D model of an urban object

3.3 Data Structures

An object is a self-contained package of information describing the characteristic and capabilities of a geographical entity. Real-world geographical features can be modeled as a collection of objects. Relationships among the objects also need to be considered. In urban objects, four properties information are required in constructing 3D urban models (Table 1).

Table 1: Urban object properties

Planimetric property	Position, shape of footprints
Vertical property	Heights, roof structure
Texture property	Visual appearance of facades
Thematic property	Object attributes

Different data sets can be collected and fused to an integral 3D-dataset with respect to different resolution methods (Köninger and Bartel 1998). Li et al. (1999), Xia (1995), and Pfund (2002) provide a relational database structure for creating and manipulating attribute information in 3D urban model. They demonstrated various 3D geometric representations and concepts such as surface based geometric representations and volume based geometric for integration topological and attribute information with geometric representations.

Some planners used software to create a GO-3DM database system for storing information, including the height of objects, roof types and images of facades (Ranzinger and Gleixner 1995, 1997).

Coors (2003) present the 3D geometry and topology in Urban Data Model (UDM) which includes the concept of multiple representations for the same feature. Each feature is associated with one of the four abstractions named point, line, and surface from planimetric properties, and body from vertical property (Figure 11). A point such as true position of a tree is represented in a zero-dimensional spatial extension. Line features like road and sidewalk have a one-dimensional spatial extension. Surfaces and bodies are represented as two- and three-dimensional objects. Thus, the concept of UDM is possible helpful for a query oriented function in this research. In addition, it supports an easy way to extract information from the database about geometric and thematic aspects of spatial features and their topological relationships.

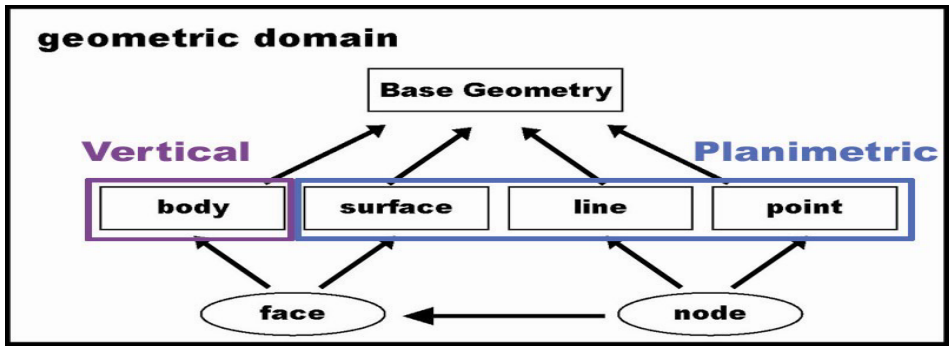

Figure 11: Geometric domain

From the concept of UDM, urban features can be represented as point, line, and polygon objects in terms of their geometric properties and generalization level (Table 2). For instance, trees and poles can be represented as point objects, roads and side walk can be represented as line features, and buildings, rivers, and grass areas can be represented as polygon objects.

Table 2: Geometric properties of urban objects

Point objects	vector	Trees, Poles, Traffic signs
Line objects	vector	Road, Sidewalk, Wall, Bridges, Highway
Polygon objects	vector	Buildings, Grass, Water area

In this research, an OpenFlight scene-description format is utilized for describing 3D database and its structure. An OpenFlight database uses geometry, hierarchy, and attributes to define models used in real time applications. Each component provides a unique contribution to the model. Geometry defines the feature in three dimensions as a set of ordered coordinate vertices. Hierarchy defines additional structures that combine the vertices of the model into logical units that are easily edited and displayed with texture property in switching both graphics and hierarchy views (Figure 12). The vertices of each side of a box make one face, and the faces of the box make one object. The term node refers to each of these structural elements in the hierarchy.

Attributes provide additional data to define the graphical, physical, and theoretical characteristics of each node (MultiGen-Paradigm 2002).

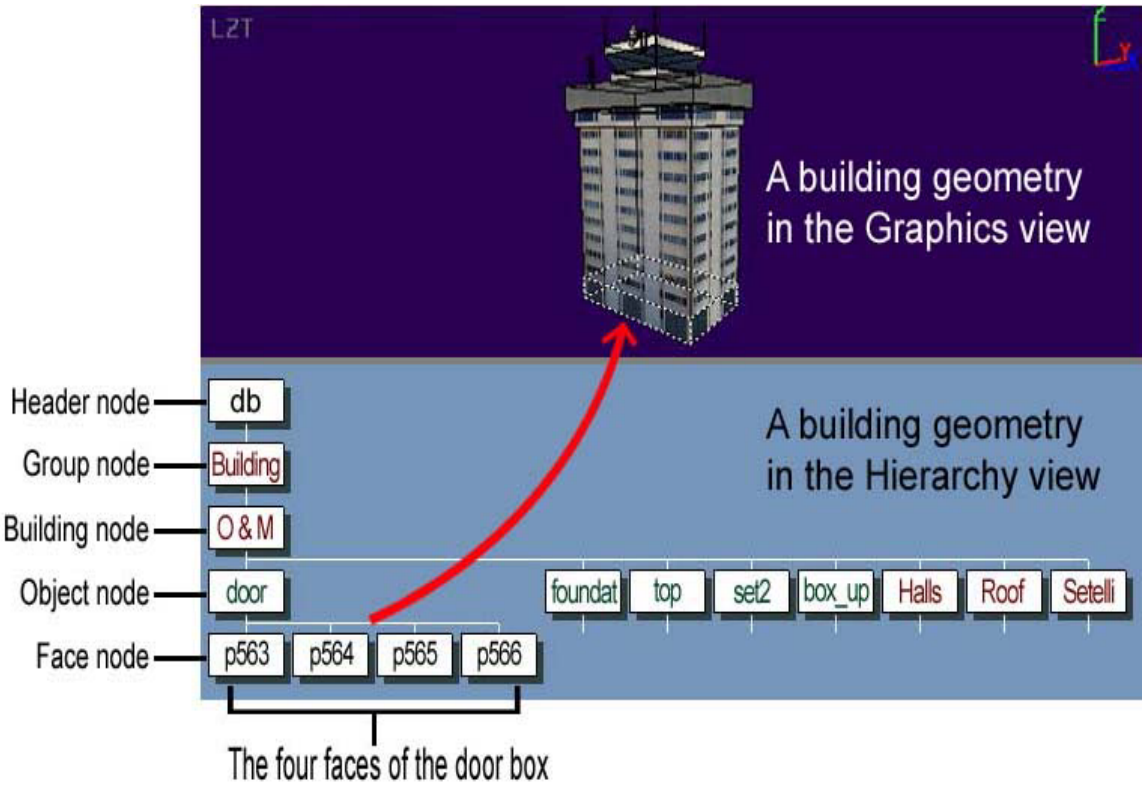

Figure 12: Graphic and hierarchy views of O&M Building

In addition, the database hierarchy defines the relationship of the nodes in a database to each other. The nodes in the hierarchy are linked together in an inverted tree, which grows from a single database header node at the top, down to object, face, and vertex nodes at the bottom (Vertex nodes do not appear in the Hierarchy view).

The basis for many spatial operations is topology. Topology is one of the mechanisms to describe relationships between spatial objects (Zlatanova et al. 2004). After the data structure is designed and the geometric properties of urban objects are extracted, the thematic attributes information is required for shape files of each urban object. For example, the thematic attributes of building including building name, building types, owner, built year, number of rooms, types of structure, etc. They are quite helpful for supporting GIS query and operations with geometrical information (position, shape, and height of objects), and thematic data (building and textural information).

For a typical urban space, urban features can be classified to five classes (Li et al. 1999). Each class can be considered as a template for urban objects. New object classes can be defined and added in terms of geometry, different levels-of-detail and related thematic data (Figure 13).

a. Tree class: With tree name, tree types, and tree position (point objects).
b. Pole class: With pole types, pole height, pole position, and pole rotation (point objects).
c. Road class: With road name and road number (linear objects).
d. Side walk class: With side walk name and number (linear objects).
e. Building class: With building name, building numbers, height, floor numbers, rotation, gross area, perimeter, and building usages (polygon objects).

f. Grass class: With grass name, grass types, grass position, and grass area (polygon objects).

g. Water class: With water types, water position, and water area (polygon objects).

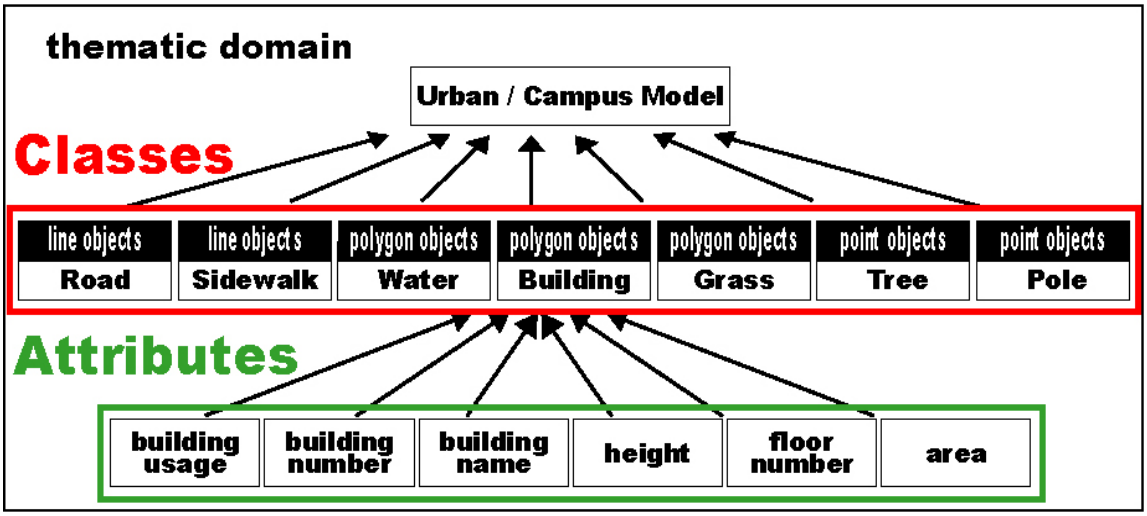

Figure 13: Thematic domain

The inclusion of thematic information is desired for each building, so it is possible for user to query for information such as building name, height, number of floors, and usage from selected buildings.

Object-oriented structure in terms of spatial analysis allows direct and continual access to attribute data. It is capable by linking feature attributes to structures designed for 3D graphical representation. Therefore, it allows the end

user to perform continuous mapping and querying in an interactive environment. Döllner and Hinrichs (2000) analyzed the integration of visualization and GIS with geo-objects by embedding the visualization technique using object-oriented method. This integration saves development effort and ensures that object information can be changed and modified by end-user in object-oriented structure.

The visual representations can be quickly updated with attribute control by interaction between objects and end users. One major column can be used as a primary key for linking associated attributes in a relational database to control or modify the object elements in object-oriented database (Figure 14). It enables users to query and manage the data in terms of object characteristics like color, rotation, and object surfaces.

The software of Model Builder 3D provides the object-oriented functions for collecting and managing objects. The planimetric information, vertical information, and texture information can be stored into a database system. Additionally, the software also provides the utility to control objects elements for dynamic alteration, and an interactive query task. Therefore, object-oriented structure is designed to support our research in manipulation and visualization of 3D objects for real-time rendering and dynamic generation of virtual models. It also enables rendering software to directly transform all the object data like geometric and texture descriptions into a display from the database.

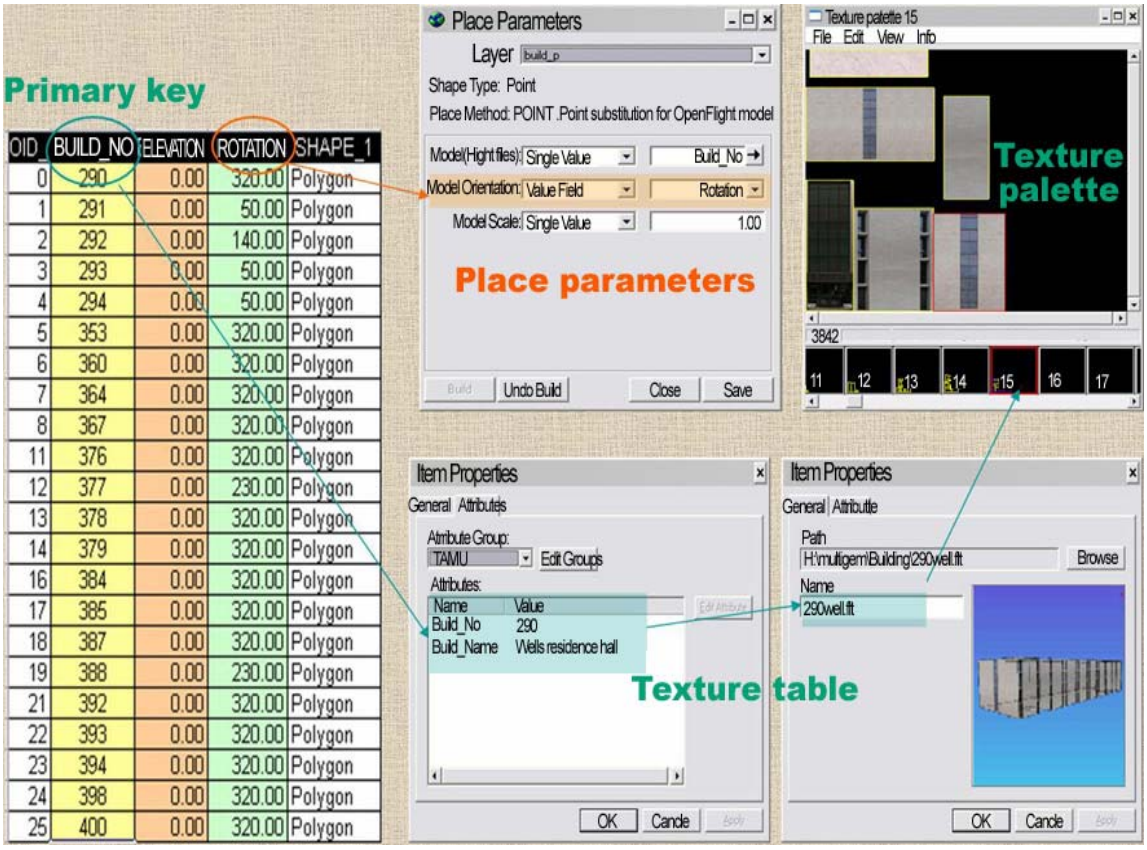

Figure 14: Attribute control. Building number is set as a primary key which can link with relative tables such as geometry and texture palette for visualization. In addition, rotation values can be modified with table of place parameters for rotating buildings

3.4 Planimetric Information

The Extraction of spatial objects from high-resolution imagery, range image data (LiDAR) or parcel data are the main processes to get the shape of buildings, trees, etc. In this research, we tried to extract these objects from LiDAR data and aerial photographs. In generally, features can be extracted directly from digital surface models as those produced by LiDAR (Elaksher and Bethel 2002).

Many researchers developed automatic or semi-automatic methods for building extraction and 3D reconstruction by using LiDAR data (Haala et al. 1998; Brenner and Haala 1999; Priestnall et al. 2000; Ding 2000; Hill et al. 2000; Haithcoat et al. 2001). Priestnall et al. (2000) examined methods for extracting surface features form a digital surface model using LiDAR. They tried to detect building edges from gradient maps and to refine the surface roughness estimates by classifying extracted surface features using topographic and spectral characteristics to discriminate between buildings and tree canopy.

Haithcoat et al. (2001) took a similar approach to building footprint extraction and 3D reconstruction. The first step is to generate a digital surface model from the LiDAR point data. The second is to extract objects higher than the ground surface. Based on the building's geometric characters such as size, height and shape, buildings are separated from other objects like trees or rivers. This approach provides a good method to distinguish buildings from other objects.

Brenner and Haala (1999) proposed the concept of reconstruction of urban area based on height data from LiDAR. By applying LiDAR data, they obtained constructive solid geometry and converted its data to boundary representation. It is possible to transform raster representation of airborne laser data to a high-qualify 3D vector representation of urban scene.

From previous researches, LiDAR is used to detect building outlines and extract plants canopy (Rottensteiner and Briese 2002). Therefore, building extraction is solved by determining approximate building outlines and the vertical dimension value is derived by building polygons.

Building representations are required for geometric properties. Hence, converted grid LiDAR data can instead of point clouds or triangular irregular network (TIN) models. It is the most efficient way to perform feature extraction from LiDAR data (Ding 2000). The methods of gradient calculation and slope information are used in determining the building shapes. Moreover, extracting spatial objects from high-resolution aerial photographs like 1-foot resolution DOQQs is an efficient and simple method to quickly extract the base shape of buildings and other features by manual work using ArcGIS software if LiDAR data is not available.

3.5 Height Information

Ding (2000) presents an efficient and automated approach from grid data instead of point clouds for generating elevation of building polygons.

For this research, it is possible to extract average building heights information. A grid format file is transformed from a LiDAR ASCII file. The grid can be overlay with building polygons by raster manipulation. After raster manipulation, building grid data can be produced with the height value.

From DOQQs images, building heights information is also derived from remote sensing knowledge. For example, the laser rangefinder can be used to measure the horizontal distances and hypotenuse length of a building. It is uncomplicated to get the vertical value by the Pythagorean Theorem calculation if the hypotenuse and the base distance are available. In addition, Shadow methods are useful to get the elevation. The length of an object's shadow on a horizontal surface is proportional to its height. On the other hand, displacement methods and parallax methods are also profitable for extracting the heights if the LiDAR data is not available.

3.6 Texture Information

Texture data capture stage is the most time consuming part of constructing 3D models. It involves the use of GIS, CAD, images, videos, and photographic technologies in imaging processes.

The campus model will be constructed using a digital terrain model, 2D features stored in a GIS, and textures derived from digital camera and digital camcorder. Buildings were placed at ground level and then extracted from footprints, or put a texture onto each plannar faces by MultiGen-Paradigm Model Builder 3D software. Green fields, water bodies and roads were draped over the terrain by the textures. This model will be enhanced with structural details for buildings, vegetation, and urban features (Pullar and Tidey 2001).

3.7 3D Model Visualization

3.7.1 LOD Concept

Models with multiple levels of detail (LOD) are intensively used to control scene complexity and to accelerate rendering for real-time visualization of complex 3D scenes. Base on map scales, each level contains different methods, which have an influence on the visual representation of urban objects. The literature provides there methods like pixel area, distance to object, dependence, and view-independent methods to preparing LOD models (Köninger and Bartel 1998; Zhu et al. 2002).

Model Builder 3D can be used for creating different level of views from low detail level to high specify level. The number of polygons can be reduced in each level to simplify the objects. The simplest level is used when the viewpoint is far away. As the viewpoint is approached to the objects, increasingly complex models allows viewer to see more detail (Multigen-Paradigm 2002).

For this research, we use three different levels-of-detail by view-independent methods. For the first level (LOD0), basic building boxes are considered as sufficient. It is planned to represent simple shape of buildings for greater distances (Figure 15A). The second level (LOD1) includes a precise roof shape with antenna and box details with generalized fronts (Figure 15B). They are shown as simple geometry with textures. The third level (LOD2) contains more detailed object geometry and facade with rich characteristic elements for

closer distance (Figure 15C). Due to general thematic data are available in all LODs, these LOD models are then stored in a database. During the rendering process, the LOD decreases with an increasing distance. Specific LOD model is selected depending on the position of the viewpoint (Zhu et al. 2002).

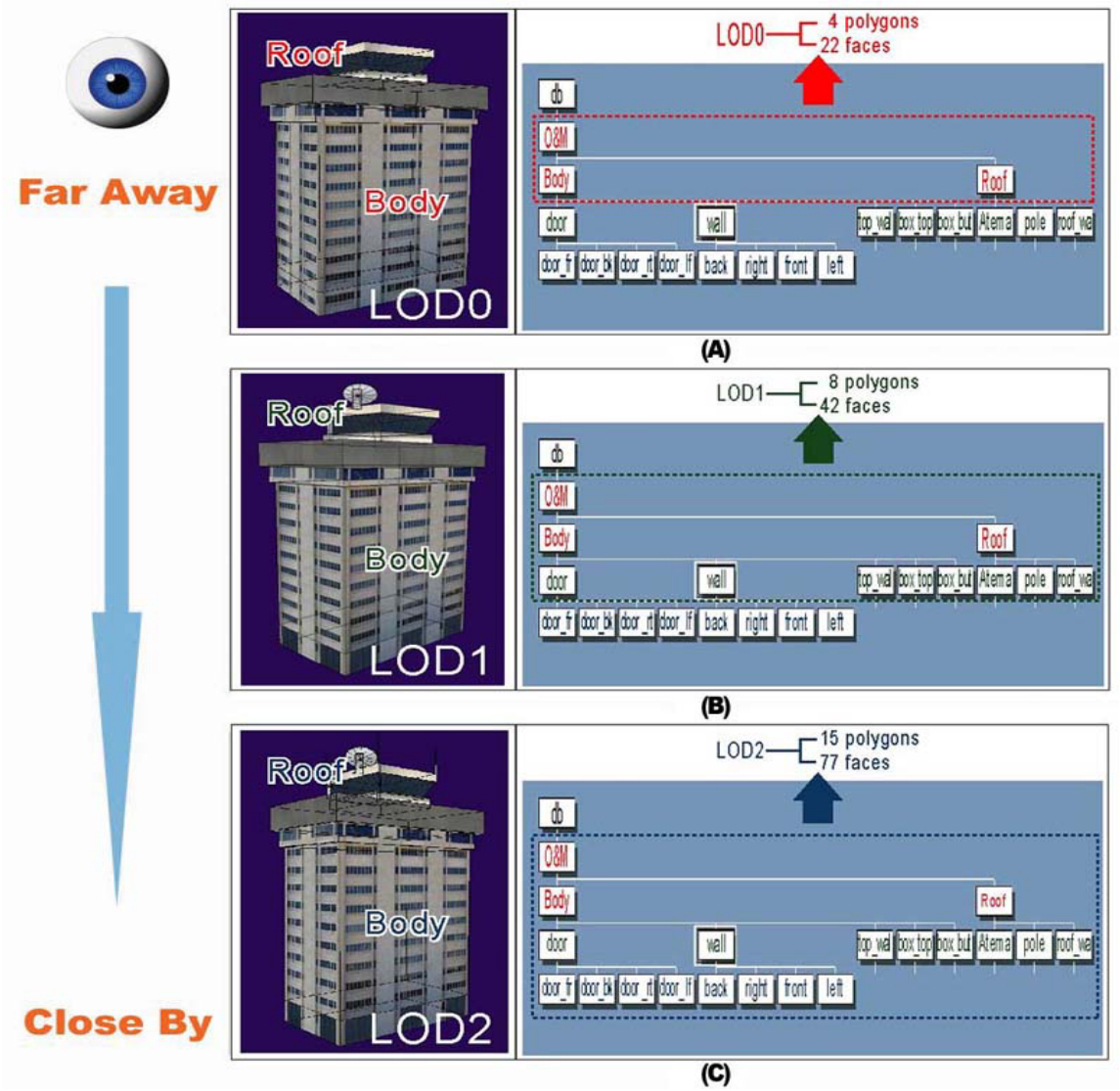

Figure 15: The concept of LOD. (A) LOD0; (B) LOD1; and (C) LOD2

3.7.2 Fly-through, Walk-through, and Animations

The visual quality of the built environment is highly valued for both aesthetic and economic considerations.

MultiGen-Paradigm Site Builder 3D can be used for employing visual simulation to fly-through or walk-through into a texture for the elevation of planning proposals. It is very useful, especially for projects dealing with the landscape and built environment (Pullar and Tidey 2001). A key component in most virtual reality systems is the ability to perform an animation of a virtual environment from different viewing positions and orientations by a virtual camera moving through the virtual environment along a fixed path. The clip of animation of Texas A&M University was shown in Figure 16.

Figure 16: The clipped animation of Kyle Field in LOD1 level

3.8 Summary

In this chapter, the generation of GIS-based 3D urban model has been discussed. Planimetric information, height data, texture, and attributes with object-oriented concept are necessary to create a 3D urban model. From these methods, 3D campus and urban models can be examined in next two chapters.

CHAPTER IV

3D CAMPUS MODEL FOR TEXAS A&M UNIVERSITY

Texas A&M University is a land grant institution located in College Station, Texas. There are many different types of buildings on campus. DOQQ (Digital Orthophoto Quarter Quads), aerial photos and laser rangefinder are used to acquire geometric information for buildings and other objects.

In a 3D campus model, buildings are of primary interest objects. Our goal is to extract the geometrical structures and attributes using photogrammetry and remote sensing methods with digital images. Relief displacement method, shadow height method, parallax method, and laser ranging method are used to capture height information for structures on campus.

4.1 Data Collection

DOQQs were obtained from the Texas Natural Resource Information System (TNRIS). It is used to extract planimetric information by supervised classification. In addition, some parts of planimetric data like building footprints, roads, and side walks were derived from TAMU GIS office for updating old information. Trees, grass, and poles information are derived by high-resolution aerial photographs and post-classification process. Building

height information is collected by the laser rangefinder and photogremmetry technique. Building attributes were acquired from TAMU facilities coordination office, and tree attribute were received from TAMU urban forestry work center. Texture data is obtained by digital video camera and digital camcorder, and processed by Adobe Photoshop 6.0 image program.

- DOQQs are 1 meter resolution digital images that combine the geometric qualities of a map with the detail of an aerial photograph. The characteristic of DOQQs image is shown in Table 3, and the DOQQs image of Texas A&M University is shown in Figure 17.

Table 3: Characteristics of DOQQs data

	DOQQs
Format:	MrSID
Projection:	UTM
Units (x,y):	Meters
Nominal scale:	1:12,000
Area:	3.75- x 3.75-minute quad (one quarter-quad)
Resolution:	1 meter ground resolution
Color:	24-bit color infrared (CIR)
Data:	1995-1996 NAPP (full range of dates from 1994-1998)
File size:	154 +/- megabytes per quarter-quad
Available:	USGS, TNRIS

Figure 17: DOQQs image of Texas A&M University

4.1.1 Hardware and Software

- Nikon Laser 400 Rangefinder: It is a simple survey equipment to acquire the height for buildings, trees, and poles. It provides quick and accurate distance measurements up to 400 meters, and is suitable for surveying campus buildings.
- Olympus C750 ultra zoom digital camera: It has astounding 40x total zoom and 4 mega-pixel CCD for capturing colorful and large range images for texturing.
- Sony DCR-TRV38 MiniDVdigital camcorder: It delivers mega-pixel resolution video from recording survey area for reviewing and texturing.
- Adobe Photoshop 6.0: It offers powerful functions to create original images or modify photos for image processes in texturing.

- Model Builder 3D/Site Builder 3D: Both of these products were made by Multigen-Paragium company. Site Builder 3D is the software for ArcGIS users to quickly transform 2D map data into highly-realistic, fully interactive realtime 3D scenes; Model Builder 3D is a companion product to Site Builder 3D that allows users to quickly generate 3D models of real-world urban objects and topography for an interactive display of 3D GIS data.
- ArcGIS version 8.3 (ESRI): It is a desktop GIS used for storing, organizing and displaying spatial information. It has an interactive interface for display and query for spatial data. Planimetric information of urban objects collected in the field was processed with ArcGIS on a Windows 2000 platform.

4.2 Data Structures and Object-oriented Models

For the campus model, the representation of object requires planimetric information, including the position and boundary shape. It also requires the information about height and surface texture. To support spatial query, attributes and properties associated with each object need to be collected. Those include name, type, height, number of floors, and built year, etc. Figure 18 shows a geometric and thematic description of O&M building object.

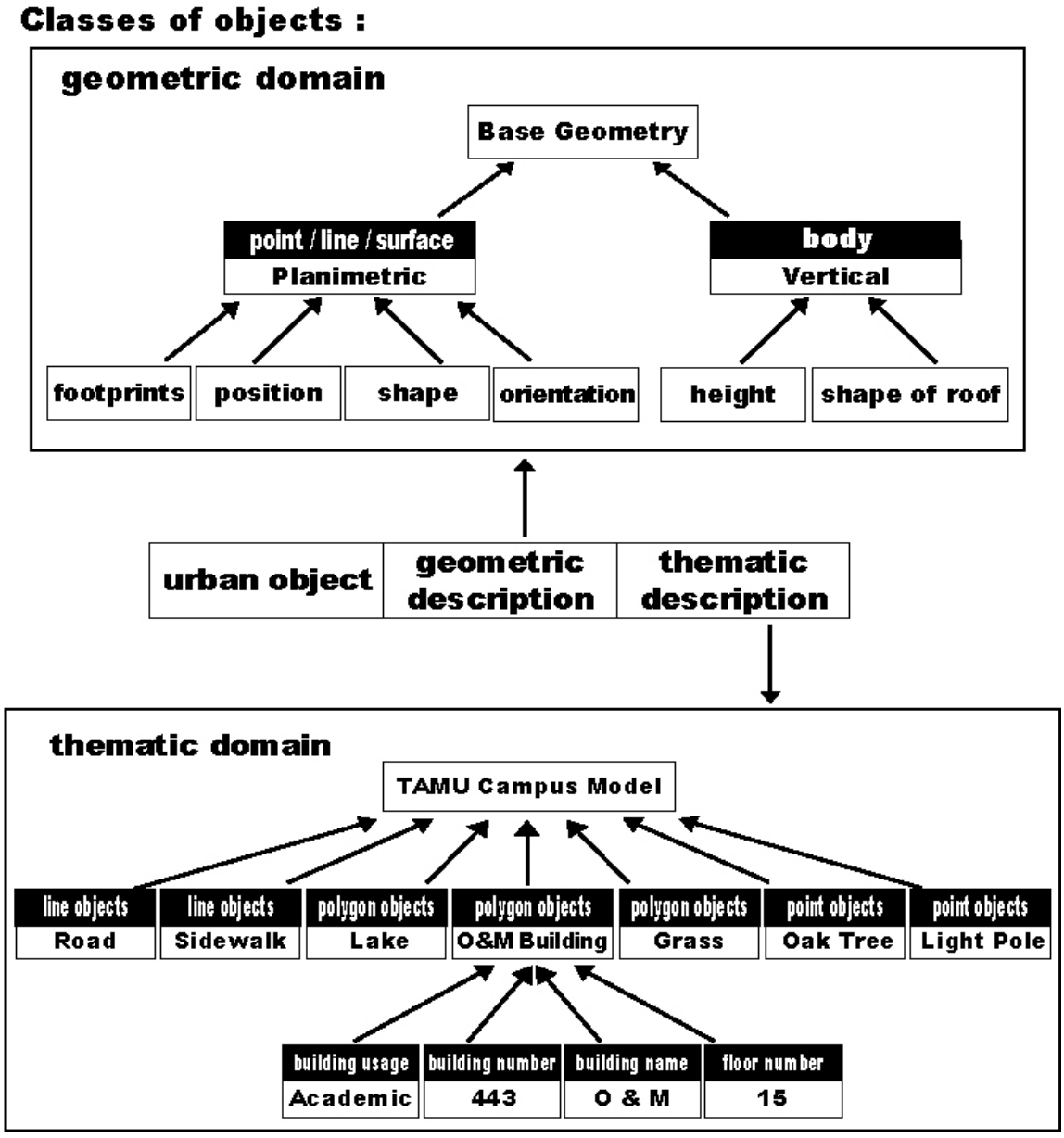

Figure 18: Geometric and thematic description of O&M Building

4.3 Planimetric Information Acquisition

2D planimetric data is necessary for constructing a model for campus objects. Previously, the planimetric footprints of urban objects are mainly

acquired by ground survey method or manually tracing by aerial photographs. In this research, an automatic method is developed for extracting planimetric data by image classification, boundary detection, and edge tracing.

4.3.1 Multi-spectral Classification

Multi-spectral classification is the one of most often used methods for extracting thematic information based on multi-spectral image data. Multi-spectral remote sensing imagery represents the reflected radiation for a specific geographic area in a number of discrete spectral bands. With multiple image bands, a particular type of campus objects exhibits a diagnostic spectral response pattern that differs from other types of objects. To identify and map various objects, a basic underlying premise is that there are detectable differences in reflected radiation observed for different types of features.

DOQQs are the infrared false color digital aerial photographs which can be used to calculate the vegetation index. The most commonly used index is the Normalized Difference Vegetation Index (NDVI). Due to the fact that DOQQ provides in MrSID format, it can be converted into three individual grids. They are: band 1 (near infrared band), band 2 (red band), and band 3 (green band). The near infrared band (band 1) and red band (band 2) grids can be used to calculate the NDVI using the following general equation:

$$NDVI = \frac{NearIR - RED}{NearIR + RED}$$

In general, trees, grasses, and other vegetation covered areas have high positive NDVI values. Healthy vegetation reflects strongly in the near infrared portion of the spectrum while absorbing strongly in the visible red. Water yields negative values due to larger red reflectance than near infrared. The NDVI values for bare soil are near zero due to their similar reflectance in both bands. Therefore, in a NDVI grid the lighter tones are associated with dense coverage of healthy vegetation. The images of near infrared band, red band, green band, and NDVI band are shown in Figure 19. We combine near infrared band, green band, and NDVI band into an individual multiple bands image for supervised classification (Figure 20).

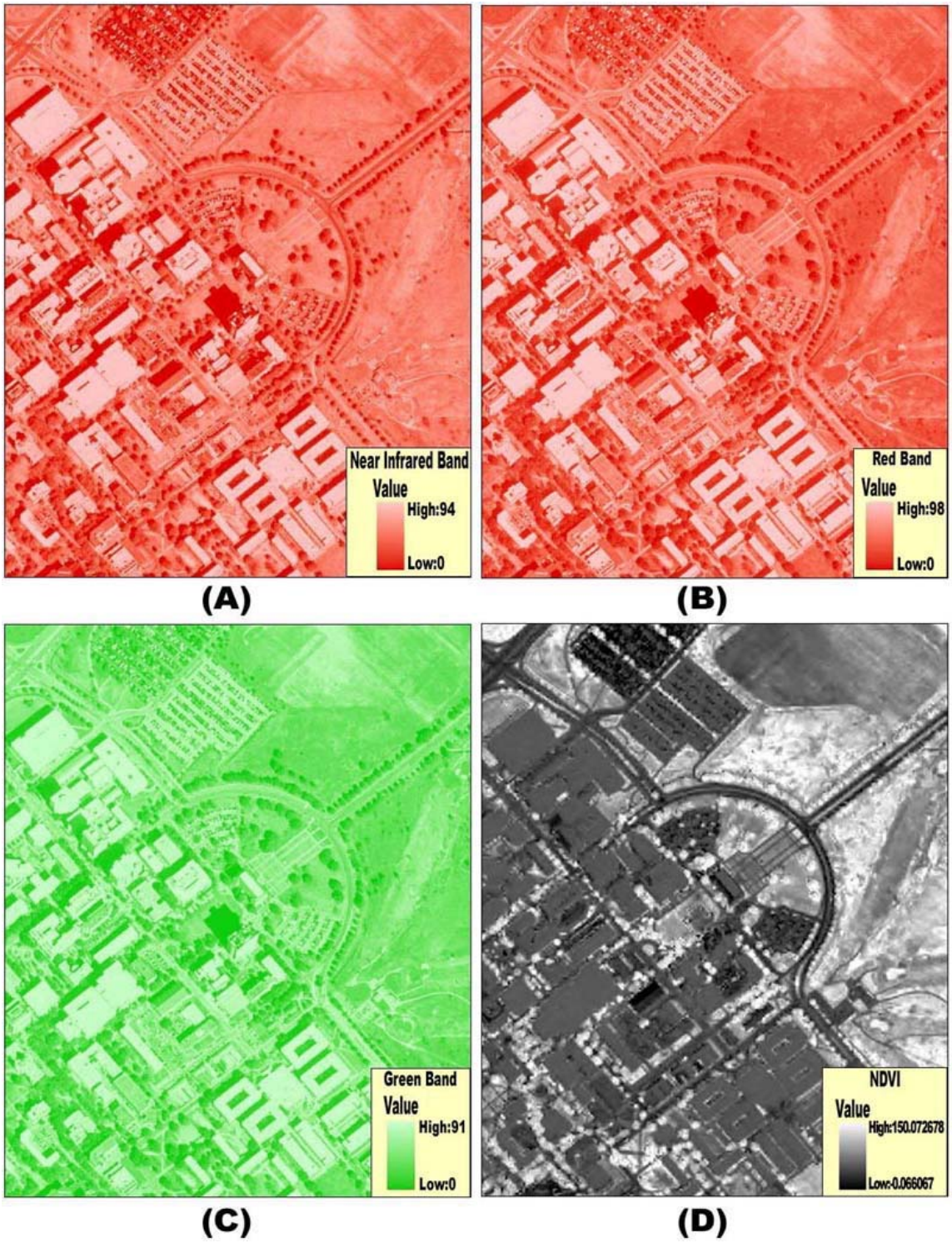

Figure 19: DOQQ and NDVI images of TAMU campus. (A) near infrared band image; (B) red band image; (C) green band image; (D) NDVI image

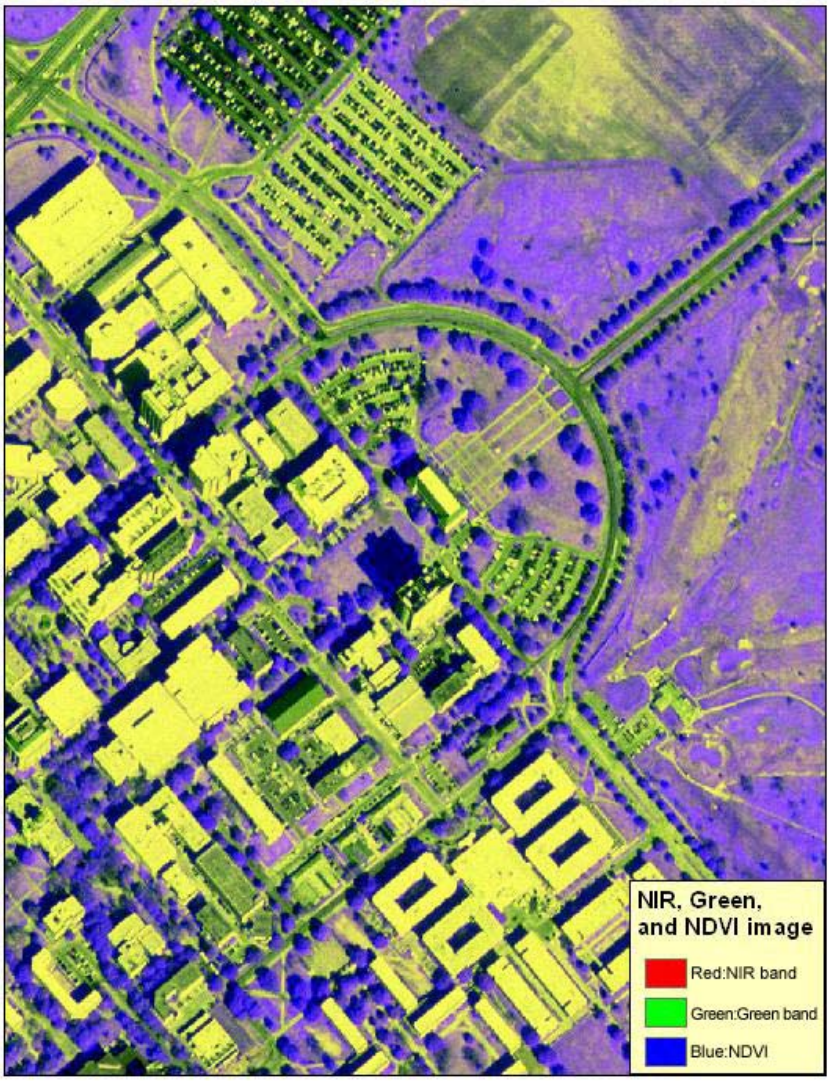

Figure 20: The NGI image of TAMU campus

A graphical scattergram are required to determine the correlation strength between spectral bands and the degree of between-class separability of multispectral data. A scattergram is a two-dimensional scatter plot of image data values for any two spectral bands. It allows graphic view to the correlation

between two image bands and the combined ability of two spectral bands for separating different types of features.

The correlation strength between NIR band and NDVI band, NIR band and green band, and green band and NDVI band are shown in Figure 21. If two spectral bands are highly correlated to each other, then data points in the scattergram will be tightly grouped along the diagonal direction. In this case, green band and NIR band contain much redundant information, and hence the combination of these two bands has a relatively weak capability to separate different terrain features (Figure 21B). If two bands are uncorrelated or weakly correlated, the data points in the scattergram will be widely spread. In this case, NIR band and NDVI band, green band and NDVI band provide different types of information. The combination of these two bands may have a better chance to separate different terrain features. In addition, A cluster of points on the scattergram often corresponds to a certain type of terrain feature as they have very similar spectral properties. The greater the distance between different clusters, the greater the potential of these two bands for accurately discriminating different classes of terrain features. A good result of scattergram for distinguishing individual identification of each feature type is shown in Figure 21A and Figure 21C.

Thus, NIR band and NDVI band combined images is used for supervised classification procedure.

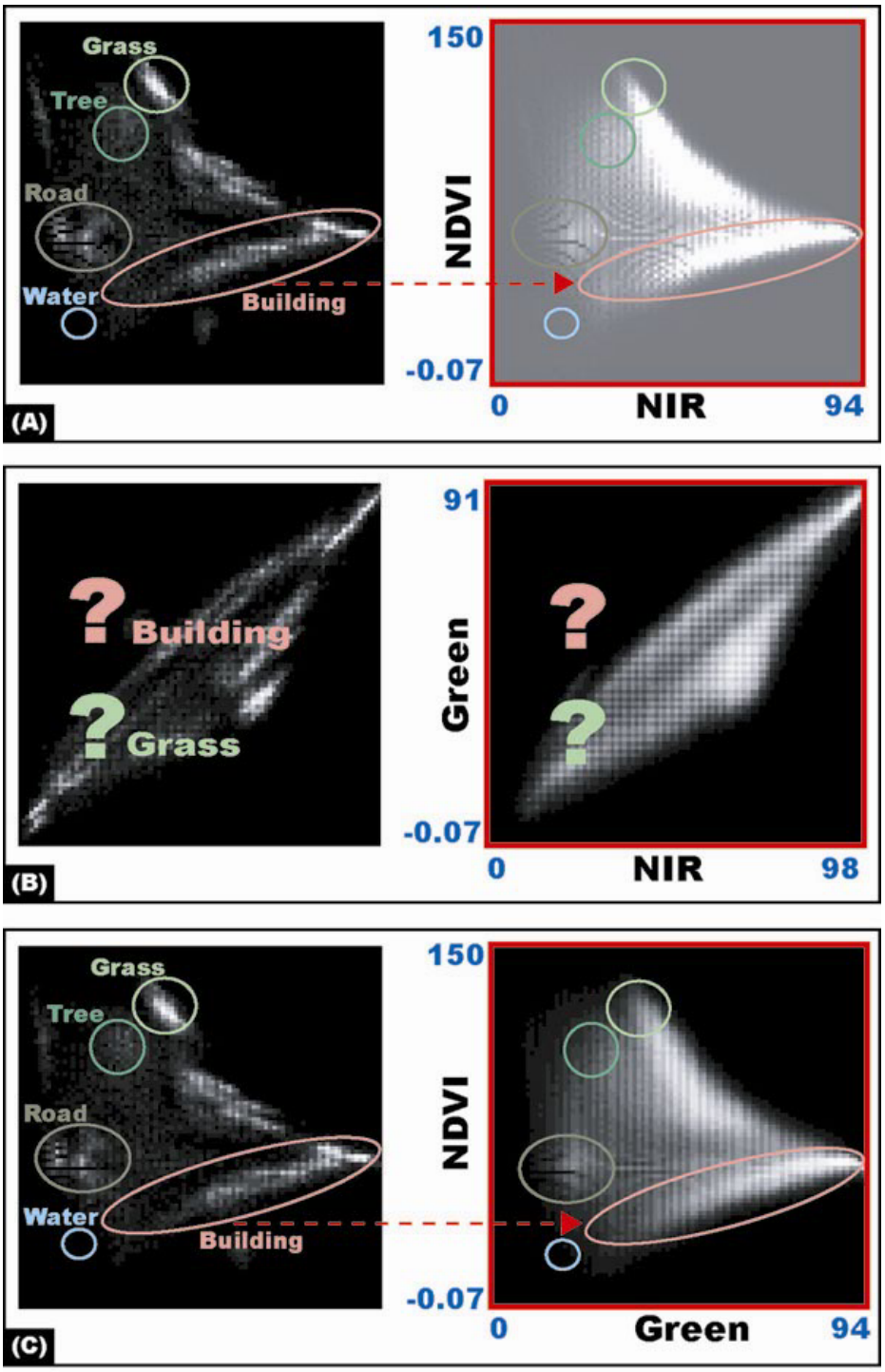

Figure 21: Scattergram analysis. (A) NIR band and NDVI band;

(B) green band and NIR band; and (C) green band and NDVI band

In supervised classification, the identity and location of feature classes or land cover types, such as building, tree, grass, water, side road, and road, are known beforehand for a limited number of some training regions through visual analysis of aerial photographs. The identified specific training areas on the multispectral imagery that represent the desired known land cover types are shown in Figure 22.

Figure 22: Training chips of urban features

The spectral characteristics of these known areas train the classification algorithm for land-cover mapping of the remainder of the image by Maximum Likelihood algorithm, namely to assign the remaining pixels in the image to one of these land cover classes. The result of supervised classification is shown in Figure 23.

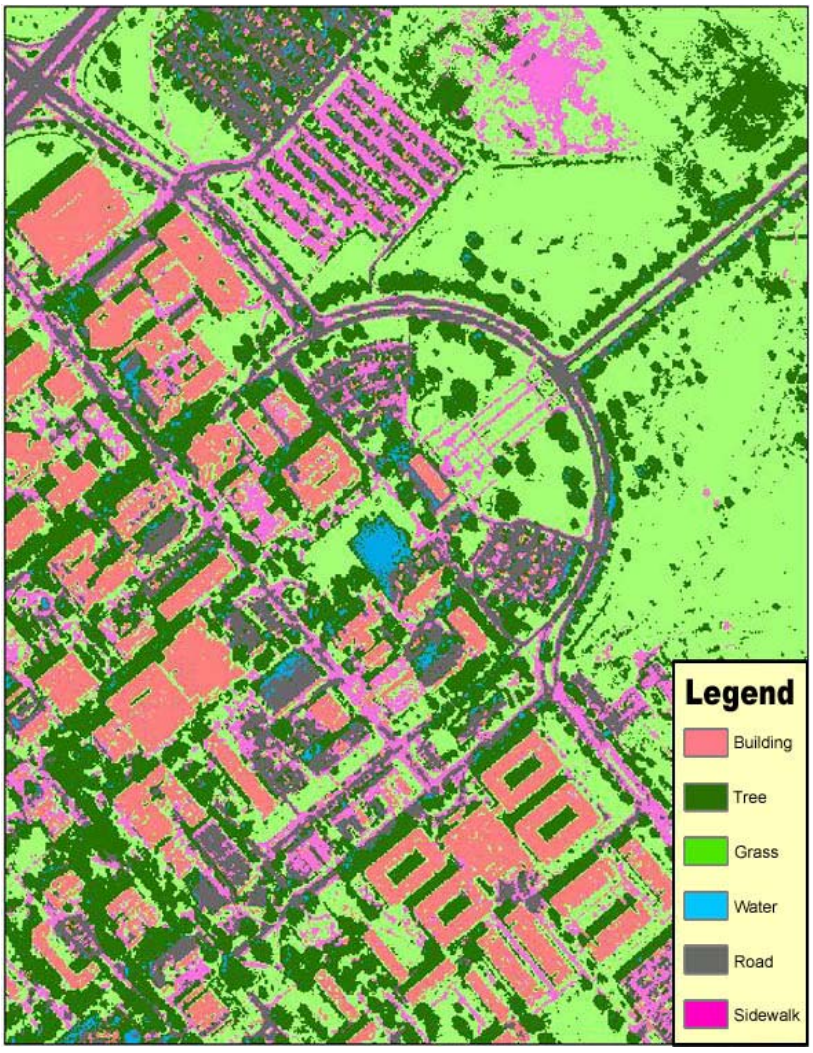

Figure 23: Classification map of TAMU campus

Multivariate statistical parameters, the mean, standard deviation, minimum value, maximum value, are calculated to each training class as its statistical signature, namely, its fundamental spectral characteristics. This signature is a statistical representation of a particular class, which is used by the decision rule to assign labels. The decision rule labels each pixel in the image according to their similarity to the class statistical signature. The table of training region statistics of NDVI band was shown in Table 4, and small standard deviation value presented the accuracy of classification for each object.

Table 4: Training region statistics of NDVI band

	Mean	Minimum	Maximum	Std Deviation
Water	0.609	0	37	4.520
Grass	65.035	59	150	4.267
Tree	78.526	72	93	5.008
Side Road	54.067	52	58	2.686
Road	43.232	38	46	2.381
Building	49.493	47	51	1.415

An accuracy assessment has been conducted to insure the validity of the information that has been extracted from the image. In this research, Kappa coefficient values are used to determine and summarized as an error matrix. To

correctly perform a classification accuracy assessment, it is necessary to systematically compare two sources of information. One is pixel value in classification map by producer's accuracy, and another is ground reference test information by user's accuracy. The reference data of check points is shown in Figure 24.

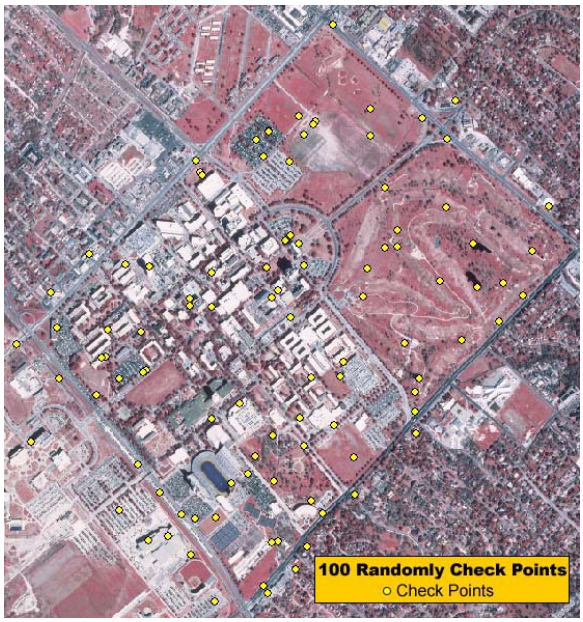

Figure 24: Random check points of reference data

The error matrix is a table of numbers that express the number of sample units assigned. It was shown in Table 5 that the columns of the table normally represent the reference data generated, and the rows of the table represent the classification generated from the remote sensed data (Jensen, 1996).

Table 5: Error matrix analysis of classification map

	Reference Data								
Classified Data	Building	Tree	Grass	Water	Road	Sidewalk	Row Total	User's accuracy	Kappa
Building	10	0	0	0	1	3	14	71.43%	0.675325
Tree	0	20	2	1	0	0	23	86.96%	0.826087
Grass	0	4	32	0	0	2	38	84.21%	0.760766
Water	0	0	0	3	0	0	3	100.00%	1.000000
Road	2	1	0	0	9	0	12	75.00%	0.715909
Sidewalk	0	0	0	0	2	8	10	80.00%	0.770115
Column Total	12	25	34	4	12	13	100		
Producers Accuracy	83.33%	80.00%	94.12%	75.00%	75.00%	61.54%			
Overall Classification Accuracy	82.00%								
Overall Kappa Statistics	76.56%								

Kappa analysis is a discrete multivariate technique used in an accuracy assessment which yields the K_{hat} statistic that is a measure of agreement or accuracy. The K_{hat} statistic is calculated as follows:

$$K_{hat} = \frac{N \sum_{i=1}^{r} xii - \sum_{i=1}^{r} (xi + xX + i)}{N^2 - \sum_{i=1}^{r} (xi + xX + i)}$$

where N is the total number of check point (N=100), r is the number of rows in the matrix (r=6), Xii is the number of check point in row i and column i, Xi and X+I are the marginal tools for row i and column i (Jensen, 1996).

$$\sum_{i=1}^{r} xii = (10 + 20 + 32 + 3 + 9 + 8) = 82$$

$$\sum_{i=1}^{r} (Xi + xX + i) = (14x12) + (23x25) + (38x34) + (3x4) + (12x12) + (10x13) = 2321$$

$$\text{therefore } K_{hat} = \frac{100(82) - 2321}{100^2 - 2321} = \frac{8200 - 2321}{10000 - 2321} = \frac{5879}{7679} = 76.56\,\%$$

K_{hat} values >0.80 represent strong agreement or accuracy between the classification map and the ground reference information. K_{hat} values between 0.40 and 0.80 represent moderate agreement. K_{hat} values <0.40 represent poor agreement (Jensen 1996). Hence, the K_{hat} values for classification map of Texas A&M University represent a moderate agreement.

4.3.2 Post-classification Processing

From the previous classification grid of campus, the boundaries of campus features can be extracted by posy-classification processing for improving their accuracies. A series of image processing steps, including region grouping and labeling, small image objects removing, morphological dilation and erosion, boundary tracing and vectorization, are applied to the classified image (Liu and Jezek 2004). Grouping and labeling algorithms convert image

regions into individual image objects. A vector-based line coverage of building boundaries is the final product.

1) The classified image is recoded as a binary image to represent building and non-building pixels. The building pixels are recorded as 1, and non-building pixels objects such as grass, water, road, and tree recorded as 0.

The binary image consists of numerous connected image areas. Any contiguous areas of feature objects in the binary image can be grouped into individual building object. A unique identification number and characterized can be labeled by its geometric shape from each image object. Based on the image object, heuristic human knowledge about the size and continuity of building and non-building shapes are applied to identify true building objects and remove false building objects.

2) Building pixels are grouped into black objects and labeled as individual image objects. Some small and irregular image objects are not true building features (Figure 25B). They are removed by merging them into non-building area (Figure 25C).

3) The non-building pixels can be grouped into background objects. Similarly, the small isolated background objects inside the building objects are removed by combing them into building objects (Figure 25D). After removal of small isolated image objects, only building and non-building objects are left.

Two morphological operations: opening and closing are used to improve the boundaries of building objects. Opening operation generally smooths the boundary of an image objects, breaks narrow isthmuses, and eliminates thin protrusions. It erases the flange of edge then dilates the contours. Closing operation also tends to smooth sections of contours but it generally fuses narrow breaks and long thin gulfs, eliminates small holes, and fills gaps in the boundary (Gonzalez and Woods 1992).

4) Each building pixel in image objects is scanned by a 3 x 3 neighborhood windows to check its four contiguous neighbors. If one or more neighbor of the building pixel belongs to background pixels, the pixel is removed as a boundary pixel. In this way, boundary pixels of building objects are delineated (Figure 25E).

5) A line tracing algorithm is utilized to trace the edge pixels and record their coordinates into a list of vector line segments in ArcoInfo ungenerate format (Figure 25F). Based on the ungenerate file, an ArcInfo line coverage can be created to represent the final building boundaries (Figure 26).

The same procedure is employed to extract the boundary of tree canopy, roads, and lakes. The boundaries of tree canopy are represented as polygon coverage. The tree point coverage is also derived from the centroid point from tree canopy polygon coverage (Figure 27).

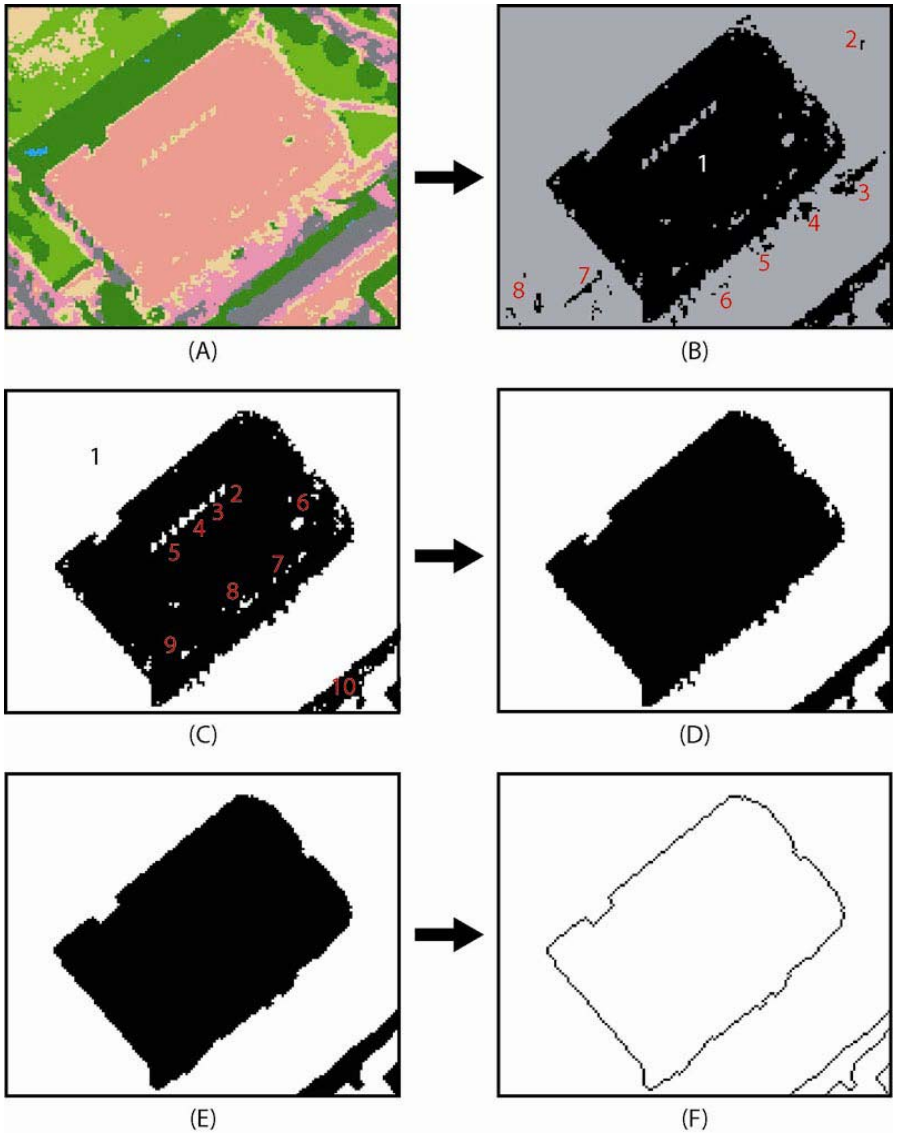

Figure 25: Post-classification processing. (A) the classification image with building pixels (pink) and pixels of non-building (green, orange, and purple); (B) building pixels are grouped into eight image objects 1 to 8; (C) small image objects 2 to 8 are removed; non-building pixels are grouped into nine background objects 1 to 10; (D) small isolated background objects 2 to 10 are removed, and only building object is left; (E) morphological dilation and erosion; and (F) tracing and vectorizing edge pixels, building edge pixels are delineated

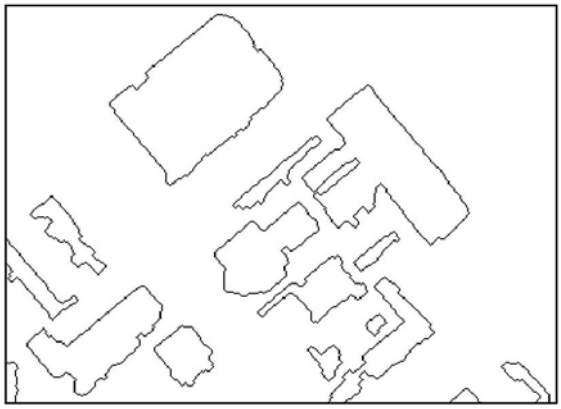

Figure 26: Building boundaries of TAMU campus

Figure 27: Boundaries of tree canopy with tree centroid points

Due to the date of DOQQs was derived in 1995, and much planimetric information lacked the latest urban objects information including reconstructed buildings, removed buildings, and built-up buildings. In addition, the result of building footprints has some problems with shadow effects and zigzag outlines by classification map and post-classification procedure. Hence, we tried to

utilize and update the planimetric data from Texas A&M University GIS office. However, it is possible to employ the latest aerial photographs for updating information while the data from GIS office was out-of-date.

Campus objects are represented as polygons, lines, and points in terms of their geometric properties and generalization level. The building, grass, and water polygon objects are shown in Figure 28. The road and side road line objects are shown in Figure 29. The tree and poles point objects are shown in Figure 30. However, it is hard to derive the pole points from image classification methods. They are identified manually from a high-resolution aerial photograph.

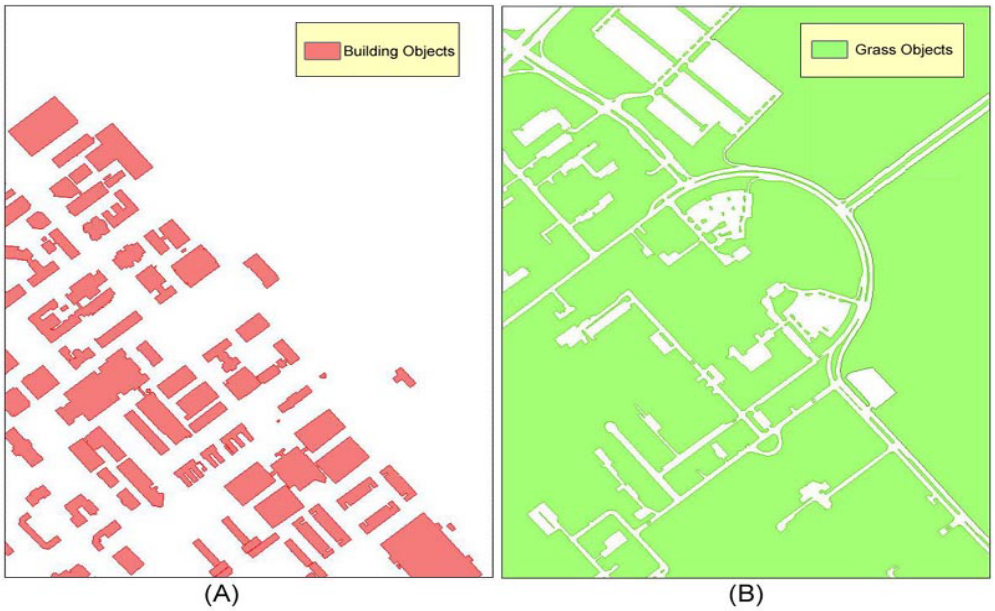

Figure 28: Polygon objects of TAMU campus. (A) building and (B) grass

Figure 29: Line objects of TAMU campus. (A) road and (B) sidewalk

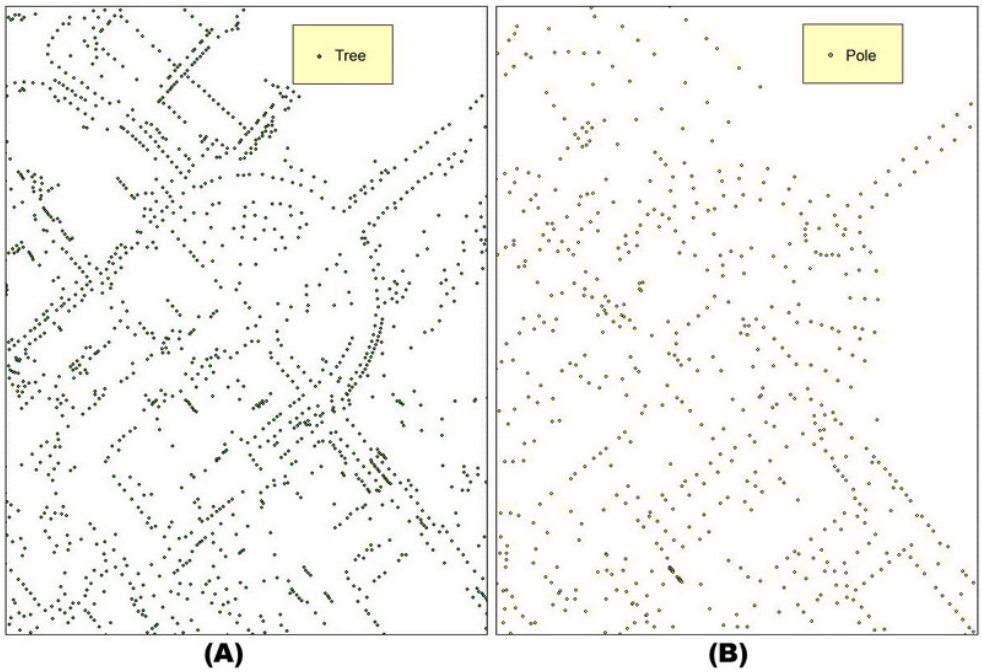

Figure 30: Point objects of TAMU campus. (A) tree and (B) pole

The combination of polygon, line, and point objects make the base updated planimetric data of campus. Figure 31 shows the result of campus planimetric information.

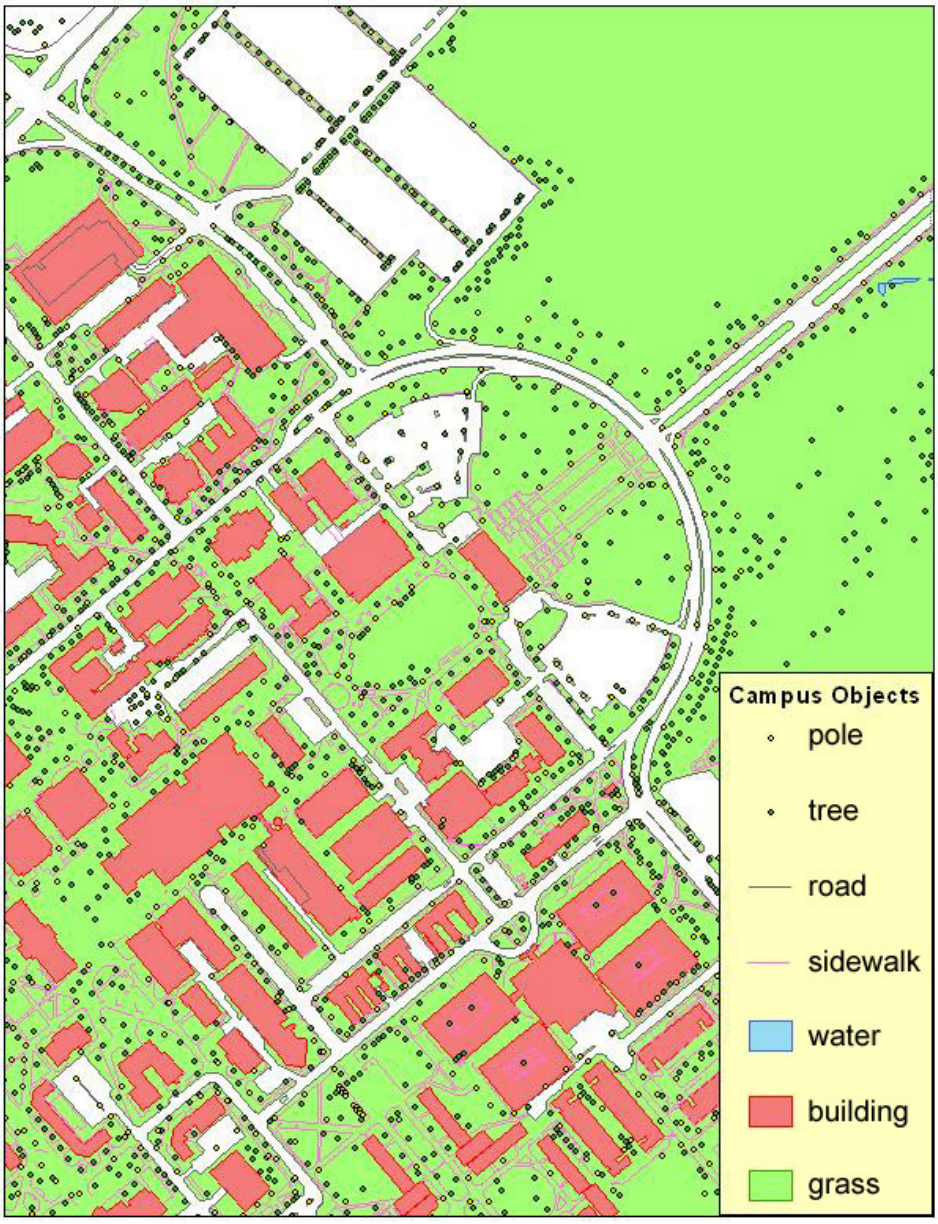

Figure 31: Campus map with planimetric information

4.4 Height Information Acquisition

Height measurements are the key information for converting 2D models into 3D ones. Four methods are used to calculate the building heights, including the relief displacement method, the shadow method, the differential parallax method, and the laser ranging method.

There are around 200 buildings in the main campus. Most of them are academic, administrative, student activities buildings, residence halls, and corps dorms. Buildings can be characterized by the number of floors, building shape, height, built-up year, or building usages. As shown in Table 6, there are about 60% buildings below 3 floors, 30% buildings with 4 floors, and 10% with more than 5 floors.

Table 6: Building patterns in main campus (Appendix A)

Number of Floors	Numbers	Percentages
1	69	36.7
2	16	8.5
3	27	14.4
4	57	30.3
Over 5	19	10.1
Total	188	100.0

Due to elevation measuring by phtogrammetry technique, it is hard to calculate the height of very low-height buildings, especial for shadow height

method, from the aerial photographs. Thus, there are three groups can be classified by number of floors for distinguishing group average heights in following similar height buildings (Figure 32):

- Group of below 3 floors: History building (HIST), Scoates hall (SCTS), and Civil engineering building (CE).
- Group of 4 floors: Architecture center (ARC), Peterson building (PETR), Butler hall (BTLR), Animal industries building (ANIN), Administration building (ADMIN), Geosciences building (HLB), and Heldenfels hall (HELD).
- Group of over 5 floors: Bright building (HRBB) and Oceanography & Meteorology building (O&M).

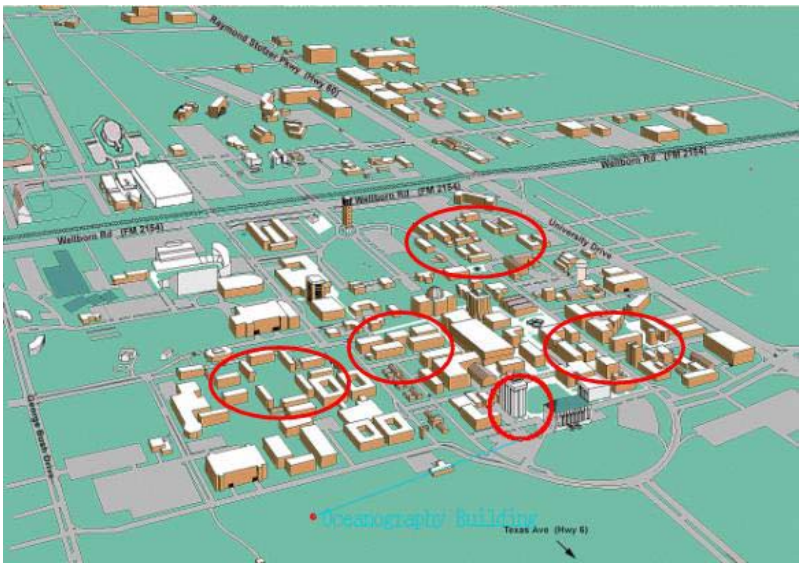

Figure 32: Distribution of selected buildings (www.tamu.edu/map)

4.4.1 Height Measurement of Photogrammetry

Two aerial photographs were scanned into a digital image file from a 9″x9″ film. They were acquired in 1987 and 1988 with different vantage points, and covered a common area of the campus (Figure 33).

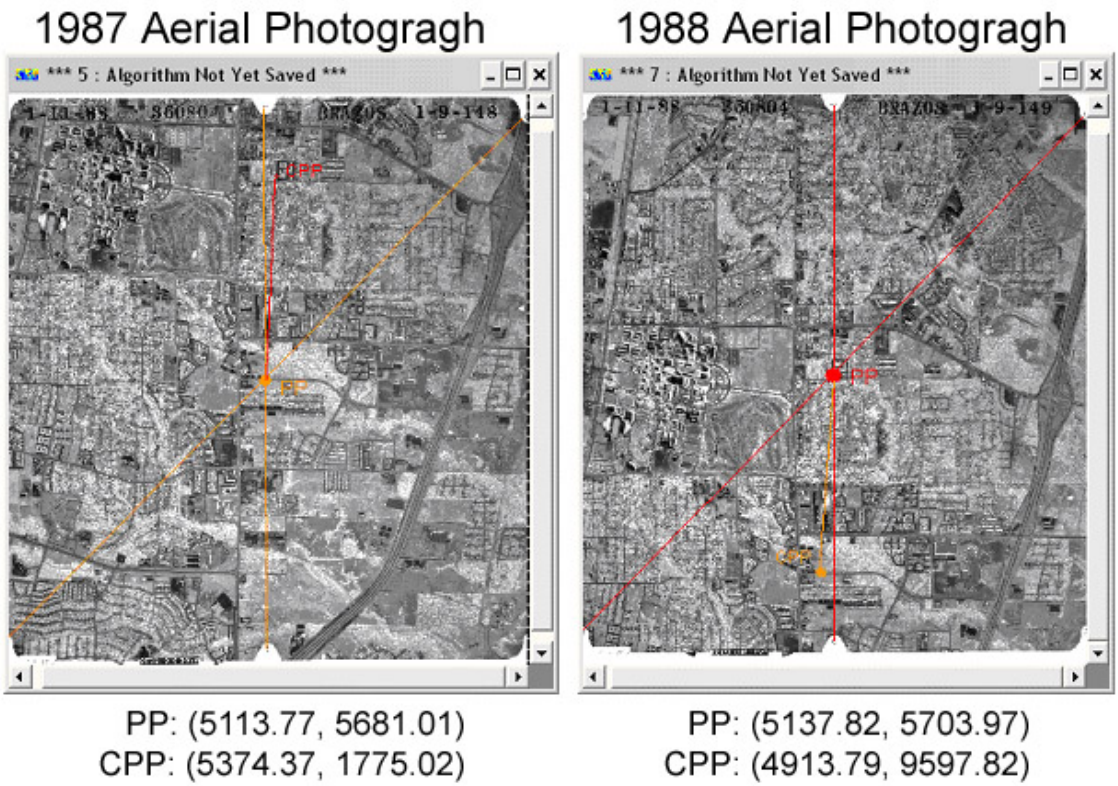

Figure 33: Two aerial photographs of 1987 and 1988

1) Relief Displacement Method: Any objects that are higher or lower than the principal point are displaced from its true planimetric (x,y) location on a vertical

aerial photograph. This displacement is referred to as relief displacement or terrain distortion. The relief displacement is outward from the principal point for objects whose elevations are above the local datum, and toward the principal point for objects whose elevation are below the local datum (Figure 34).

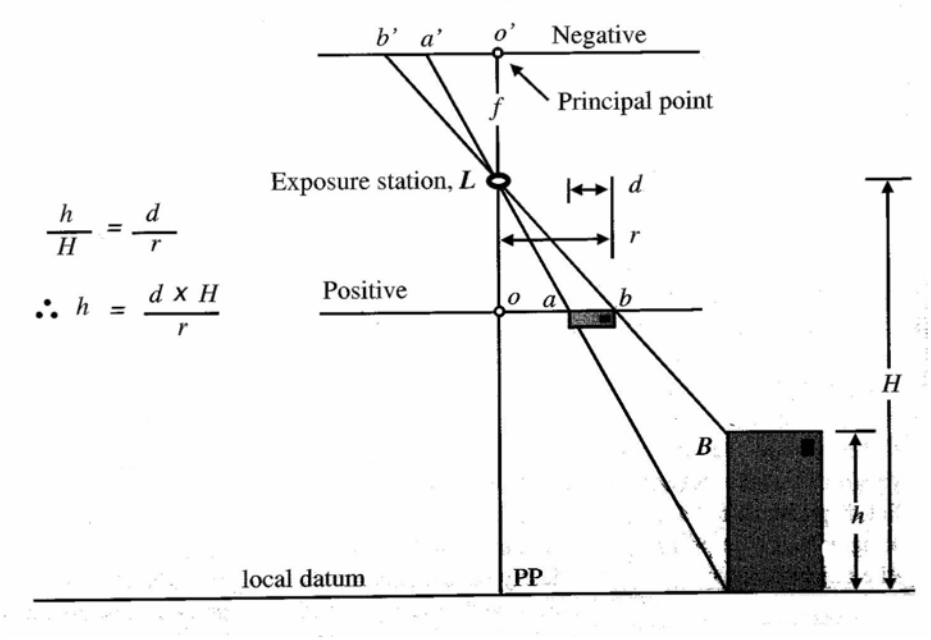

Figure 34: Relief displacement method (Jensen 2000)

Height of an object can be derived from relief displacement using the following formula:

$$h = \frac{D}{R} \times H$$

Where h is height of the object referenced to the local datum; H is the altitude above the local datum; d is object length from base to top on the image; r is radial distance from the photo nadir (principal point) to the top of the object.

For example, the elevation of the Bell Tower and the History Building can be derived using the 1987 aerial photograph.

Given:

Principal point: (5113.77, 5681.01)

Aircraft flying altitude: 3421 m

- Height of the Bell Tower

  Top : (926.66, 1573.53)

  Bottom: (975.64, 1623.37)

  D= $\sqrt{(927-976)^2+(1574-1623)^2}$ = 69.30

  R= $\sqrt{(927-5114)^2+(1574-5681)^2}$ = 5865.02

  $h=\frac{D}{R}\times H=\frac{69.3}{5865.02}\times 3421=40.42m$

- Height of the History Building

  Top : (2455.15, 1888.41)

  Bottom: (2463.39, 1902.00)

  D= $\sqrt{(2455-2463)^2+(1888-1902)^2}$ = 16.12

  R= $\sqrt{(2455-5114)^2+(1888-5681)^2}$ = 4632.18

$$h = \frac{D}{R} \times H = \frac{16.12}{4632.18} \times 3421 = 11.91m$$

The heights of remaining buildings are derived in the same procedure, and final results are shown in Table 7.

2) Shadow Method: The height of an object may be computed by measuring the length of the shadow on vertical aerial photography. Because the rays of the sun are essentially parallel throughout the area shown on vertical aerial photographs, the length of an object's shadow on a horizontal surface is proportional to its height (Figure 35).

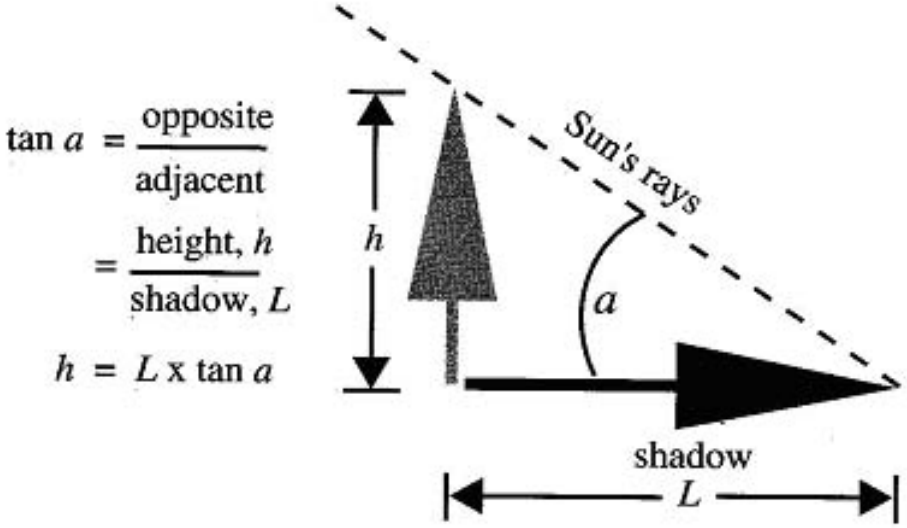

Figure 35: Shadow method (Jensen 2000)

The height of an object can be derived from the formula below:

$$h = L \times \tan \alpha$$

Where α is the sun elevation angle; L is the shadow length.

The sun elevation angle is first calculated by using the Bell Tower whose height is already known.

Given height of the Bell Tower: 40.42 m

- Shadow length of the Bell Tower:

  Show top : (1059.09, 1548.93)

  Shadow bottom: (982.64, 1616.48)

  Shadow length:

  $$\text{L}=\sqrt{(1059-983)^2+(1549-1616)^2}=101.32m$$

  $$\alpha = \arctan \frac{h}{L} = \arctan \frac{40.42}{101.32} = 21.75^\circ$$

The sun angle is calculated to be 21.75°. The sun elevation angle can be used for deriving the heights of other buildings by measuring shadow lengths.

- Height of the History Building

  Shadow top : (2496.99, 1878.94)

  Shadow bottom: (2471.54, 1894.21)

  L= $\sqrt{(2497-2472)^2+(1879-1894)^2}$ = 29.15

  $h = L \times \tan\alpha = 29.15 \times \tan 21.75 = 11.63m$

The heights of other buildings are derived using the same procedure. The final results are shown in Table 7.

3) Differential Parallax Method: The difference in the absolute stereoscopic x-parallaxes of two points imaged on a stereopair of photographs. This is usually employed in the determination of the height of objects. Almost all topographic maps are made based on the measurement of differential parallax (Figure 36). The equation for differential parallax method is as follows:

$$h = \frac{dP}{P + dP} \times H$$

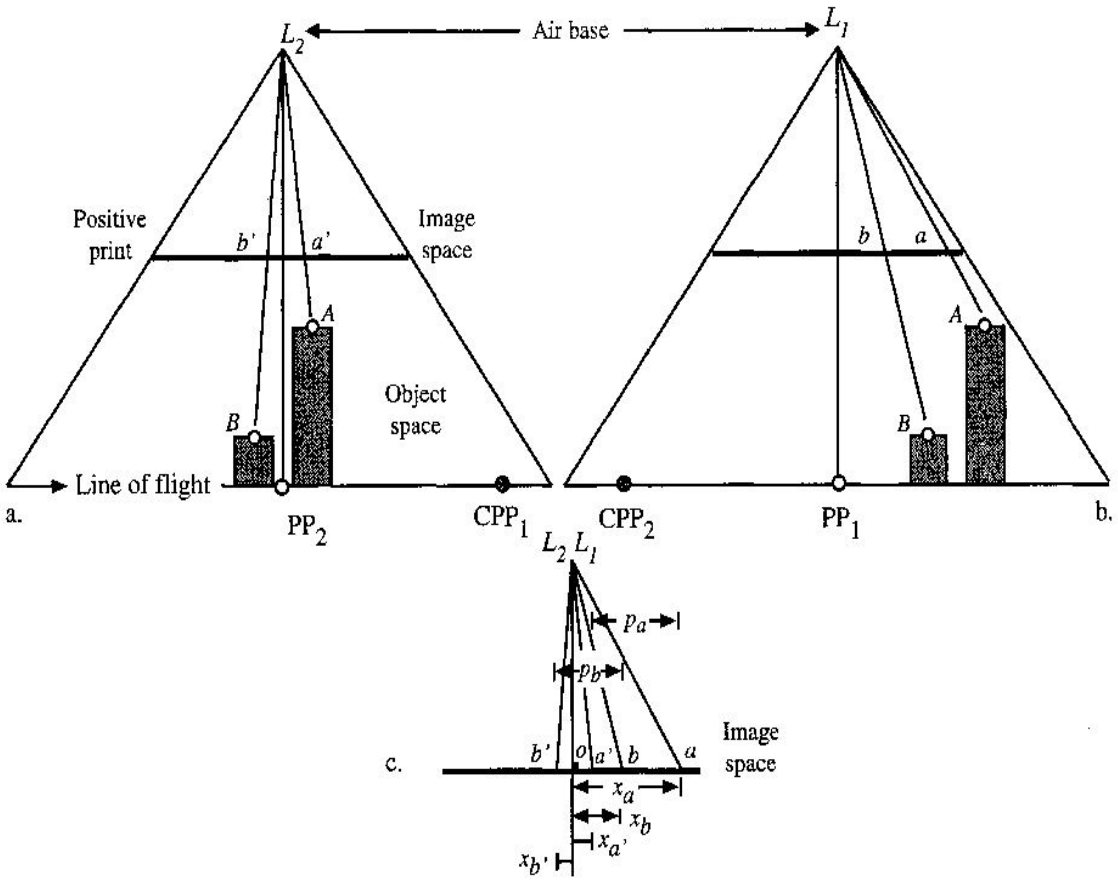

Figure 36: Differential parallax method (Jensen 2000)

Where h is the height of the object; H is the altitude of aircraft above the local datum; P is the absolute stereoscopic parallax at the base of the object, dP is the differential parallax between the base and top of the object.

The average of air base value should be calculated from image 1987 aerial photograph and 1988 aerial photograph.

$$d87 = \sqrt{(5114-5374)^2 + (5681-1775)^2} = 3914.64$$

$$d88 = \sqrt{(5138-4914)^2 + (5704-9598)^2} = 3900.44$$

Average base of the stereopair (pixels) = (3914.64 + 3900.44)/2 = 3907.54 pixels.

After the value of air base was considered, measured the differential parallax (dp) between the base and top of the object is required. The parallax of the top and the parallax of the base of the object can be measured from fiducial line.

For History building, the computation procedure is as fallows:

1998 aerial photo:

Top : (2197.27, 5926.24), Fiducial line: (2197.27, 5745.67)

Bottom: (2210.58, 5927.84), Fiducial line: (2210.58, 5745.67)

$$X_{top} = \sqrt{(2197-2197)^2 + (5926-5746)^2} = 180$$

$$X_{base} = \sqrt{(2211-2211)^2 + (5928-5746)^2} = 182$$

1987 aerial photo:

Top : (2455.15, 1888.41); Fiducial line: (2455.15, 5620.80)

Bottom: (2463.39, 1902.00); Fiducial line: (2463.39, 5621.26)

$$X'_{top} = \sqrt{(2455-2455)^2 + (1888-5621)^2} = 3733$$

$$X'_{base} = \sqrt{(2463-2463)^2 + (1902-5621)^2} = 3719$$

$$P_{top} = 180 - 3733 = -3553$$

$$P_{base} = 182 - 3719 = -3537$$

$$dP = -3553 - (-3537) = -16$$

$$h = \frac{16}{3908+16} \times 3421m = 13.95m$$

The heights of other buildings are derived by the same procedure. The final results are shown in Table 7.

4) Laser Ranging Method: The ground rangefinder provides quick and accurate distance measurement. For this research, Nikon Laser Rangefinder is used to determine height data from line-of-sight distance (hypotenuse) in meters and horizontal distance (base) in meters. It can up to 400 meters (437 yards), and is suitable for a diverse range of user applications. The height value can be calculated using the Pythagoras theorem (Figure 37), and the height of selected buildings is shown in Table 7.

$$Height = \sqrt{hypotenuse^2 - base^2}$$

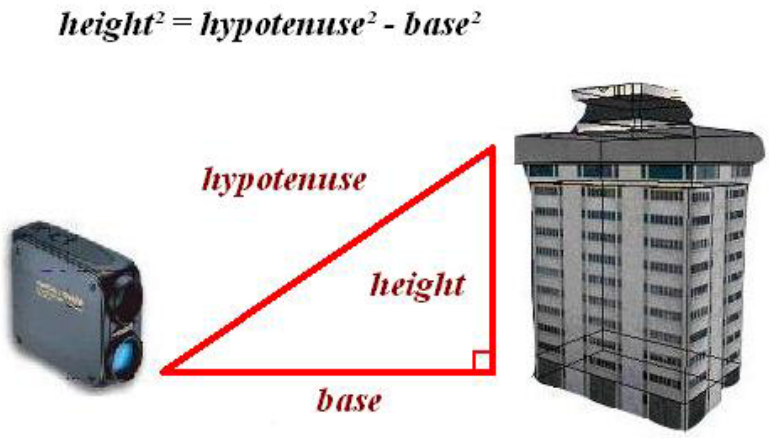

Figure 37: Laser ranging method

Table 7: Comparison of height values with different methods

Build No	Build Code	Relief Displacement	Shadow	Differential Parallax	Laser Ranging
353	HRBB	31.12	29.81	35.20	38.68
398	ARCA	12.10	X	14.51	13.71
432	ARCB	18.35	18.21	20.82	19.86
443	O&M	59.53	57.23	64.37	65.81
444	PETR	17.92	X	20.03	18.87
465	BTLR	13.87	X	16.19	15.66
470	HIST	11.91	11.63	13.95	13.67
472	ANIN	18.84	19.16	23.42	21.89
473	ADMIN	14.72	14.58	16.61	16.79
478	SCTS	11.30	12.02	14.57	13.50
492	CE	10.75	10.21	13.25	11.05
511	HLB	14.81	X	16.91	16.61
521	HELD	17.05	16.86	19.66	18.78

(Meters)

Based on the ground laser measurement, height values from differential parallax method are close to laser ranging measurement. Comparison shows that differential parallax method is more accurate than relief displacement method and shadow method. Hence, height values from differential parallax method are desired as the height standard in campus models. Table 8 shows the average height for each floor of the buildings and average height of each group.

Table 8: Average floor height of selected buildings

Building Number	Building Code	Floors	Peri-meter (ft)	Gross Area (ft^2)	Height (m)	Average Floor Height (m)
398	ARCA	3	1,174	116,619	14.51	4.84
470	HIST	3	450	39,887	13.95	4.65
478	SCTS	3	914	62,228	14.57	4.86
492	CE	3	1,068	56,537	13.25	4.42
Group 1 Average Height						4.9((16.27 ft
432	ARCB	4	494	86,447	20.82	5.21
444	PETR	4	970	84,831	20.03	5.01
465	BTLR	4	380	29,699	16.19	4.05
472	ANIN	4	854	44,856	23.42	5.47
473	ADMN	4	650	69,898	16.61	4.15
511	HLB	4	1,120	40,476	16.91	4.23
521	HELD	4	890	104,949	19.66	4.91
Group 2 Average Height						4.7((15.48 ft
353	HRBB	9	630	148,837	35.20	3.91
443	O&M	15	676	180,316	64.37	4.29
Group 3 Average Height						4.1((13.45 ft

For entire buildings whose heights cannot be derived from aerial photos, their heights are determined by multiplying the number of floors and the group average height (Appendix A).

4.5 Object Attributes Acquisition

Attribute data are very important for querying about appropriate information including building name, number of floors, number of rooms, usage, building location, and street name, and directions. For the campus model, attribute data are obtained from Facilities coordination office and GIS office in Texas A&M University.

4.6 Object Textures Acquisition

Texturing is a technique to map an image onto a geometrical shape to provide special effects or a level of realism that is not geometrically practical. For campus, textures are classified in general groups with similar surfaces or colors such as garages and dorms, and unique groups with individual and complex surfaces. Textures also can be derived from digital camera or video camcorder and be processed with image processing software. In addition, a texture palette file is an ASCII file that specifies the contents of the texture palette. It is useful for saving and loading related sets of texture patterns in the research. The texturing procedure is shown in Figure 38.

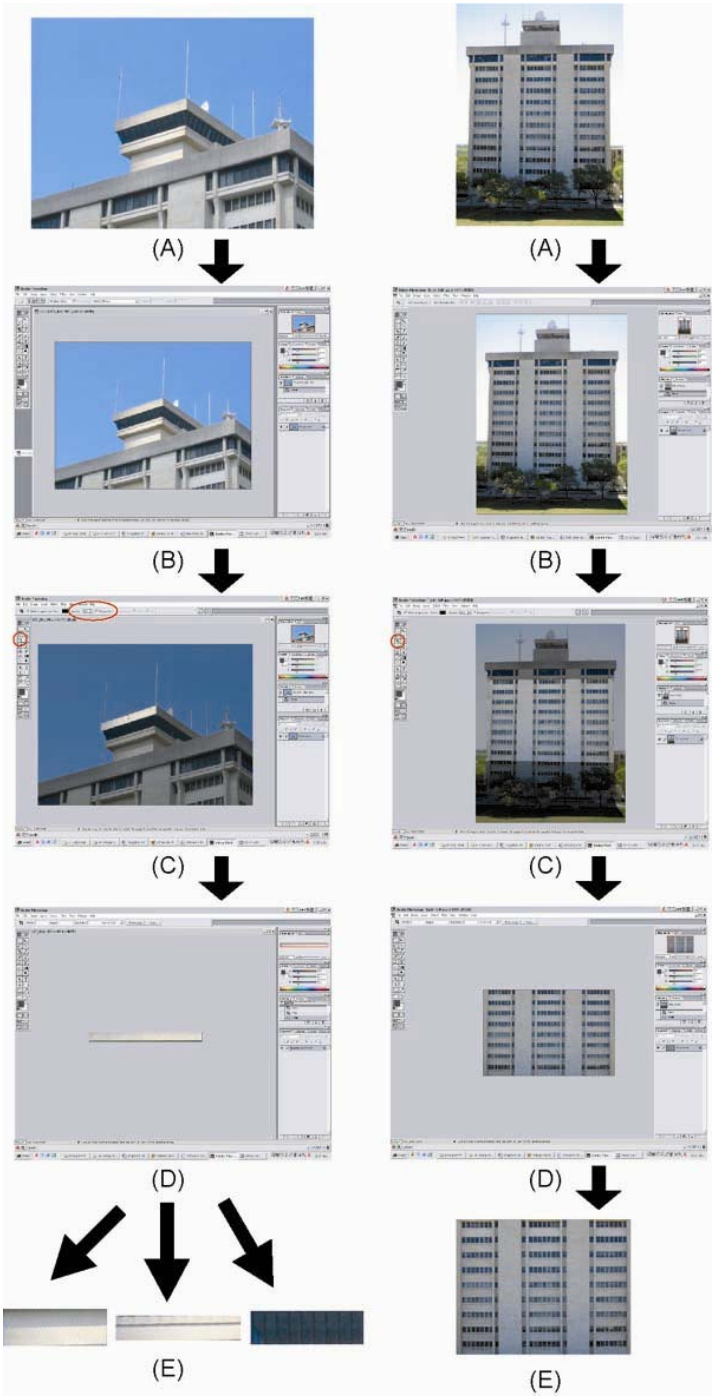

Figure 38: Texturing. (A) take pictures of building surface by digital camera; (B) loading into image processing software; (C) facades selecting; (D) cropping perspective image into rectangle shape; and (E) making pieces of images from selected surface

4.7 3D Campus Model Construction Procedure

Geometric models and texture mapping are accomplished by using Multigen-Paradigm Model Builder 3D software. 1) The building shapefiles are converted into a CAD drawing interchange format (DXF). Then load the data and pick up an object from campus footprints. 2) Raise the walls from bottom using the height data from previous acquisition. The geometric model construction procedure is shown in Figure 39.

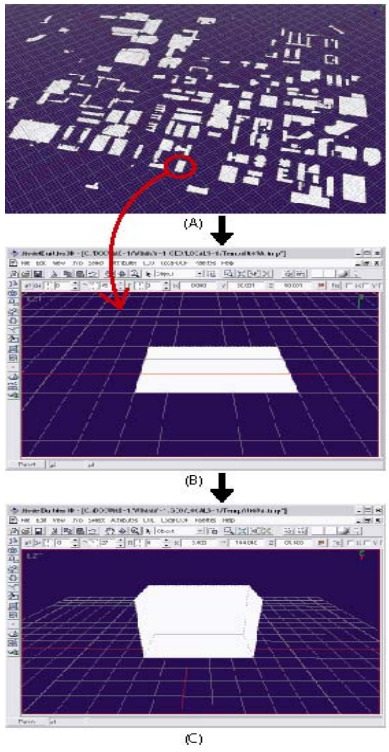

Figure 39: Geometry procedure. (A) select a building object from campus converted footprints from ArcGIS shapefiles; (B) paste the object on the bottom; and (C) rise up the walls according to height data which was derived form previous methods

3) Put more detail geometric shape such as roof and facades with different level of LOD layer. Then mapping selected image piece from texture palette to desired solid face. The texture mapping procedure is shown in Figure 40 and entire urban objects with textures were shown in Appendix B.

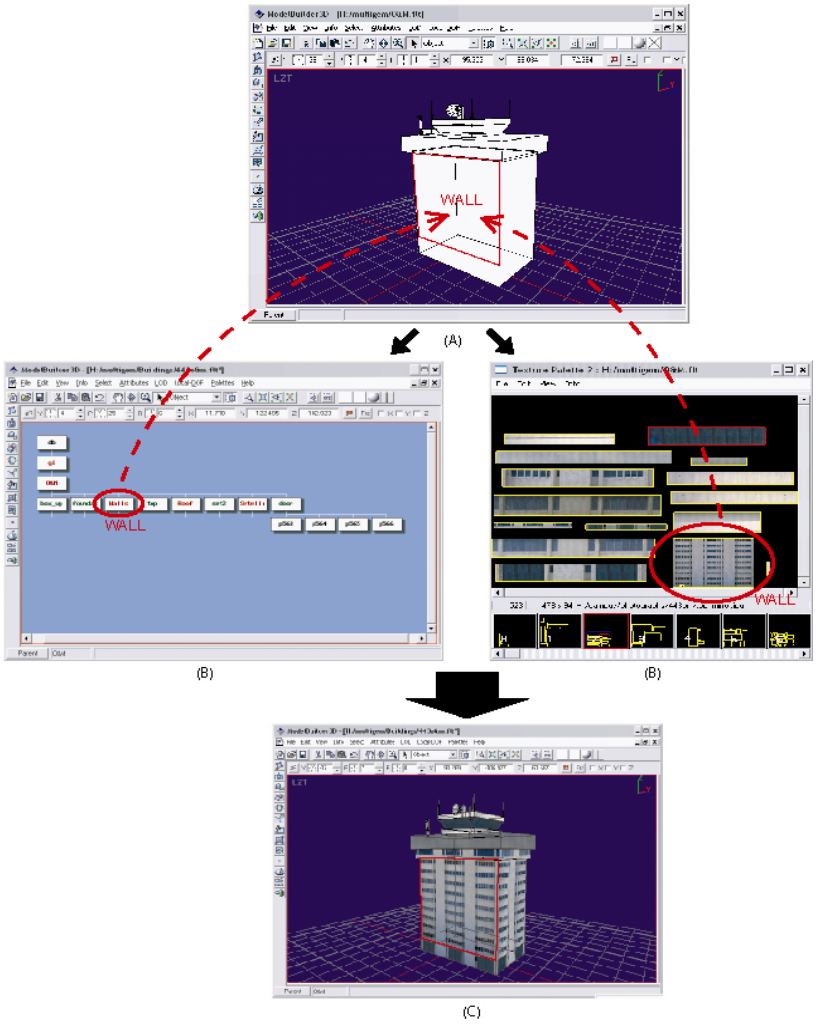

Figure 40: Texture mapping procedure. (A) modify more detail for building object; (B) structuring a database hierarchy of selected objects, and fitting selected image piece from texture palette to desired solid face; and (C) build a 3D building model

4) Load all updated 2D shapefiles such as pole point, tree point, pave line, side line, water polygon, building polygon, and grass polygon from ArcGIS into Site Builder 3D model (MultiGen-Paradigm 2003), and link them into 3D object models constructed by Model Builder 3D (Figure 41).

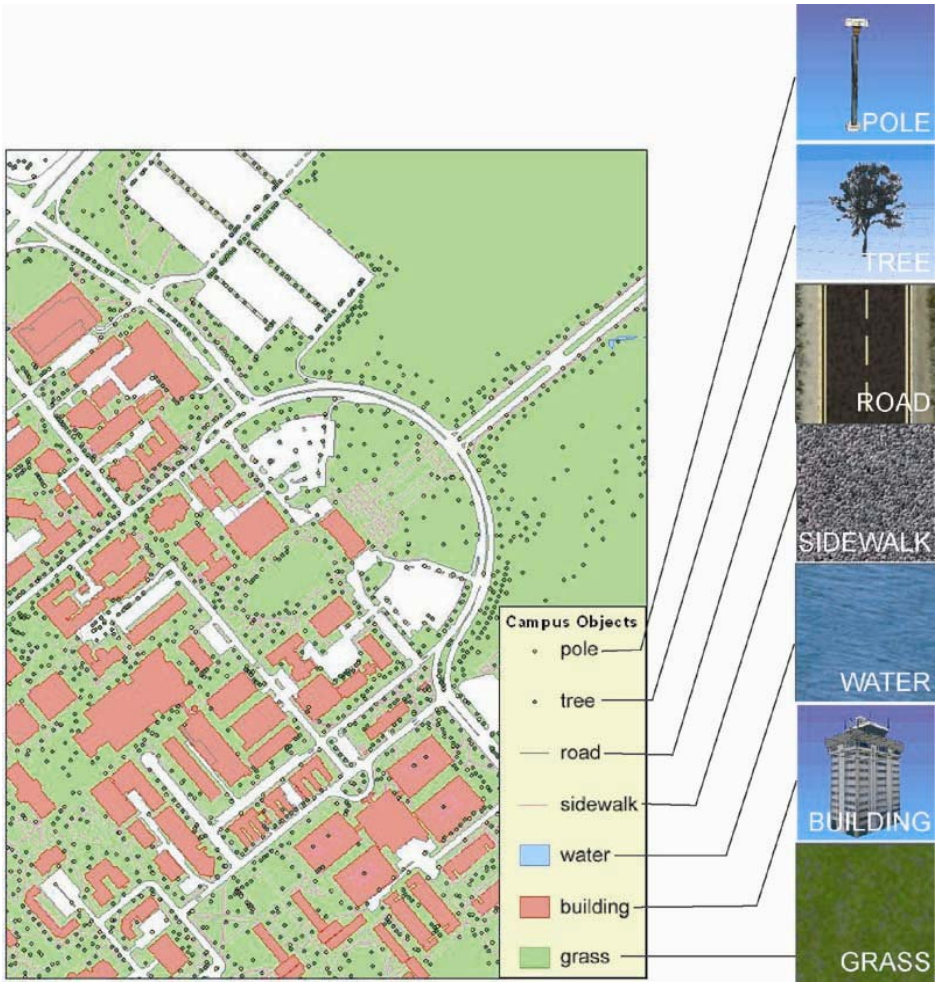

Figure 41: Data linkage. Linking 2D objects such as pole point, tree point, pave road line, side road line, water polygon, building polygon, and grass polygon with 3D object models built by Model Builder 3D software

5) The interactive visualization was created by lunching 3D viewer of 3DS: Visual clips of Texas A&M University were shown in Figure 42 and Figure 43.

Figure 42: 3D scene of TAMU campus

Figure 43: Bird view of TAMU campus

6) The route of fly-through or walk-through can be desired with LOD concept and environment control for creating an animation (Figure 44). The animation can be used as a visual campus tour.

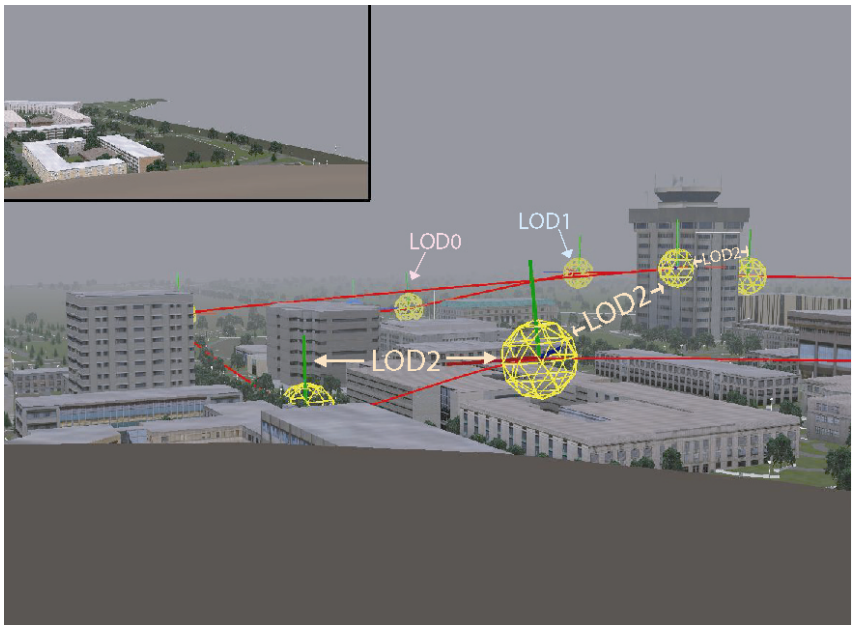

Figure 44: A LOD path setting with fog for animation editing

4.8 Campus Navigation

A 3D model of TAMU campus shows the details of the buildings and their surroundings to support object recognition and query about appropriate information like building name, street name, routes and directions (Figure 45). One application is to help new students or tourists to get familiar with Texas A&M campus. It also can be used for campus planning, emergency management, and law enforcement operation.

Figure 45: Campus information query and navigation

CHAPTER V

3D URBAN MODEL FOR DOWNTOWN HOUSTON

Houston, the fourth largest city in the United States, is located at the southeastern part of Texas (Figure 46). It has a large number of modern buildings that define the city's skyline. Downtown Houston represents a higher concentration of skyscrapers, making it an ideal area for the 3D representations.

Figure 46: Location of Houston (CNN.com)

LiDAR data is used to update and extract planimetric and vertical information for urban objects. The building footprints are updated and modified with LiDAR data. Combining building footprints and LiDAR data, the

height information of urban objects are determined. By applying building texture information acquired by digital camera and video camera, a 3D urban model with photorealism quality has been constructed. With 3D urban information, the solar radiation pattern in downtown Houston is simulated for different seasons.

5.1 Data Collection

The planimetric data from City of Houston GIS (COHGIS) provides an abundant and specific data of urban features with outlines and attributes. COHGIS developed and maintains GIS data layers regarding building footprints, roads, and associated attributes. However, these data were produced in 1985 and the information was out-of-date and lacks the latest developments and height information. Thus, LiDAR data are helpful for updating the data for downtown Houston urban model.

LiDAR data were obtained from the Harris County Flood Control District (HCFCD), and DOQQs were obtained from the Houston-Galveston Area Council (HGAC). They are used to extract planimetric information by boundary detection and tracing. Height information about buildings, highways, or trees is extracted by LiDAR data. Texture data are obtained by digital video camera and digital camcorder, and processed by Adobe Photoshop 6.0 image program.

LiDAR data in this research is a 15 feet ground resolution with State Plane coordinate system. The data is in ASCII format and arranged in 3 columns: latitude, longitude, and elevation in feet. DOQQs are 1 foot resolution digital images that combine the geometric qualities of a map with the detail of an aerial photograph. Hardwares used in this research are Olympus C750 ultra zoom digital camera and Sony DCR-TRV38 MiniDVdigital camcorder. Software used in this research are Adobe Photoshop 6.0, Model Builder 3D/Site Builder 3D, and ArcGIS version 8.3 (ESRI).

The images of LiDAR and DOQQs are shown in Figure 47, and their characteristics are list in Table 9.

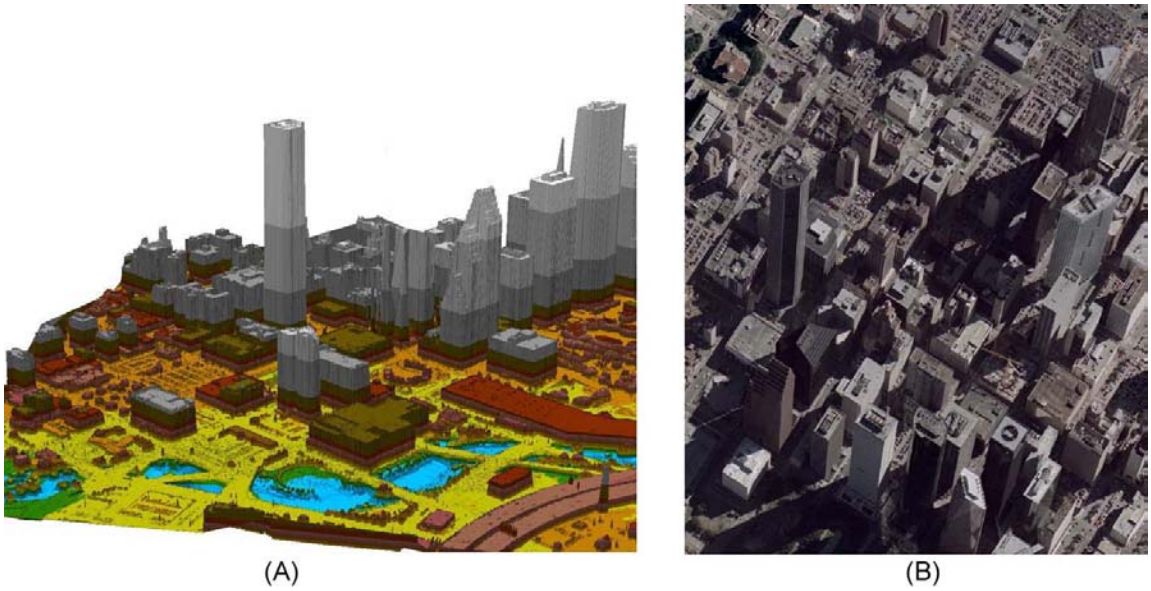

Figure 47: Images of downtown Houston. (A) LiDAR data; (B) DOQQs image

Table 9: Characteristics of LiDAR and DOQQs data

	LiDAR	DOQQs
Format:	ASCII	MrSID
Projection:	State Plane	State Plane
Units (x,y):	Feet	Feet
Nominal scale:	N/A	1:12,000
Area:	3.75- x 3.75-minute quad (one quarter-quad)	3.75- x 3.75-minute quad (one quarter-quad)
Resolution:	15 feet ground resolution	1 foot ground resolution
Color:	N/A	Nature color
Data:	November, 2001	January, 2002
Available:	HCFCD	HGAC

5.2 Overview of LiDAR Technique

Some problems remain for extracting feature planimetric information with aerial images. First, in the region with dense high-rise buildings, building shadows and occultation limit the use of aerial photos in extraction of planimetric geometry of buildings (Figure 47B). It is difficult to obtain a complete representation of building boundaries and shapes, using supervised classification, or even using manual delineation. Second, vertical nadir view of aerial photos often lacks information about building facades due to steep observation angles (Figure 47B). Third, extraction of height information with relief displacement and shadow method from single aerial photo is time

consuming. Differential parallax method with stereo aerial photos is limited by building shadows and occultation and also very costly for a large urban area.

The use of LiDAR technology along with digital imagery for urban modeling and visualization is an efficient method to extract the planimetric and height information. LiDAR is a relatively new technology that has proven to be effective in extracting high-resolution information both quickly and efficiently (Serr 2000). With LiDAR, data can be collected under a variety of adverse environmental conditions, including low sun angles and darkness. (Brenner and Haala 1999; Veneziano et al. 2003). LiDAR data can be used to detect buildings and their approximate outlines and extract planar roof faces for roof structures (Rottensteiner and Briese 2002).

Priestnall et al. (2000) examines methods for extracting and generalize feature edges from the unsupervised classification of the LiDAR Digital Surface Model (DSM) with a simple filtering procedure. Haithcoat et al. (2001) use an automated approach to generate a Digital Surface Model (DSM) from LiDAR, and extracts objects higher than the ground surface. Based on general knowledge of the characteristics of man-made objects, buildings are separated from other features. Building footprints can be derived from simplified orthogonal algorithm.

Palmer and Shan (2002) tried to use an automated process to model and to visualize most urban buildings from grid LiDAR data. They combine the

manual and automated procedures for resolving shortcomings of each and choose the best use of resolution potentials for both LiDAR and orthoimaging.

Zhou et al. (2004) developed a new method to interpolate LiDAR raw data into a grid DSM with discontinuous buildings. LiDAR points are located in the polygon of roof surfaces, and then the planar equation is employed for generating DSM grid.

LiDAR (Light Detection and Ranging) is a rapid technique for acquiring surface height information. It offers surface elevation data for a large range area with a high accuracy and spatial resolution (Priestnall et al. 2000). In this research, a digital object is obtained by removing a bare earth DEM (Digital Elevation Model) grid from the raw LiDAR DSM grid. Then, the digital object grid is used for building footprints detection, segmentation processing, and height data extraction. Figure 48 shows the 3D rendering of the LiDAR data in downtown Houston.

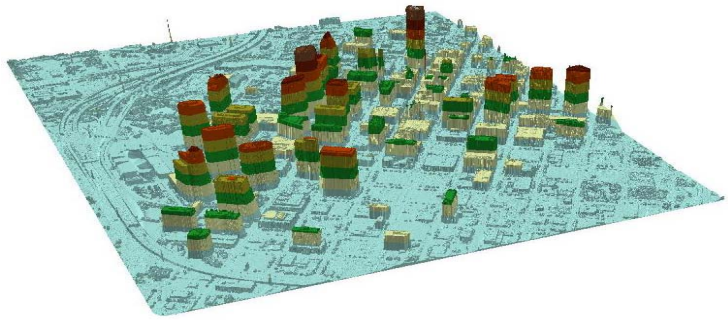

Figure 48: 3D rendering of LiDAR data

5.3 Planimetric Information Acquisition

2D planimetric data is necessary for constructing an urban model. Conventionally, field surveying and photogrammetric mapping are the most widely used methods to get surface terrain information and urban features. . In the construction of TAMU campus model, the planimetric footprints of urban objects are updated by the classification and segmentation of digital aerial photos. For the downtown Houston model, similar procedure of segmentation is applied to LiDAR range data for detecting building footprints, tree canopy, and highways.

Before segmentation procedure, there are two methods to distinguish building footprints and tree canopies. One is watershed analysis, the other is slicing method. In watershed analysis, flipped elevation LiDAR grid is necessary to obtain depth of sinks. The outlines of urban objects are delineated after filling sinks by calculating the depth of sinks. From the characteristics of man-made features, building shapes are distinguished from irregular tree canopies. In slicing method, slicing LiDAR grid into many levels of height values is used to obtain the specific range of height value and accuracy shape in each building polygon (Figure 49).

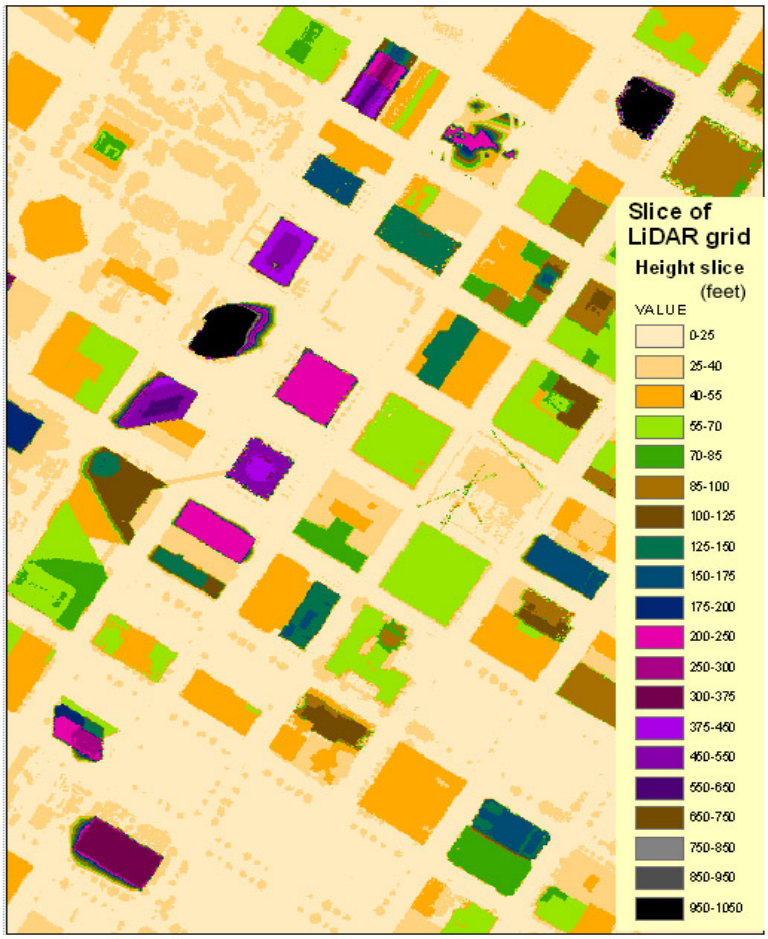

Figure 49: Sliced grid of downtown Houston

In segmentation procedure, the LiDAR grid is recoded as a binary image to represent building and non-building pixels using thresholding method. From the level of each slice and shapes of tree canopies from watershed analysis, the maximum height value of tree canopies is determined with 40 feet. We employ this value to recode building pixels (height value over 40 feet) as 1, and non-building pixels as 0 (Figure 50B).

Building pixels are grouped into black objects with a unique label. Some small and irregular image objects are not true building features. They are removed by merging them into non-building region (Figure 50C).

After removal of remaining and small isolated image objects, only large building and non-building background are left. Morphology and line tracing are employed for vectorization process to extract the final building boundaries (Figure 50D). The same procedures are employed for extracting the boundary of tree, river, and highway (Figure 51).

Due to the existent planimetric data from COHGIS is out-of-date and lacks the latest developments, LiDAR data are required for updating and modifying the data for downtown Houston urban model. Figure 52 shows the different building footprints between COHGIS data and LiDAR data. Removed or new buildings can be easily identified by comparing LiDAR and COHGIS building footprints.

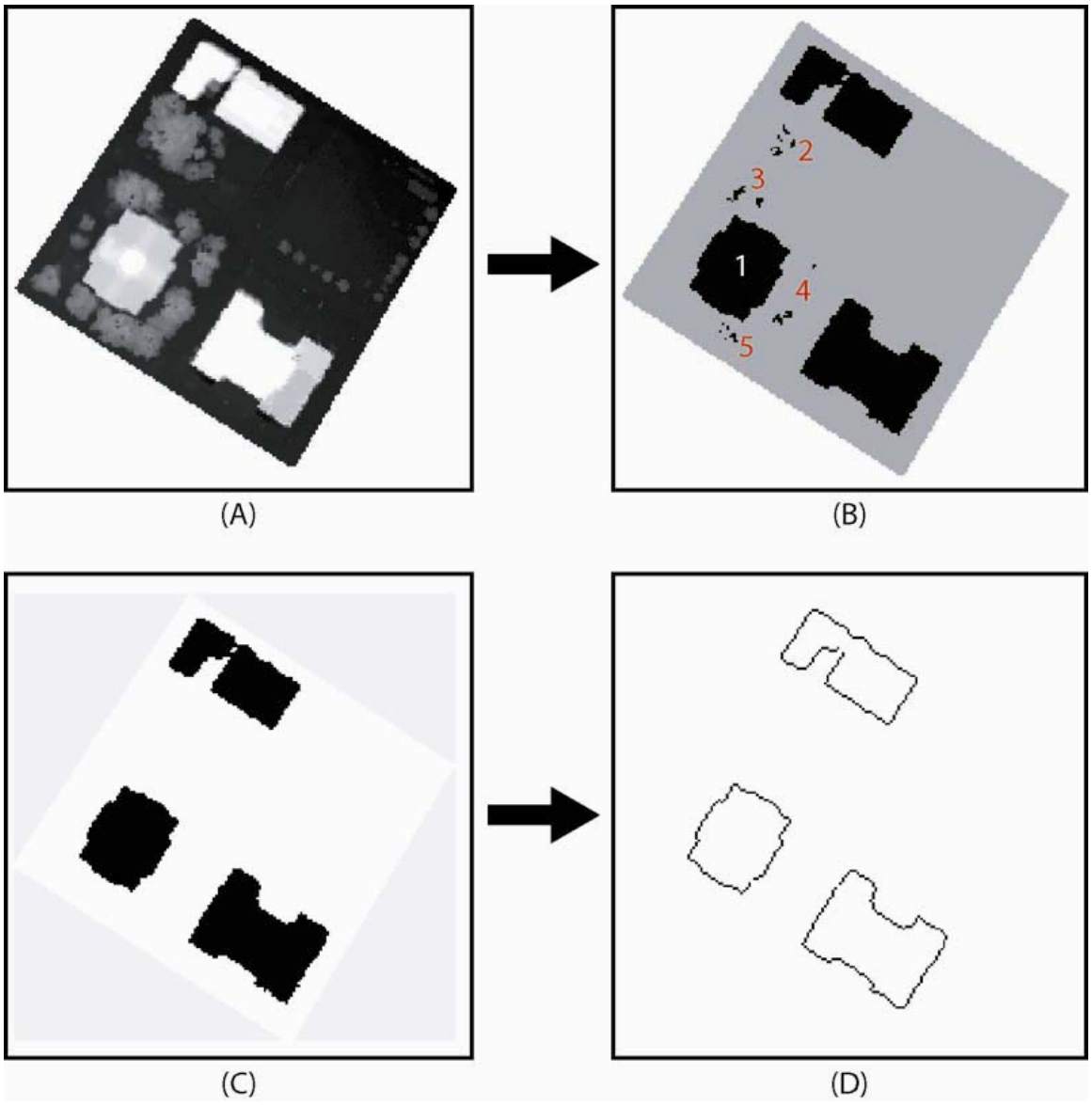

Figure 50: Segmentation processing. (A) segmented image with building pixels (height value over 40 feet) and pixels of non-building (height below 40 feet); (B) building pixels are grouped into four image objects 1 to 5; (C) small image objects 2 to 5 are removed; and only building and non-building background are left; (D) after morphology, tracing, and vectorizing edge pixels, building edge pixels are delineated

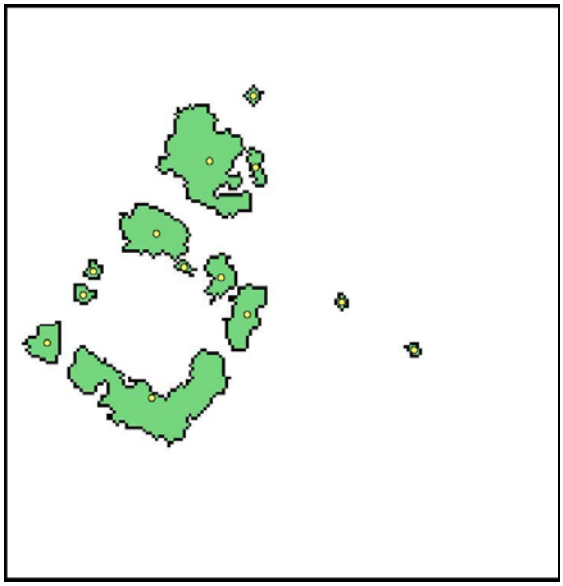

Figure 51: Boundaries of tree canopy and tree points

Due to the dense points of LiDAR data, it is hard to derive the road, sidewalk, stop sign, light pole and traffic signal information. The efficient way to obtain and update these data is identified manually from a high-resolution aerial photograph overlay with LiDAR grid. Figure 53 shows different shapes of highway and roads between GOHGIS data and DOQQ image.

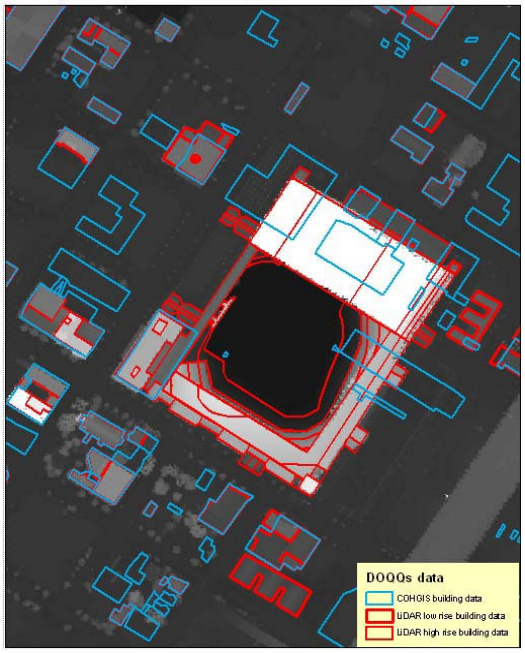

Figure 52: Building footprints. Blue edges are shown from COHGIS,

and red outlines are derived from LiDAR

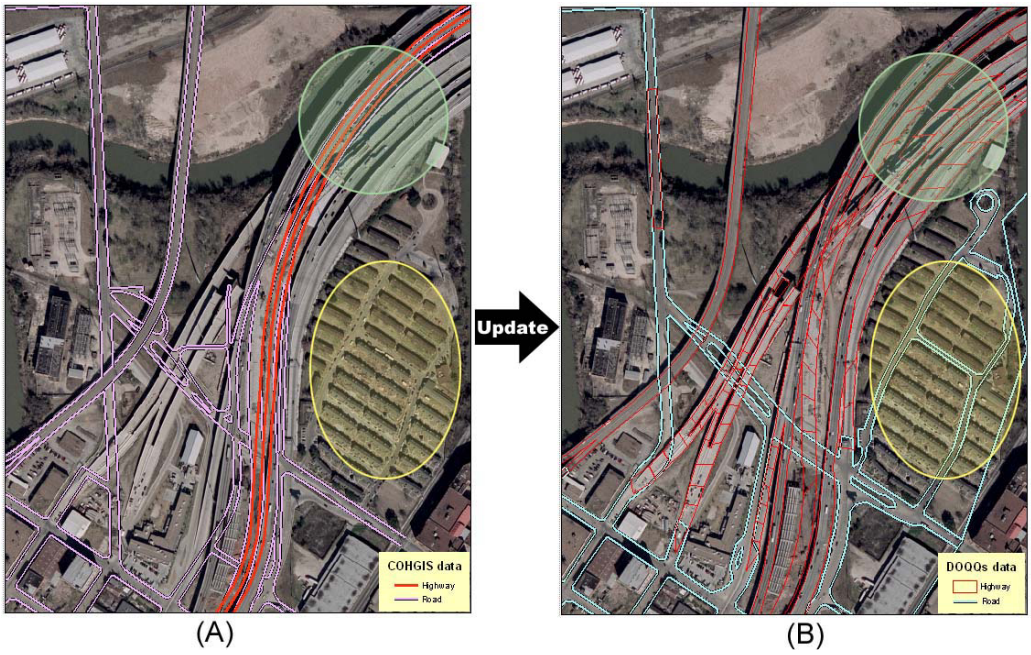

Figure 53: Highway and road outlines. (A) COHGIS data (B) updated outlines on DOQQs image

Urban objects are represented as polygons, lines, and points in terms of their geometric properties and generalization level. The final result of building, water, and highway polygon objects are shown in Figure 54. The roads and sidewalk line objects are shown in Figure 55. The tree, light pole, and traffic signal point objects are shown in Figure 56 (Light pole, traffic signal, stop sign point objects are delineated manually using DOQQs image and LiDAR).

Figure 54: Polygon objects. Buildings, highways, and water

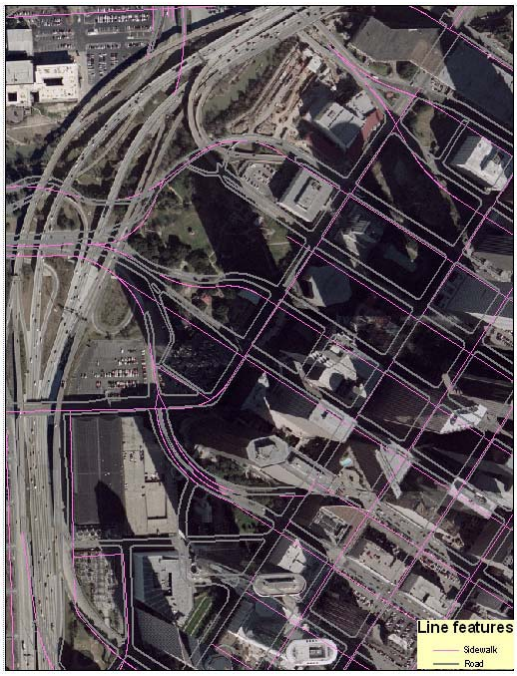

Figure 55: Line objects. Sidewalks and roads

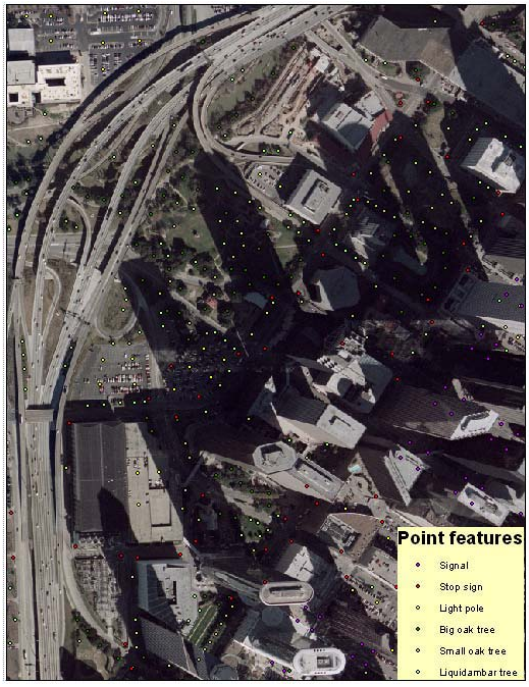

Figure 56: Point objects. Traffic signals, stop signs, light poles, and three species of trees

The combination of polygon, line, and point objects make abundant data of updated planimetric data. The result of urban planimetric information of downtown Houston is shown in Figure 57.

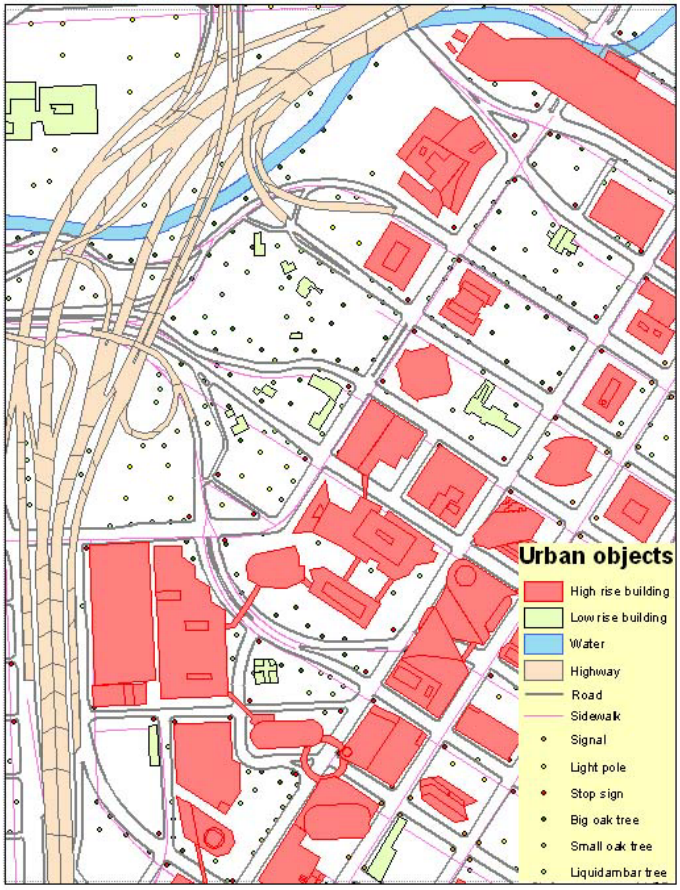

Figure 57: Map of downtown Houston with planimetric data

5.4 Height Information Acquisition

The shape and the height of building objects are quantified by a C++ program. The shape indicators include area and perimeter, and the height of

building objects are characterized by maximum height, minimum height, mean height, and median height. Median height values are used as the height standard for each building. Table 10 lists the height information in the median height column, and Appendix C list height values of entire buildings.

Table 10: Building height values derived from LiDAR

BLDG NO	Area	Peri-meter (ft)	BLDG Name	AD NO	Street Name	Max Height (ft)	Min Height (ft)	Mean Height (ft)	Median Height (ft)
11	6693.63	369.74	Harris County Vehicle Maintenance	426	Austin	93.38	49.97	63.89	63.39
22	3408.88	240.95		1100	Louisiana	78.81	51.06	73.04	72.66
23	131310.5	1576.3	Palais Royal	917	Main	146.14	48.56	117.84	134.62
24	23362.00	600.50				742.64	41.14	271.57	107.42
30	2887.88	221.47	Americana Building	811	Dallas	84.19	47.22	65.07	70.02
45	29188.00	729.32	4 Houston Center	1300	McKinney	160.58	54.77	138.97	139.75
47	72205.25	1082.8	Garage	1400	Louisiana	192.53	47.10	165.70	173.10
48	32384.75	870.68				91.83	48.09	52.72	49.21
49	5581.50	386.10	Garage	1600	Smith	69.07	49.17	66.96	68.38
54	5098.38	477.27	Travis Tower	1300	Main	76.91	47.89	51.53	49.06
59	63700.88	1009.6	Crowne Plaza Cullen Center	1700	Smith	147.18	45.06	127.53	121.66
60	3055.75	219.79	Exxon Garage	1616	Milam	86.06	47.46	71.77	77.28
74	2364.50	205.95	Kellogg, Brown & Root Tower Garage	701	Jefferson	69.71	50.14	63.88	64.36
90	9628.00	406.04	First Church Of Christ Scientist	1720	Main	65.52	46.29	61.12	62.86

In addition, there are some different height values of roof which stored in a building polygon. If the height value were calculated as one polygon, sometimes it has an incorrect height value for describing irregular roof or complex buildings. Thus, sliced LiDAR data is used to acquire more accurate height values for each divided individual building polygon. Figure 58 shows the incorrect height value from a building polygon and correct height values in each sliced polygons.

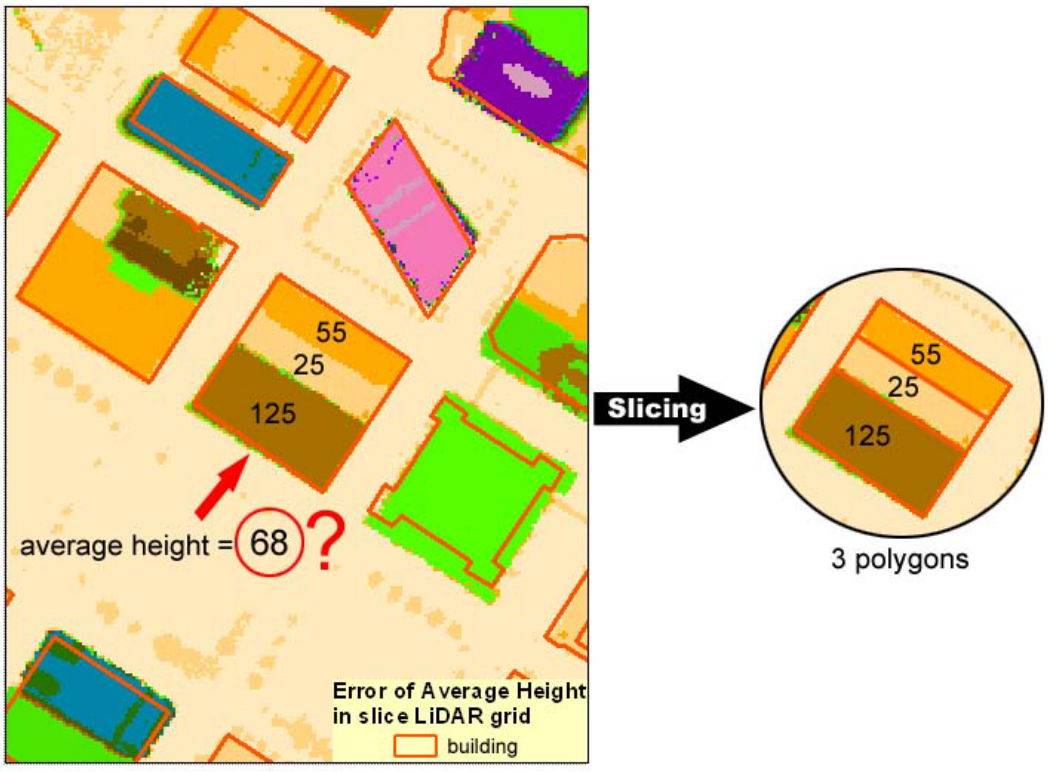

Figure 58: A sliced building polygon into three individual polygons

5.5 Object Attributes Acquisition

Attribute data is the element for querying about appropriate information with building name, number of floors, usage, location, street name, or orientation, etc. For the urban model, attribute data is obtained from City of Houston Planning and Development Department. Figure 59 shows an example of attributes information from COHGIS. It includes owner, address, built year, number of floors, and zip code, etc.

FID	OWNER	ADDRNO	STNAME	YRBUILT	STORY	MAIL1	MCITY_ST	MZIP	MZIP4	SUBD	USEG
0	OCCIDENTAL INVESTMENT CO	02409	AUSTIN	1968	1	2402 AU	HOUSTON	77004	1008	HOLMAN OUTLOT 7	5
1	REDWINE ROBERT L	00000	AUSTIN		1	2323 RO	HOUSTON	77005	2605	HOLMAN OUTLOT 7	9
2	REDWINE ROBERT L	00000	MC ILHENNY		1	2323 RO	HOUSTON	77005	2605	HOLMAN OUTLOT 7	9
3	REDWINE ROBERT L	00000	MC ILHENNY		1	2323 RO	HOUSTON	77005	2605	HOLMAN OUTLOT 7	9
4	MINISTRY JESUS CHRIST LIFE	02301	CAROLINE	1961	2	CENTER	HOUSTON	77004	1013	HOLMAN OUTLOT 8	4
5	FORTIER SO SAM	02307	CAROLINE	1958	1	5407 AU	SPRING TX	77379	0000	HOLMAN OUTLOT 8	3
6	ROESCH ROLAND E	02309	CAROLINE		1	7550 KIR	HOUSTON	77030	4376	HOLMAN OUTLOT 8	9
7	ROESCH ROLAND E	02311	CAROLINE		0	4535 HO	BELLAIRE T	77401	5806	HOLMAN OUTLOT 8	9
8	WASHINGTON DOROTHY M	00000	MC ILHENNY		1	2323 CA	HOUSTON	77004	1033	HOLMAN OUTLOT 8	3
9	F W SERVICES INC	02310	AUSTIN	1964	1	PO BOX	HOUSTON	77252	2146	HOLMAN OUTLOT 8	5
10	F W SERVICES INC	00000	AUSTIN		1	PO BOX	HOUSTON	77252	2146	HOLMAN OUTLOT 8	9

Figure 59: Attributes information from COHGIS

5.6 Object Textures Acquisition

Repeated textures can be found in the urban area, especial for high-rise building region. In terms of the characteristics of skyscrapers and buildings in downtown Houston, four types of building surfaces can be classified: glass texture, normal texture, traditional texture, and garage texture (Figure 60).

The image chips for these textures are created from digital camera or camcorder and developed by image processing software. The chips are mapped and manipulated onto a geometrical shape to provide special effects or a level of realism for the general buildings. They provide a highly economical alternative and less time consuming on texturing for similar texture of buildings. For mapping unique or complicated buildings, texture chips have to be acquired separately. The entire urban objects with textures are shown in Appendix D.

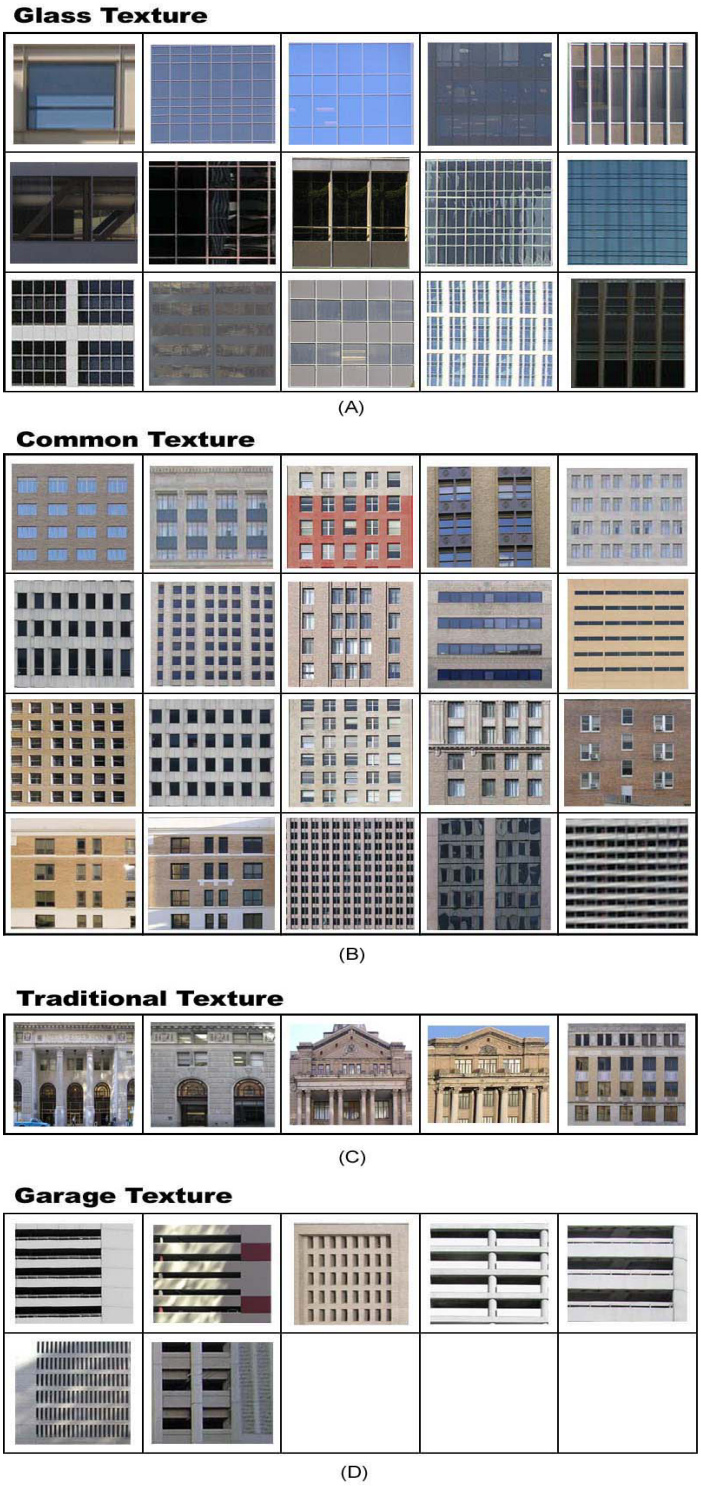

Figure 60: Texture catalog. (A) glass texture; (B) common texture;

(C) traditional texture; (D) garage texture.

5.7 3D Urban Model Construction Procedure

Similar to the procedure of the TAMU campus model, load all updated 2D objects including light pole point, traffic signal point, stop sign point, tree point, road line, sidewalk line, water polygon, building polygon, and highway polygon from ArcGIS into Site Builder 3D model, and link them into 3D objects constructed by Model Builder 3D (Figure 61).

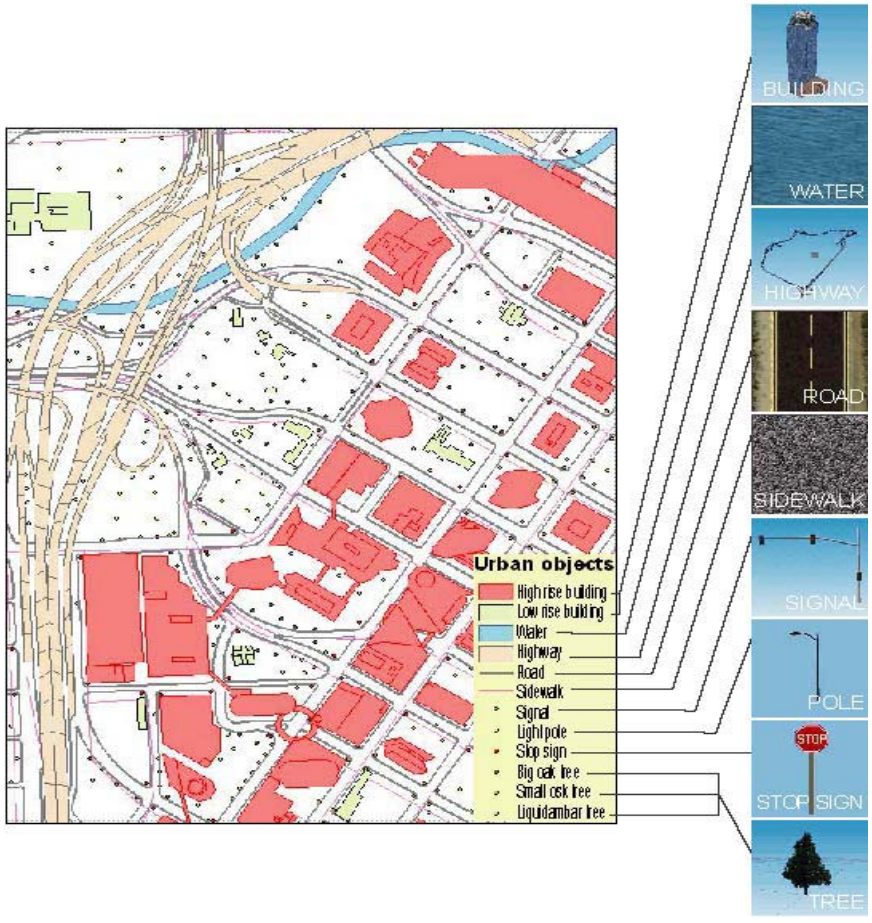

Figure 61: Elements of urban objects. Linking 2D objects such as point, line, and polygon with 3D object models built by Multigen-Paradigm Model Builder 3D

Finally, the interactive visualization was created by lunching 3D viewer of Multigen-Paradigm Site Builder 3D. Examples are shown in Figure 62 and Figure 63.

Figure 62: Bird view of downtown Houston

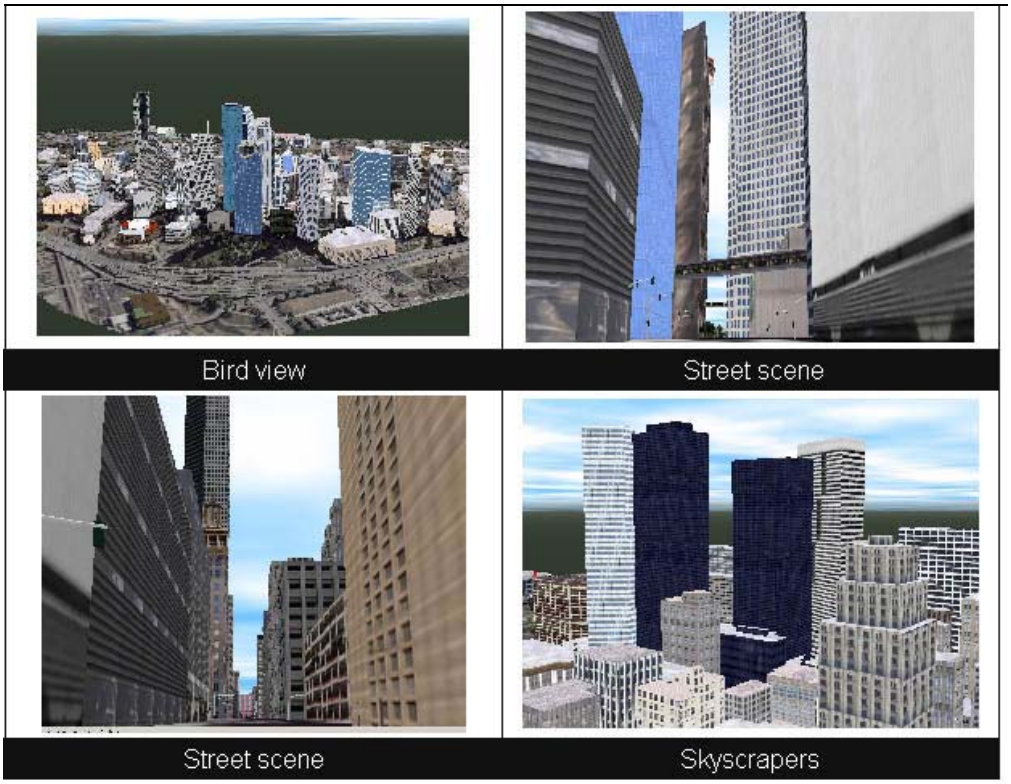

Figure 63: 3D scene of downtown Houston

5.8 Solar Radiation Analysis with 3D Urban Models

3D urban models have many potential applications. For car navigation, it helps the driver easily recognize landmarks and directions from the navigator. For urban planner, site location and aesthetic considerations of landscaping are also useful for scenario analysis and urban planning. For environment analysis, for instance, the building shadows can be utilized for solar radiation analysis.

Solar radiation is the major energy source on earth, and the spatial difference of solar radiation affects the vegetation yield in different species.

Different amount of incoming sun radiation may be affected by the spatial pattern of buildings in the urban area. 3D urban models can help Houston city planners to make a plan regarding where and what species of trees and grasses to be planted in terms of the spatial distribution of solar radiation for different seasons.

A solar flux model is used to calculate the solar radiation volume based on high-resolution LiDAR data for the downtown. The amount of shortwave radiation under clear-sky conditions is computed by an Arc Macro Language (AML) program (Kumar et al. 1997; Zimmermann 2000). The spatial variations of radiation for different months are evaluated.

Plants require solar radiation for photosynthesis, and their growth rate is proportional to the amount of sunlight received. The amount of radiation is reduced by the low sun angles in winter, and increased by the higher angles in summer (Kumar and Skidmore 2000). Young and Smith (1980) determined appropriate insolation value ranges for sun plants and shade plants. According to the spatial distribution of solar radiation in different months, the downtown region is divided into sun-plant suitable area and shade-plant suitable area (Figure 64). This provides the scientific basic for urban planners to choose and plant appropriate species of trees, bushes, grasses, and flowers for different location in the downtown area.

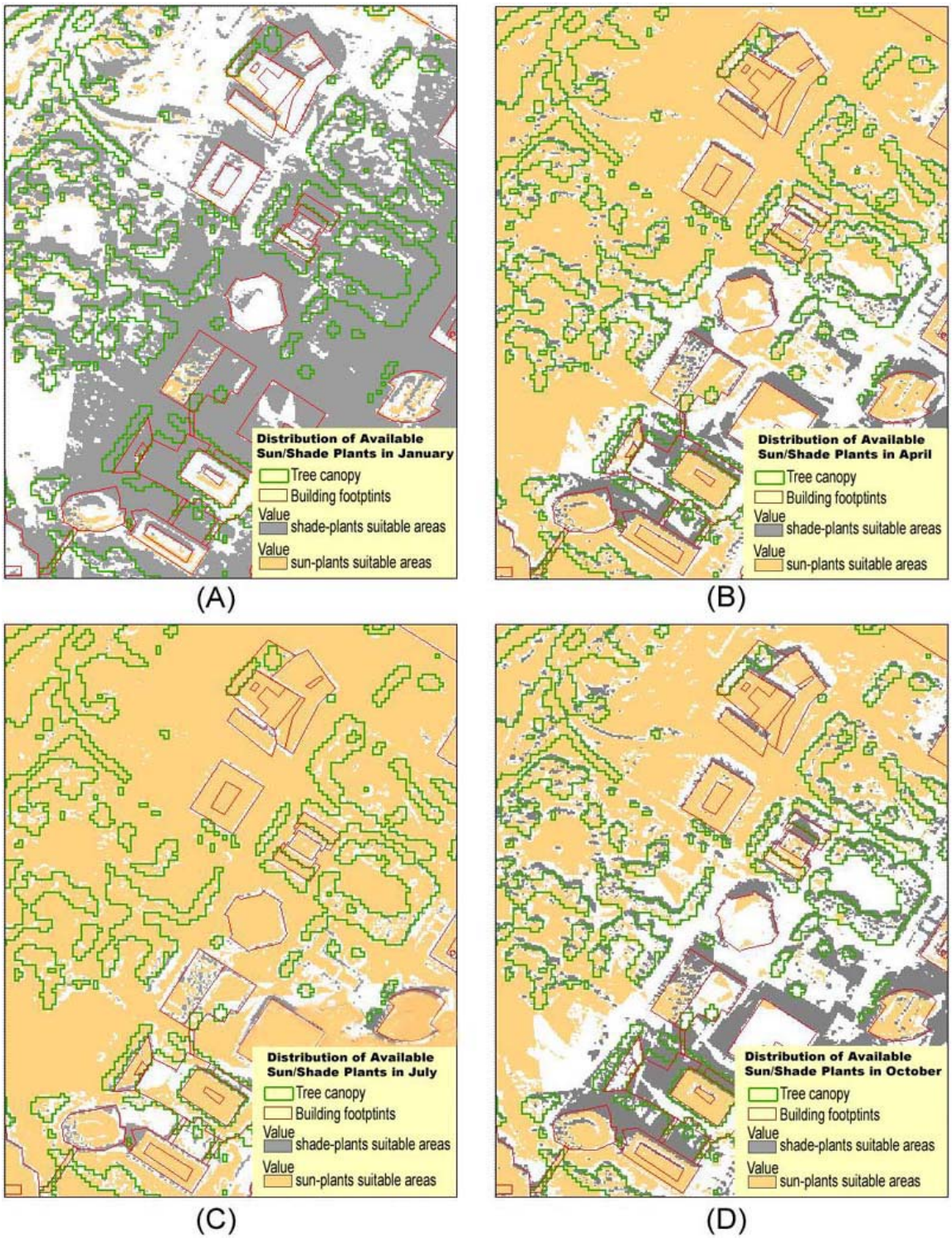

Figure 64: Distribution of suitable sun/shade plants areas. (A) distribution in January; (B) distribution in April; (C) distribution in July; and (D) distribution in October

CHAPTER VI

CONCLUSIONS

Traditionally, 3D urban models are constructed by architects using balsa wood or foam blocks. With the advance of computer visualization technology, the interest and application of digital urban models have been rapidly growing. In the recent decade, an increasing number of digital and virtual urban models have been developed to replace tangible physical wooden models.

Panoramic imaging, VRML, and CAD technology are three major methods used for constructing and visualizing digital urban models. Despite their unique advantages, these three methods suffer from the inadequacy in handling a large urban area and the absence of functionality to perform spatial query, analysis and numerical modeling. To address these limitations, this research proposed a GIS-based 3D urban modeling method. This method is supported by close coupling ArcGIS software and MultiGen-Paradigm Site Builder 3D software. Using the object-oriented approach, the urban features are abstracted into various objects. In terms of their geometric properties, these objects are classified as points, lines, polygons, surfaces, and bodies. In terms of their thematic properties, the objects are classified into buildings, water bodies, roads, sidewalks, grasslands, trees, poles, highways, etc. It has been proven that the grouping urban objects into different classes facilitates the adoption of

appropriate strategies and techniques for acquiring and managing geometric, texture and thematic attributes of urban objects. The geometric and thematic properties of urban objects are derived and managed in ArcGIS environment, the texture properties, object models and visual simulations are managed and realized in MultiGen-Paradigm Site Builder 3D environment.

Texas A&M University campus model and downtown Houston model have been implemented to offer proof-of-concept, namely, to demonstrate the advantages of the GIS-based approach. These two prototype applications show that the GIS-based 3D urban modeling method by coupling ArcGIS and MultiGen-Paradigm Site Builder 3D software can realize the desired functionalities in georeferencing, geographical measurements, spatial query, spatial analysis, and numerical modeling in 3D visual environment. The various GIS data layers and remote sensing data can be easily incorporated for model construction. Geographical coordinates, distance, area, volume, and massing of urban objects can be measured. The linked thematic and geometric attributes of urban objects can be queried in ArcGIS.

With the established GIS functionality, the line-of-sight analysis can be undertaken for locating best location of transmitter base station for telecommunication industry, and the viewshed analysis can be performed for property developers to visualize the proposed buildings and facilities and their associated views in context. In addition, 3D urban models can be applied to

spatial cognition for simulating urban features, landscapes, and landmarks. They are helpful for military to simulate a combat in urban environment, homeland security to plan and prevent emergencies and disasters in simulate environment, or tourism to display attractions for tourist. This research also demonstrated that the shadow effects of buildings can be quantified and simulated with a built-in AML numerical solar radiation model. The GIS-based 3D urban modeling method also keeps the advantages of the previous 3D urban modeling methods in photorealism and flexible visualization. As demonstrated, 3D walk-through or fly-by simulations can be created by interactively controlling the moving path and levels of detail by varying the position and angle of view point. To the author's best knowledge, the downtown Houston model developed in this research is the first digital 3D urban model for the City of Houston. The Texas A&M campus model is the first GIS-based digital model for the campus, although the VRML and panoramic models were developed previously.

Despite the growing interest in 3D urban models and the increased capabilities of 3D urban modeling software, the constructions and applications of 3D urban models in many cities are severely constrained by the unavailability of 3D geometric information. This research demonstrated that the airborne Lidar data and high-resolution aerial images can be utilized to extract both planimetric and vertical information for urban objects, which can be used to

create and update 3D urban database. This research designed and tested automated algorithms to detect and trace the urban object footprints from aerial imagery or airborne LiDAR data. The algorithms are applicable to utilize for other areas. The construction of the downtown Houston model demonstrated that the airborne LiDAR data provide the most efficient and accurate means to capture vertical measurements for urban objects. When the airborne data are not available as in the case of the Texas A&M University campus model, the relief displacement method, the shadow method, and the differential parallax method can be applied to single or stereo aerial images to derive the height information for buildings. The differential parallax method is recommended if the stereo pairs of aerial photographs are available since it produces the height measurements with a higher accuracy. When stereo pairs of aerial photographs are not available, reasonable height measurements are still can be derived by the relief displacement method or shadow method from single aerial photographs.

It should be noted that the footprints derived from aerial photographs or LiDAR data are only rough approximations to the real objects, and small zigzag features can be observed on the derived footprint boundaries. This is because of the limited spatial resolution of aerial photographs or LiDAR data. In the future, the algorithms may to be further improved by using Hough transformation to fit straight lines to the zigzag footprints. In addition, neither Texas A&M University campus model nor downtown Houston model contains the detailed

roof morphology information. With airborne LiDAR, polyhedra may be mathematically fitted to represent detailed roof morphology.

For 3D geometric information, a prismatic block model can be created by the extrusion of urban objects in proportional to the height of the objects. Such a model lacks architectural details of building facades and does not convey compelling sense of realistic urban environment. By mapping photographic texture onto individual urban objects, photorealistic visualization can be achieved. The two prototype applications show that the high-resolution aerial images can be used to create textures for background areas or open spaces. But, terrestrial images are recommended to create texture for urban objects. For unique, complicated buildings and landmarks, texture information needs to be collected by taking digital images from all sides with a digital frame camera or a video camera. For each type of ordinary and simple objects, only one representative object needs to be selected for texture acquisition. At present, making texture chips from the photographs and linking texture chips to individual objects largely depend on manual operations, and therefore require significant effort, time and cost. The efficient algorithms and techniques for texture information capture and processing need to be addressed and developed in the future research.

REFERENCES

Batty M. 2000. The new urban geography of the third dimension. *Environment and Planning B: Planning and Design* 27: 483–484.

Batty M., D. Chapman, S. Evans, M. Haklay, S. Kueppers, N. Shiode, A. Smith, and P. Torrens. 2000. Visualizing the city: Communicating urban design to planners and decision-makers. Centre for Advanced Spatial Analysis, University College London, London, U.K.
http://www.casa.ucl.ac.uk/visualcities.pdf
(last date accessed: 10 August 2003).

Brail R. and R. Klosterman. 2001. *Planning support systems: Intergrating geographic information systems, models, and visualization tools*. ESRI, Redlands, C.A., 443p.

Brenner C. and N. Haala. 1999. Rapid production of virtual reality city models. *GeoInforamtion System* 12(2): 22-28.

Chen D., M. Ho, and M. Ouhyoung. 1998. VideoVR: A real-time system for automatically constructing panoramic images from video clips. *Proceedings of IFIP Workshop on Modelling and Motion Capture Techniques for Virtual Environments*, 26-28 November, Geneva, Switzland, pp.140-143.

Chen S. 1995. Quicktime VR – An image-based approach to virtual environment navigation. *Computer Graphics SIGGRAPH Annual Conference*, 6-11 August, Los Angeles, California, pp. 29-38.

Çöltekin A. 2002. An analysis of VRML-based 3D interfaces for online GISs: Current imitations and solutions. *Surveying Science in Finland* 20(1-2): 80-91.

Coors V. 2003. 3D GIS in networking environments. *Computer, Environment and Urban Systems* 27(4): 345-357.

Ding A. 2000. An efficient fully-automated approach for extracting 3D building polygons from raw LiDAR data.
http://www.terrapoint.com/News_DingURISA2000.html
(last date accessed: 10 October 2003).

Döllner J. and K. Hinrichs. 2000. An object-oriented approach for integrating 3D visualization systems and GIS. *Computer & Geosciences* 26(1): 67-76.

Elaksher A. and J. Bethel. 2002. Reconstructing 3D buildings from LiDAR data. *ISPRS Commission III, Symposium 2002*, 9-13 September, Graz, Austria, pp. 91-96.

Evans S. and A. Hudson-Smith. 2001. Information rich 3D computer modeling of urban environments. Centre for Advanced Spatial Analysis, University College London, London, U.K.
http://www.casa.ucl.ac.uk/paper35.pdf
(last date accessed: 21 August 2003).

Gonzalez R. and R. Woods. 1992. *Digital image processing*. Addison-Wesley, New York, N.Y., 716p.

Haala N., C. Brenner, and K. Anders. 1998. 3D urban GIS from laser altimeter and 2D map data. *ISPRS Journal of Photogrammetry and Remote Sensing* 32: 339-346.

Haithcoat T., W. Song, and J. Hipple. 2001. Building footprint extraction and 3D reconstruction from LiDAR data. *IEEE/ISPRS Joint Workshop on Remote Sensing and Data Fusion over Urban Areas*, 8-9 November, Rome, Italy, pp. 74-78.

Hill J., L. Graham, R. Henry, D. Cotter, and D. Young. 2000. Wide-area topographic mapping and applications using airborne light detection and ranging (LiDAR) technology. *Photogrammetric Engineering & Remote Sensing* 66 (8): 908-914.

Hu J., S. You, and U. Neumann. 2003. Approaches to large-scale urban modeling. *IEEE Computer Graphics and Applications* 23(6): 62-69.

Jensen J. 1996. *Introductory digital image processing: A remote sensing perspective*. Prentice-Hall, Upper Saddle River, N.J., 318p.

Jensen J. 2000. *Remote sensing of the environment: An earth resource perspective.* Prentice-Hall, Upper Saddle River, N.J., 544p.

Köninger A. and S. Bartel. 1998. 3D-GIS for urban purposes. *GeoInformatica* 2(1): 79-103.

Kumar L., A. Skidmore, and E. Knowles. 1997. Modeling topographic variation in solar radiation in a GIS environment. *International Journal of Geographical Information Science* 11(5): 475-497.

Kumar L. and A. Skidmore. 2000. Radiation-vegetation relationships in a eucalyptus forest. *Photogrammetric Engineering & Remote Sensing* 66(2): 193-204.

Kumaradevan P. and S. Kumar. 2001. Virtual reality and distributed GIS. GIS Development. *Proceedings of GITA Annual Conferences*, 4-7 March, San Diego, California, pp. 32-41.

Li Q., W. Shi, and B. Yang. 1999. 3D city modeling based on an integrated data model. *Proceedings of Geoinformatics '99 Conference*, 19-21 June, Ann Arbor, Michigan, pp. 1-8.

Li R. 1994. Data structures and application issues in 3-D geographic information systems. *GeoMatica* 48(3): 209-224.

Lin C. and R. Nevatia. 1998. Building detection and description from a single intensity image. *Computer Vision and Image Understanding* 72(2): 101-121.

Liu H. and K. Jezek. 2004. Automated extraction of coastline from satellite imagery by integrating canny edge detection and locally adaptive thresholding methods. *International Journal of Remote Sensing* 25(5): 937-958.

Mahoney D. 1998. Merging CAD and GIS. *Computer Graphics World* 21(3):45-50.

MultiGen-Paradigm. 2002. *The Model Builder 3D desktop tutor*. MultiGen-Paradigm Inc., San Jose, C.A., 154p.

MultiGen-Paradigm. 2003. *Site Builder 3D user's guide*. MultiGen-Paradigm, Inc., San Jose, C.A., 192p.

Naimark M. 1998. Field cinematography techniques for virtual reality applications.
http://www.naimark.net/writing/gifu.html
(last date accessed: 5 May 2004).

Palmer T. and J. Shan. 2002. A comparative study on urban visualization using LiDAR data in GIS. *Journal of the Urban and Regional Information Systems Association* 14(2): 19-26.

Pesce M. 1996. *VRML flying through the web*. New Riders, Indianapolis, I.N., 367p.

Pfund M. 2002. 3D GIS architecture: A topological data structure. *GIM International* 16(2): 35-37.

Pintaric T., U. Neumann, and A. Rizzo. 2000. Immersive panoramic video. *Proceedings of the 8th ACM International Conference on Multimedia*, 30 October-4 November, Los Angeles, California, pp. 493-494.

Priestnall G., J. Jaafar, and A. Duncan. 2000. Extracting urban features from LiDAR digital surface models. *Computers, Environment and Urban Systems* 24: 65-78.

Pullar D. and M. Tidey. 2001. Coupling 3D visualisation to qualitative assessment of built environment designs. *Landscape and Urban-Planning* 55: 29-40.

Ranzinger M. and G. Gleixner. 1995. Changing the city: Datasets and applications for 3D urban planning. *GIS Europe* 4(2): 28-30.

Ranzinger M. and G. Gleixner. 1997. GIS datasets for 3D urban planning. *Computer, Environment and Urban Systems 21*(2): 159-173.

Rau J. and L. Chen. 2001. Semi-automatic approach for building reconstruction using split-merge-shape method. Center for Space and Remote Sensing Research, National Central University, Chung-Li, Taiwan.
http://www.crisp.nus.edu.sg/~acrs2001/pdf/055JYRau.pdf
(last date accessed: 8 August 2004).

Rottensteiner F. and C. Briese. 2002. A new method for building extraction in urban areas from high-resolution LiDAR data. *International Archives of Photogrammetry and Remote Sensing* 34 (3A): 295 - 301.

Schoonmaker S. 2003. *The CAD guidebook: A basic manual for understanding and improving computer-aided design*. Marcel Dekker, New York, N.Y., 323p.

Serr D. 2000. Use of LiDAR in creating accurate terrain elevation models for floodplain mapping.
http://www.emporia.edu/earthsci/student/serr1/project.htm
(last date accessed: 10 March 2004).

Sheppard S. 1989. *Visual simulation: A user's guide for architects, engineers, and planners*. Van Nostrand Reinhold, New York, N.Y., 215p.

Shiode N. 2001. 3D urban models: recent developments in the digital modeling of urban environments in three-dimensions. *GeoJournal* 52(3): 263-269.

Sinning-Meister M., A. Gruen, and H. Dan. 1996. 3D city models for CAAD-supported analysis and design of urban areas. *ISPRS Journal of Photogrammetry and Remote Sensing* 51(4): 196-208.

Smith A., M. Dodge, and S. Doyle. 1998. Visual communication in urban planning and urban design. Centre for Advanced Spatial Analysis, University College London, London, U.K.
http://www.casa.ucl.ac.uk/urbanplan.pdf
(last date accessed: 31 August 2003).

Veneziano D., R. Souleyrette, and S. Hallmark. 2003. Integrating LiDAR and photogrammetry in highway location and design. *Proceedings of the 2003 Transportation Research Board Annual Meeting*, 12-16 January, Washington D.C., pp. 1-17.

Weidner U. 1996. An approach to building extraction from digital surface models. *Proceedings of 18th ISPRS Congress*, 9-19 July, Vienna, Austria, pp. 924-929.

Xia F. 1995. *Three dimensional GIS for environmental modeling: A surface water quality modeling example*. PhD Dissertation, University of New York at Buffalo, Buffalo, New York, 230p.

Xiao B. 1996. Building a VRML of Texas A&M main campus. Center for the Study of Digital Libraries, Department of Computer Science, Texas A&M University.
http://www.csdl.tamu.edu/~b0x9330/tour/techinfo/techvrml.htm
(last date accessed: 10 October 2003).

Young D. and W. Smith. 1980. Influence of sunlight photosynthesis, water relations, and leaf structure in the understory species arnica cordifolia. *JSTOR Ecology* 61(6): 1380-1390.

Zhou G., C. Song, J. Simmers, and P. Cheng. 2004. Urban 3D GIS from LiDAR and digital aerial images. *Computer & Geosciences* 30(4): 345-353.

Zhu Q., D. Li, Y. Zhang, Z. Zhong, and D. Huang. 2002. CyberCity GIS (CGIS): Integration of DEMs, images, and 3D models. *Photogrammetric Engineering & Remote Sensing* 68(4): 361-367.

Zimmermann N. 2000. The AML code of shortwavc. http://www.wsl.ch/staff/niklaus.zimmermann/programs/aml1_2.html (last date accessed: 15 April 2004).

Zlatanova S. 1999a. An alternative for a 3D GIS. *Proceedings of the International symposium on Modern Information and GPS Technology–Aspects and Implications of Their Application*, 12 November, Sofia, Bulgaria, pp. 221-231.

Zlatanova S. 1999b. VRML for 3D GIS. *Proceedings of the 15th SCCG*, 28 April-1 May, Budmerice, Slovakia, pp. 74-82.

Zlatanova S., A. Rahman, and W. Shi. 2004. Topological models and frameworks for 3D spatial objects. *Computer & Geosciences* 30(4): 419-428.

APPENDIX A

The list of building attributes of TAMU main campus

Building Number	Building Name	Number of Floors	Peri-meter (ft)	Gross Area (ft^2)	Height (m)	Group Average Height (m)
290	WELLS RESIDENCE HALL	3	744	67,283	14.88	4.96
291	RUDDER RESIDENCE HALL	3	744	67,283	14.88	4.96
292	EPPRIGHT RESIDENCE HALL	3	744	67,283	14.88	4.96
293	APPELT RESIDENCE HALL	3	860	82,767	14.88	4.96
294	LECHNER RESIDENCE HALL	3	670	59,541	14.88	4.96
350	ALBRITTON BELL TOWER	6	105	13,800	24.60	4.10
353	BRIGHT BUILDING	9	630	148,837	36.90	4.10
357	VENDING MACHINE BOOTH	1	101	579	4.96	4.96
360	STEED RESEARCH & CONDITIONING LAB	1	771	26,250	4.96	4.96
362	TENNIS COURT RESTROOMS	1	100	869	4.96	4.96
364	SMITH TENNIS CENTER	1	255	1,855	4.96	4.96
367	KYLE FIELD	4	589	149,895	18.88	4.72
369	READ BUILDING	2	601	153,886	9.92	4.96
370	HENSEL PARK PICNIC SHELTER	1	140	1,225	4.96	4.96
371	HENSEL PARK PICNIC SHELTER #1	1	150	1,200	4.96	4.96
372	HENSEL PARK PICNIC SHELTER #2	1	150	1,700	4.96	4.96
373	HENSEL PARK RESTROOMS	1	140	256	4.96	4.96
376	CHEMISTRY BUILDING ADDITION	5	928	115,797	20.50	4.10
377	SOUTH SIDE NO. 3 - SATELLITE PLANT	1	566	12,338	4.96	4.96

378	SOUTH SIDE PARKING GARAGE	4	1,769	628,040	18.88	4.72
379	UNIVERSITY CENTER PARKING GARAGE	4	1,311	487,664	18.88	4.72
380	FLORICULTURE BUILDING A	1	50	120	4.96	4.96
381	FLORICULTURE BUILDING B	1	64	152	4.96	4.96
382	FLORICULTURE BUILDING C	1	84	516	4.96	4.96
383	KOLDUS BUILDING	3	1,511	110,272	14.88	4.96
384	SANDERS CORPS OF CADETS CENTER	1	718	19,363	4.96	4.96
385	CIVIL ENGINEERING LAB BUILDING	8	1,096	157,844	32.80	4.10
387	RICHARDSON PETROLEUM ENGINEERING BUILDING	11	540	113,700	45.10	4.10
388	NORTHSIDE PARKING GARAGE	4	1,395	621,774	18.88	4.72
389	GROUNDS MAINTENANCE POTTING SHED	1	108	560	4.96	4.96
391	ENGINEERING/PHYSICS LAB BUILDING	5	836	115,288	20.50	4.10
392	ENGINEERING/PHYSICS OFFICE TOWER	5	376	46,953	20.50	4.10
393	LINDSEY BUILDING	1	922	22,666	4.96	4.96
394	UNDERWOOD RESDIENCE HALL	4	858	81,730	18.88	4.72
396	BUS STOP SNACK BAR - ROSS & IRELAND	1	100	600	4.96	4.96
398	LANGFORD ARCHITECTURE CENTER BUILDING A	5	1,174	116,619	20.50	4.10
400	SPENCE HALL	4	420	31,952	18.88	4.72
401	KIEST HALL	4	420	31,952	18.88	4.72
402	BRIGGS HALL	4	345	31,952	18.88	4.72
403	FOUNTAIN HALL	4	345	31,952	18.88	4.72
404	GAINER HALL	4	476	33,904	18.88	4.72
405	LACY HALL	4	476	31,052	18.88	4.72

406	LEONARD HALL	4	490	31,952	18.88	4.72
407	HARRELL HALL	4	478	31,952	18.88	4.72
408	WHITELY HALL	4	490	31,952	18.88	4.72
409	WHITE HALL	4	478	31,952	18.88	4.72
410	HARRINGTON HALL	4	478	31,952	18.88	4.72
411	UTAY HALL	4	490	31,952	18.88	4.72
412	MOSES RESIDENCE HALL	4	540	40,828	18.88	4.72
413	MOORE RESIDENCE HALL	4	845	40,828	18.88	4.72
414	CROCKER RESIDENCE HALL	4	520	40,828	18.88	4.72
415	DAVIS-GARY RESIDENCE HALL	4	522	40,828	18.88	4.72
416	BIZZELL HALL	3	604	34,004	14.88	4.96
417	HART RESIDENCE HALL	4	877	50,416	18.88	4.72
419	LEGETT RESIDENCE HALL	4	430	45,134	18.88	4.72
420	MILNER HALL	4	310	48,268	18.88	4.72
422	WALTON RESIDENCE HALL	4	1,105	51,494	18.88	4.72
424	HOTARD RESIDENCE HALL	4	400	18,500	18.88	4.72
425	HENDERSON HALL	3	650	22,185	14.88	4.96
426	HUGHES RESIDENCE HALL	4	452	38,957	18.88	4.72
427	FOWLER RESIDENCE HALL	4	686	57,696	18.88	4.72
428	KEATHLEY RESIDENCE HALL	4	686	57,696	18.88	4.72
429	MCINNIS RESIDENCE HALL	4	410	31,184	18.88	4.72
430	SCHUHMACHER RESIDENCE HALL	4	520	38,957	18.88	4.72
431	MACHINE SHOP POWER PLANT	1	265	3,577	4.96	4.96
432	ARCHITECTURE BUILDING B	4	494	86,447	18.88	4.72
433	MOSHER RESIDENCE HALL	5	1,240	155,430	20.50	4.10
434	LUEDECKE BUILDING (CYCLOTRON)	2	750	80,464	9.92	4.96

435	HARRINGTON EDUCATION CENTER OFFICE TOWER	10	540	130,844	41.00	4.10
436	REED-MCDONALD BUILDING	4	586	77,435	18.88	4.72
438	HARRINGTON EDUCATION CENTER CLASSROOM BUILDING	4	707	61,860	18.88	4.72
439	CAIN HALL	4	960	92,812	18.88	4.72
440	COMMONS	2	830	84,500	9.92	4.96
441	KRUEGER RESIDENCE HALL	4	1,230	112,133	18.88	4.72
442	DUNN RESIDENCE HALL	4	1,230	112,133	18.88	4.72
443	OCEANOGRAPHY & METEOROLOGY BUILDING	15	676	180,316	61.50	4.10
444	PETERSON BUILDING	4	970	84,831	18.88	4.72
445	TEAGUE RESEARCH CENTER	3	582	63,515	14.88	4.96
446	RUDDER TOWER	13	1,203	302,240	53.30	4.10
447	ASTON RESIDENCE HALL	4	1,160	113,388	18.88	4.72
448	ADAMS BAND HALL	3	928	55,248	14.88	4.96
449	BIOLOGICAL SCIENCES BLDG. WEST	4	590	96,038	18.88	4.72
450	DUNCAN DINING HALL	2	1,160	128,482	9.92	4.96
453	G. ROLLIE WHITE COLISEUM	3	1,232	177,838	14.88	4.96
454	MEMORIAL STUDENT CENTER	3	2,466	368,935	14.88	4.96
456	MILITARY SCIENCES BUILDING	3	520	43,808	14.88	4.96
457	FOREST SCIENCE BUILDING	3	527	16,364	14.88	4.96
458	FLORICULTURE GREENHOUSE	1	520	11,456	4.96	4.96
459	HORTICULTURE GREENHOUSE	1	400	7,612	4.96	4.96
460	FOREST GENETICS - GREENHOUSE	1	570	12,047	4.96	4.96
461	COKE BUILDING	2	370	24,466	9.92	4.96

462	ACADEMIC BUILDING	4	720	82,555	18.88	4.72
463	PSYCHOLOGY BUILDING	4	798	38,469	18.88	4.72
464	STATE CHEMIST BUILDING	2	362	20,027	9.92	4.96
465	BUTLER HALL	3	380	29,699	14.88	4.96
467	BIOLOGICAL SCIENCES BLDG. EAST	4	722	62,273	18.88	4.72
468	EVANS LIBRARY	4	1,997	509,189	18.88	4.72
469	CENTRAL CAMPUS PARKING GARAGE	6	742	179,154	24.60	4.10
470	HISTORY BUILDNG	3	450	39,887	14.88	4.96
471	PAVILION	2	600	40,062	9.92	4.96
472	ANIMAL INDUSTRIES BUILDING	5	854	44,856	20.50	4.10
473	WILLIAMS ADMINISTRATION BUILDING	4	650	69,898	18.88	4.72
474	YMCA BUILDING	4	550	33,814	18.88	4.72
476	FRANCIS HALL	3	650	36,850	14.88	4.96
477	ANTHROPOLOGY BUILDING	3	696	51,592	14.88	4.96
478	SCOATES HALL	3	914	62,228	14.88	4.96
480	BOLTON HALL	4	480	39,686	18.88	4.72
481	HEATON HALL	2	390	13,640	9.92	4.96
482	FERMIER HALL	4	300	19,074	18.88	4.72
483	THOMPSON HALL	3	840	81,404	14.88	4.96
484	CHEMISTRY BUILDING	5	2,131	205,393	20.50	4.10
490	HALBOUTY GEOSCIENCES BUILDING	4	1,196	120,874	18.88	4.72
492	CIVIL ENGINEERING BUILDING	2	1,068	56,537	9.92	4.96
493	BELL BUILDING	4	840	51,802	18.88	4.72
495	SBISA DINING HALL	2	1,290	94,233	9.92	4.96
496	LAUNDRY	1	625	27,457	4.96	4.96
498	CENTRAL UTILITIES PLANT	3	2,065	71,164	14.88	4.96
499	GRAPHIC SERVICES	1	790	26,865	4.96	4.96
501	CONCRETE MATERIALS LABORATORY	2	336	9,600	9.92	4.96

502	HYDROMECHANICS LABORATORY	2	680	27,150	9.92	4.96
506	NAGLE HALL	4	400	32,306	18.88	4.72
511	HEEP LABORATORY BUILDING	3	1,120	40,476	14.88	4.96
512	ALL FAITHS CHAPEL	1	760	8,999	4.96	4.96
513	DOHERTY BUILDING	3	766	42,336	14.88	4.96
514	FACILITIES PLANNING & CONSTRUCTION	2	1,250	22,134	9.92	4.96
516	COMPUTING SERVICES CENTER	1	390	30,014	4.96	4.96
517	COMPUTING SERVICES ADDITION	3	520	26,220	14.88	4.96
518	ZACHRY ENGINEERING CENTER	5	1,100	324,400	20.50	4.10
519	MOORE COMMUNICATIONS CENTER	1	630	17,861	4.96	4.96
520	BEUTEL HEALTH CENTER	3	671	63,318	14.88	4.96
521	HELDENFELS HALL	4	890	104,949	18.88	4.72
524	BLOCKER BUILDING	6	1,100	257,953	24.60	4.10
525	VOLATILE STORAGE BUILDING	1	94	515	4.96	4.96
547	WATER TOWER STORAGE	1	130	1,846	4.96	4.96
548	CLEMENTS RESIDENCE HALL	4	762	62,156	18.88	4.72
549	HAAS RESIDENCE HALL	4	900	69,668	18.88	4.72
550	MCFADDEN RESIDENCE HALL	1	603	62,156	4.96	4.96
628	GARAGE	4	1	4,000	18.88	4.72
629	WAREHOUSE - STUDENT APT	1	1	7,400	4.96	4.96
630	VICE PRESIDENT'S RESIDENCE	2	477	5,502	9.92	4.96
634	PRESIDENT'S RESIDENCE	2	468	8,550	9.92	4.96
635	GROUNDS MAINTENANCE STORAGE	1	56	118	4.96	4.96

652	NEELEY RESIDENCE HALL	4	900	69,668	18.88	4.72
653	HOBBY RESIDENCE HALL	4	603	62,156	18.88	4.72
654	GENERATOR SHED	1	56	188	4.96	4.96
655	GOLF COURSE MAINTENANCE SHOP	1	1	4,000	4.96	4.96
668	HENSEL APT MAINTENANCE BLDG	1	1	1,797	4.96	4.96
671	GROVE BAND STAND(Demolished 2003)	1	146	461	4.96	4.96
672	GOLF COURSE CLUBHOUSE	1	1	4,751	4.96	4.96
677	GOLF COURSE HALFWAY HOUSE	1	1	560	4.96	4.96
682	WISENBAKER ENGINEERING RESEARCH CENTER	3	1,288	177,704	14.88	4.96
685	GROUNDS MAINTENANCE - TRACTOR SHED	1	318	4,400	4.96	4.96
715	CHEMISTRY CHEMICAL STORAGE	1	78	387	4.96	4.96
717	STORAGE AND LAB--CYCLOTRON	1	260	3,000	4.96	4.96
718	STORAGE--CYCLOTRON	1	90	617	4.96	4.96
726	GROUNDS MAINTENANCE GREENHOUSE 4	1	256	3,046	4.96	4.96
728	GROUNDS MAINTENANCE GREENHOUSE 5	1	256	3,055	4.96	4.96
729	BIOLOGY GREENHOUSE	1	156	1,300	4.96	4.96
732	SOIL & CROP SCIENCE GREENHOUSE	1	288	4,162	4.96	4.96
733	GROUNDS MAINTENANCE GREENHOUSE	1	288	4,162	4.96	4.96
740	MCNEW LABORATORY	3	366	20,904	14.88	4.96
742	GROUNDS MAINTENANCE STORAGE	1	169	3,350	4.96	4.96

747	GROUNDS MAINTENANCE SUPPLY BLDG	1	342	4,800	4.96	4.96
821	GROUNDS MAINTENANCE STORAGE	1	101	225	4.96	4.96
824	GROUNDS MAINTENANCE IMPLEMENT SHED	1	338	1,400	4.96	4.96
825	FLORICULTURE STORAGE BLDG	1	61	234	4.96	4.96
828	GROUNDS SHOP WAREHOUSE	1	314	5,976	4.96	4.96
829	GROUNDS MAINTENANCE OFFICE SHOP/STOR	1	314	5,976	4.96	4.96
831	GROUNDS MAINTENANCE GREENHOUSE	1	284	3,392	4.96	4.96
1027	NURSERY FLORAL FIELD LABORATORY	1	284	4,040	4.96	4.96
1129	FLORICULTURE GREENHOUSE	1	144	2,270	4.96	4.96
1130	FLORICULTURE GREENHOUSE	1	255	3,100	4.96	4.96
1132	MOTOR VEHICLE MAINTENANCE SHOP	1	1	3,180	4.96	4.96
1133	VEHICLE & EQUIP STORAGE SHED	1	1	7,508	4.96	4.96
1190	FLORICULTURE RESEARCH GREENHSE	1	268	3,509	4.96	4.96
1191	FLORICULTURE GROWING FACILITY	1	114	5,515	4.96	4.96
1195	NON SURGICAL ANIMAL PROCEDURE	1	1	900	4.96	4.96
1579	SMALL UPLAND FOWL RES. LAB.	1	1	2,880	4.96	4.96
1701	TEXAS A&M POLO CLUB STABLES	1	372	6,048	4.96	4.96
3099	BUSINESS MANAGEMENT SERVICES BUILDNG (name pending)	2	419	17,368	9.92	4.96

3198	University Apartments Community Center	1	734	17,384	4.96	4.96
3199	CHILDREN'S CENTER	1	1	10,127	4.96	4.96
3200	CONNALLY BUILDING	7	936	123,961	28.70	4.10
3201	STATE HGTRS THERMAL PLANT	1	272	900	4.96	4.96
3400	UNIVERSITY SERVICES BLDG	1	1,642	153,000	4.96	4.96
8900	STUDENT LIFE TEMPORARY BUILDING	1	1	1	4.96	4.96
8901	RESIDENCE LIFE TEMPORARY BUILDING	1	1	1	4.96	4.96
9351	WATER TOWER	10	139	5,160	41.00	4.10

APPENDIX B

The list of geographical urban shapes and textures of TAMU main campus

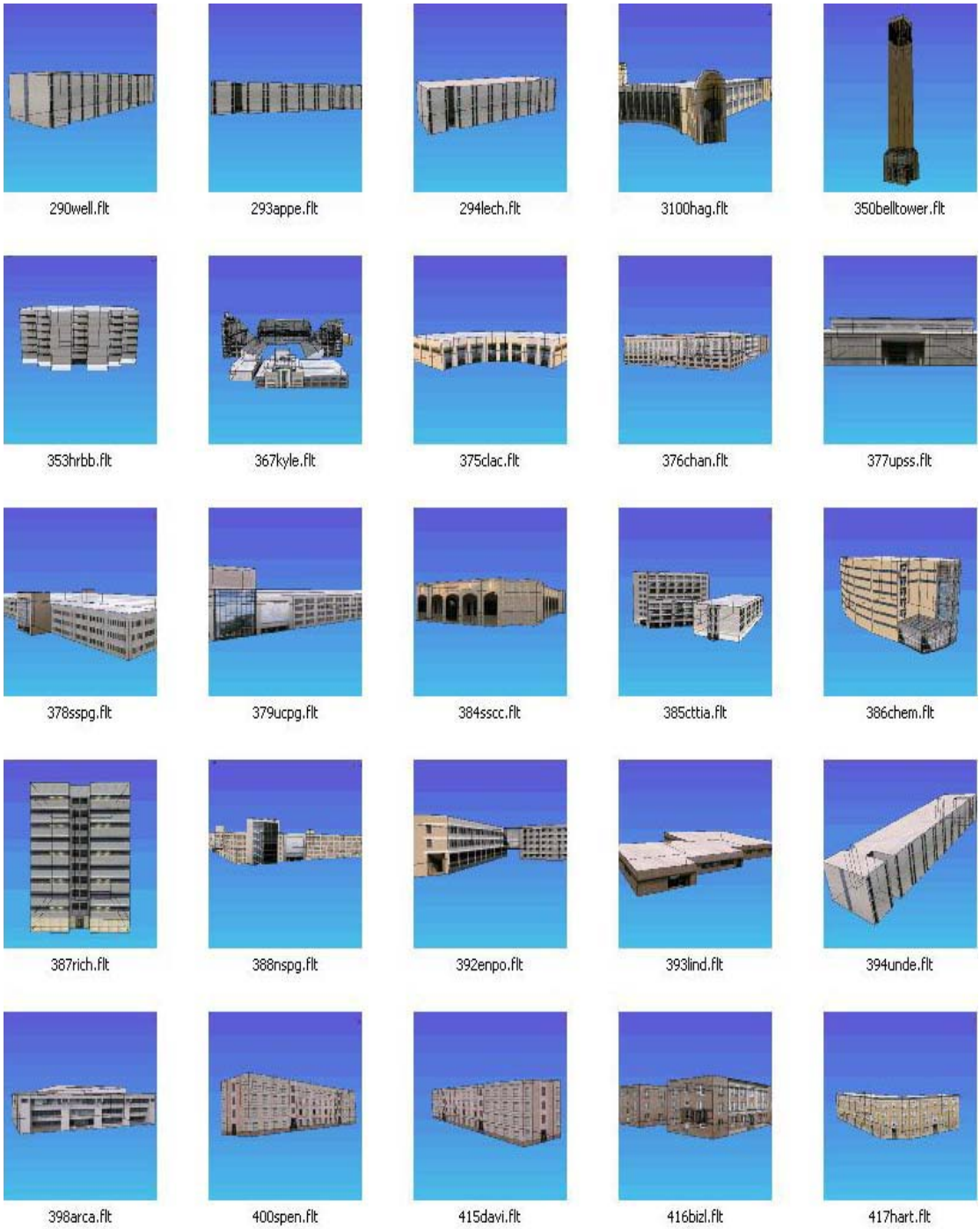


420miln.flt


422walt.flt


4241usps.flt


424hota.flt


425hend.flt


426hugh.flt


427fowl.flt


429mcin.flt


432arcb.flt


434cycl.flt


435edct.flt


436rdmc.flt


438edcc.flt


439cain.flt


440sao.flt


443o8m.flt


444petr.flt


445teag.flt


448adam.flt


454MSC.flt


456mils.flt


457taes.flt


459htgh.flt


461coke.flt


462acda.flt


463psyc.flt


464stch.flt


465btlr.flt


467bsbe.flt


468libr.flt


468scc.flt


469ccpg.flt


470hist.flt


471pav.flt


472anin.flt


473admn.flt


474ymca.flt


476francis.flt


477anth.flt


478scts.flt


480bolton.flt


481heat.flt


482ferm.flt


483thom.flt


490halb.flt


492ce.flt


493bell.flt

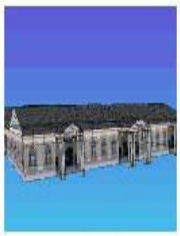
495sbsa.flt


4963watertower.flt


498ppmb.flt


501conc.flt


502hylb.flt


506ngle.flt


511hlb.flt


512chpl.flt


513drty.flt


514fp&c.flt


518zach.flt

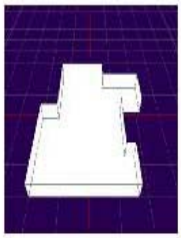
519kamu.flt


520beut.flt


521held.flt


524bloc.flt


548clem.flt

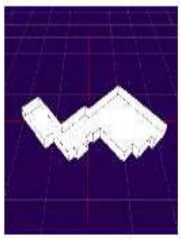
630prvp.flt


634pres.flt


672golf.flt


682werc.flt

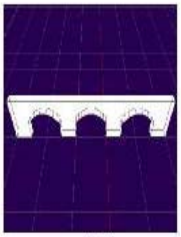
arch.flt


flag.flt


flag1.flt


lodge.flt


lodge1.flt


pool.flt


signal02.flt


stlight1.flt


stlight3.flt


stlight4.flt


stlight5.flt

stopSign.flt


streetLight1.flt


TreeBigOak.flt


TreeLiquidambar.flt


TreeOak.flt

APPENDIX C

The list of building attributes of downtown Houston

BDG NO	Area	Peri-Meter (ft)	BDG Name	ADD RNO	Street Name	Max Height (ft)	Min Height (ft)	Mean Height (ft)	Median Height (ft)
1	2474.00	199.13				55.11	39.40	50.97	51.04
3	25489.88	732.26				72.61	41.06	62.82	66.83
5	38335.00	785.26				131.74	42.31	116.87	115.71
6	2994.50	262.61				67.80	37.50	49.43	48.96
8	3730.13	331.12				80.95	42.89	65.90	70.03
11	6693.63	369.74	Harris County Vehicle Matenance	426	Austin	93.38	49.97	63.89	63.39
15	45236.88	971.36				760.20	47.75	409.49	473.14
17	2827.50	240.10				94.78	49.26	78.28	78.52
19	35153.13	789.16				498.98	39.80	202.83	82.81
21	3448.00	289.42				77.34	46.61	61.98	62.17
22	3408.88	240.95		1100	Louisiana	78.81	51.06	73.04	72.66
23	131310.50	1576.32	Palais Royal	917	Main	146.14	48.56	117.84	134.62
24	23362.00	600.50				742.64	41.14	271.57	107.42
30	2887.88	221.47	Americana Building	811	Dallas	84.19	47.22	65.07	70.02
33	8269.50	358.84				115.03	47.72	82.26	82.71
40	834.25	123.39				93.65	47.75	67.16	62.90
45	29188.00	729.32	4 Houston Center	1300	McKiney	160.58	54.77	138.97	139.75
47	72205.25	1082.81	Garage	1400	Louisiana	192.53	47.10	165.70	173.10
48	32384.75	870.68				91.83	48.09	52.72	49.21
49	5581.50	386.10	Garage	1600	Smith	69.07	49.17	66.96	68.38
50	5402.88	296.17				95.92	59.91	85.83	86.22
54	5098.38	477.27	Travis Tower	1300	Main	76.91	47.89	51.53	49.06
55	24656.88	679.16				781.14	44.41	219.04	95.53
59	63700.88	1009.61	Crown Plaza Cullen Center	1700	Smith	147.18	45.06	127.53	121.66

60	3055.75	219.79	Exxon Garage	1616	Milam	86.06	47.46	71.77	77.28
61	28556.25	698.90				604.12	45.04	274.59	145.03
63	1664.75	200.69				78.10	46.59	58.16	58.71
67	2494.75	224.82				77.05	50.61	69.34	71.26
69	3057.88	236.04				74.30	45.94	58.04	58.80
70	4132.38	327.63				62.49	47.44	59.39	61.11
72	14500.50	481.97				97.76	45.91	85.89	86.13
74	2364.50	205.95	Kellogg, Brown & Root Tower Garage	701	Jefferson	69.71	50.14	63.88	64.36
78	12143.63	446.24				82.68	46.29	72.72	73.95
79	6044.00	332.87				101.94	47.42	81.29	93.64
81	4684.50	291.07				70.99	45.59	64.25	65.92
82	8701.00	387.59				92.69	46.36	83.85	85.32
84	15401.38	476.34				368.77	45.40	294.74	341.31
88	6455.88	341.34				72.37	45.72	58.23	58.28
90	9628.00	406.04	First Church Of Christ Scientist	1720	Main	65.52	46.29	61.12	62.86
92	29742.75	736.53				345.82	49.99	202.84	123.29
93	6883.00	458.75				101.67	51.26	84.81	86.96
94	3133.75	225.29	Old Heaven On Earth Inn	1800	Travis	89.08	49.40	64.82	64.55
96	16815.13	770.59				77.88	44.62	67.24	73.81
97	2377.50	200.96	U-Haul	1622	Caroline	77.67	46.04	68.66	71.52
98	2954.25	228.54				64.04	45.93	59.34	61.14
101	28861.25	731.65				118.71	46.70	97.10	99.20
102	9438.00	397.03				74.98	45.51	70.28	71.98
104	6145.00	346.45				74.51	46.89	69.21	70.31
106	4408.13	299.62				73.57	45.76	59.02	59.25
107	3597.00	261.51				65.23	47.49	62.10	63.13
109	9898.63	397.99	Garage	1801	Main	82.19	45.35	57.69	58.01
110	59672.38	1013.70	AT&T	1407	Jefferson	235.53	44.81	116.85	97.20
111	31593.50	785.41				351.73	43.87	254.69	323.40
113	5303.00	303.80				63.95	45.22	51.67	47.30
114	33467.25	935.09				106.36	34.58	58.43	57.11
115	4863.50	296.38				94.73	33.82	74.55	78.04

117	22983.63	635.08				129.86	33.11	77.46	84.17
118	19511.63	605.06				86.98	34.18	55.82	53.32
120	100773.00	3152.56				76.18	34.44	50.57	52.97
123	19565.25	596.81				84.02	34.82	64.12	66.59
124	261015.63	2607.68				143.13	27.11	83.09	82.85
125	138446.50	1826.70				187.25	18.08	105.59	95.08
127	1208.50	139.25				83.55	36.16	54.79	56.40
129	8292.25	369.32				42.83	19.65	39.16	41.08
131	63420.50	1078.64				169.91	23.19	146.85	146.96
132	106168.00	1413.26				102.28	33.93	64.13	64.75
133	3415.38	358.64				43.99	23.83	42.37	42.88
134	3998.25	366.00				43.90	26.82	41.69	42.56
135	28934.88	722.18				107.23	32.74	65.00	59.63
136	4790.75	401.82				44.76	24.43	40.94	43.31
137	19222.38	792.59				78.49	27.13	63.91	67.15
138	8073.75	363.42				72.78	23.58	64.91	66.35
139	11185.75	456.68	Dixon Building	800	Comerce	78.25	10.96	53.82	57.62
140	4811.25	395.50	Spaghetti Warehouse	901	Comerce	52.30	24.91	41.54	43.97
141	4053.00	375.58	Magnolia Ballroom	120	Milam	55.79	27.72	42.30	42.53
142	4760.75	391.37				66.25	25.71	43.85	45.22
143	4767.50	386.29				44.36	23.98	41.02	42.64
144	39606.38	1300.60	Fire Station #1	410	Bagby	267.35	34.85	127.42	126.07
145	10899.88	445.46				104.07	37.20	90.53	89.22
146	4592.63	384.34				61.38	28.90	46.09	47.00
147	21297.50	702.75	Bayou Lofts	913	Franklin	50.55	31.34	42.53	47.62
148	4931.50	390.60				45.09	24.33	41.40	43.61
149	3986.75	268.37				72.66	24.67	61.77	64.18
150	39348.25	1067.31	Chase Drive-In	701	Congress	96.09	13.19	76.42	85.33
152	5005.00	388.43				50.94	29.27	45.72	48.75
153	352.25	77.12				86.01	41.10	48.84	43.38
154	4567.38	387.81				62.89	26.23	44.17	44.96
156	6000.00	378.77				65.02	31.64	47.03	48.46

157	4302.00	380.68				44.93	25.03	42.45	43.59
158	78821.75	1496.94				149.17	35.71	130.20	144.24
159	4644.00	365.30				53.36	31.75	47.62	51.03
160	4581.88	298.07				160.88	35.86	97.46	93.66
161	4400.13	368.82	Wortham Center	501	Texas	48.76	28.02	45.93	47.34
162	11045.25	558.99				73.21	37.32	56.58	57.00
164	27900.13	716.63				172.99	34.21	145.13	156.94
165	3936.50	356.83	Hermann Lofts	801	Congress	46.48	29.09	43.76	44.72
166	64813.38	1143.52	Bank One Drive-In	619	Preston	69.11	22.25	53.49	54.56
167	20960.88	581.22	Market Square Garage	300	Milam	81.56	4.06	52.59	51.79
168	3203.75	281.65				71.00	33.84	51.65	53.51
169	4699.63	387.21				49.67	28.53	45.35	48.05
170	4239.13	365.71	Texas Meat Packing Building	1119	Comerce	47.74	27.28	44.45	46.21
172	4147.25	363.49				73.50	32.28	51.42	51.57
173	2793.88	250.36				57.29	35.78	51.85	55.29
174	40999.63	1324.88				228.55	41.67	104.25	75.58
175	2288.00	236.32				48.59	27.53	43.80	47.65
176	3955.00	266.32				42.84	26.65	35.98	39.38
177	17721.63	535.69		220	Main	132.65	5.86	85.60	86.92
178	4981.38	395.71				61.33	34.32	53.51	55.81
179	2497.50	239.36				60.02	38.56	56.08	58.27
180	4541.25	367.92				50.81	30.21	46.52	49.20
183	36382.13	1042.85				87.63	29.48	67.41	67.41
185	46168.63	1220.31	Harris County Garage	102	Fannin	252.88	41.20	186.81	162.85
186	3773.13	338.22				52.36	39.76	48.91	49.29
187	4976.38	391.55				63.61	37.86	58.26	59.81
188	14427.50	510.94	Jury Assembly Building/ Garage	201	Main	404.23	39.45	333.15	385.40
189	55386.13	1258.27				157.31	38.17	99.49	90.79
190	4686.75	373.33	Hogg Palace	401	Louisiana	59.46	32.83	51.58	53.58

192	3364.25	299.58				59.09	44.24	53.63	54.09
193	3708.00	332.60	Bayou Place	601	Smith	57.24	29.80	49.73	52.12
194	4578.63	379.63				66.48	43.68	61.43	62.80
195	5296.88	395.61				62.38	36.05	55.57	57.96
196	19134.63	637.71				242.25	221.99	236.51	237.09
198	57625.88	1046.10				129.73	45.81	84.19	79.85
199	3284.38	315.06				49.73	33.95	47.10	48.19
200	3910.63	327.32	Majestic Metro	911	Preston	58.32	32.00	51.88	54.01
201	4697.13	389.33				69.56	42.52	64.08	65.60
203	7274.88	381.92				193.98	63.50	179.43	181.77
205	5242.75	395.96				65.84	38.62	58.67	61.14
206	33756.13	840.99				165.12	36.40	88.72	88.13
207	7627.38	353.10				58.90	48.99	56.10	56.24
209	16842.13	524.12	Alley Theater	615	Texas	165.56	33.73	150.74	150.09
210	3640.75	315.34				60.60	34.80	54.57	56.88
211	3024.00	279.88				71.78	46.86	66.26	67.74
212	56424.25	950.18	Family Law Center	201	Fannin	220.19	25.76	195.25	212.49
213	4501.88	358.43				68.68	42.06	62.61	64.34
214	2912.25	268.21				96.44	53.38	90.29	92.37
215	47986.75	1170.93	County Jail	1301	Franklin	190.32	26.69	54.34	36.61
216	3810.50	324.46				63.76	37.79	57.14	59.88
217	2493.50	237.63	Sweeney Building			71.72	46.50	67.77	68.63
218	4393.50	361.74	Rice Ritten House Garage	506	Milam	70.33	44.69	65.24	66.74
219	4555.25	293.53				93.20	40.69	84.97	87.61
220	16240.00	562.39				69.53	44.14	66.57	67.34
221	29496.88	729.97				206.16	45.13	182.29	185.87
222	4431.25	367.03				66.64	40.36	60.70	62.44
223	4797.50	336.39	Harris County Adm. Building	1001	Preston	79.26	42.87	58.76	59.45
224	4482.00	359.17				71.28	45.76	65.97	67.52
226	13476.38	584.69				69.06	33.25	61.96	64.83
227	26330.50	714.73				226.87	45.49	109.52	94.55

230	67040.75	1035.33	State National Bank	420	Main	186.49	40.46	135.52	125.82
232	14131.75	493.88	Houston Chronicle	801	Texas	72.85	33.54	51.73	52.21
233	67721.75	1043.47				91.58	39.40	68.96	72.83
234	26963.63	730.82				218.35	42.42	132.20	130.46
236	5307.50	308.37				83.85	49.36	75.26	76.95
237	11242.63	424.49	Harris County Civil Courts	301	Fannin	69.59	43.48	61.98	66.17
238	12393.25	507.01				213.44	43.70	127.93	165.15
239	65555.50	1024.16				141.06	48.12	127.82	128.78
240	2527.38	265.11	Scanlan Building	405	Main	43.81	39.13	40.75	40.56
241	68220.88	1057.17	Jones Hall	615	Louisiana	288.29	45.68	154.03	110.27
242	1155.25	136.96				62.62	35.96	54.11	54.00
243	19875.75	620.47				77.72	39.83	59.56	58.14
244	4954.50	281.93	The Rice	518	Main	149.63	43.82	97.01	126.04
245	74721.00	1197.70				71.98	45.06	69.45	70.04
246	22030.63	598.48				146.85	40.41	80.06	74.62
248	40587.38	930.60				235.16	38.70	143.11	158.22
250	38186.63	872.29				99.50	41.67	76.53	85.05
251	17453.63	573.70				110.83	44.95	80.75	76.56
252	18009.00	528.81				1049.54	44.73	1013.89	1039.07
254	30876.00	796.42				237.89	55.57	121.78	92.58
255	3504.38	250.95	Chase Tower	600	Travis	75.13	43.28	70.04	72.87
256	1786.13	194.37				70.90	45.73	62.12	62.03
257	61563.25	988.51	Binz Building	1001	Texas	569.40	43.86	196.91	114.43
258	31528.13	766.33				92.87	38.66	79.20	79.93
261	10136.25	401.00				179.75	44.72	110.56	153.13
262	52173.00	913.88	City Hall/Visi-tors Bureau	900	Bagby	290.68	45.39	255.86	268.30
263	18298.75	559.77	Old Sam Houston Hotel	1119	Prairie	113.10	44.71	93.77	102.61
265	22919.88	742.82	Chase Center	601	Travis	67.59	43.60	60.69	61.18

267	11631.38	434.04				68.96	48.09	63.20	63.29
268	2793.25	211.58				85.24	43.31	77.32	82.98
269	10174.50	523.63				80.23	41.41	69.16	74.39
270	52501.38	1168.71				121.11	44.47	74.48	77.60
271	62436.25	999.53				305.97	45.39	177.28	186.45
272	3929.13	262.22				93.40	52.44	87.32	91.29
273	4041.25	277.94	Christ Church Cathederal	1117	Texas	65.93	43.38	59.18	60.49
274	15801.25	542.30	Houston Club Building	811	Rusk	129.20	39.61	97.38	114.23
275	7320.13	369.80				82.64	43.78	74.06	74.67
276	5097.63	310.75	Harris County Annex 2 Building	1302	Preston	110.05	46.68	97.72	99.55
277	5684.25	303.16	Two Shell Plaza	777	Walker	65.72	46.48	59.22	60.48
278	2376.38	247.63	Londale Hotel	1217	Prairie	75.31	43.33	63.82	67.40
280	4788.50	300.96				98.50	52.36	86.55	87.32
281	7887.88	357.91				314.93	45.51	249.35	293.93
282	61358.00	992.44				475.57	59.38	240.30	223.02
283	10586.00	513.05	Library	500	McKiney	110.38	43.73	78.06	65.62
284	3432.88	266.34	Chase Bank Building	707	Travis	68.23	44.28	63.65	65.29
285	2596.50	213.45	Texas Tower	608	Fannin	58.89	44.95	56.57	57.45
286	26685.25	910.41				396.29	45.02	187.63	111.65
287	9179.63	383.69	One Shell Plaza	900	Louisiana	71.46	63.03	69.87	69.92
288	62632.50	1001.07	The Keystone Lofts	609	Fannin	455.81	50.54	196.92	217.40
289	24559.00	696.38				71.64	46.41	69.53	70.01
290	6748.25	370.86	Esperson Buildings	808	Travis	68.98	45.89	62.53	62.77
291	18688.63	550.09				125.17	42.75	66.31	45.26
292	24772.13	696.88				82.67	44.01	66.53	64.01
293	12438.13	456.88				126.74	61.08	90.23	89.65

294	14432.50	521.84				261.94	61.16	222.98	244.49
295	30604.63	746.84				268.49	45.15	186.18	181.50
296	61773.00	1073.00				258.00	46.42	156.69	162.32
297	6776.50	460.56	Downtown District Operations Center	727	Main	88.74	43.96	59.02	57.50
299	2437.00	255.69				74.87	55.52	69.85	71.16
300	20139.38	904.23				47.62	43.34	45.22	45.50
301	63050.63	1004.40				339.79	45.65	232.04	202.70
302	6728.25	328.18				101.18	63.36	90.83	90.70
303	41741.63	904.24				66.84	42.62	57.00	61.34
304	11943.75	439.34				107.63	70.11	91.86	91.83
305	50263.63	1604.17				278.10	44.02	189.26	214.15
306	57161.75	955.62				423.31	81.89	227.84	126.81
307	10249.88	483.55				83.46	43.22	68.74	70.72
308	67056.50	1035.67	Garage	1100	Smith	186.11	46.28	114.01	97.59
309	15153.88	549.80	Great Southwest Life	1300	Texas	181.66	43.99	85.86	60.77
310	19399.63	657.02	West Building	911	Main	181.71	42.56	75.07	71.37
311	14577.75	493.16				320.72	46.30	187.83	239.50
312	63681.38	1007.78				358.91	46.94	219.03	186.10
313	4901.13	296.41				110.30	44.18	87.10	82.66
314	43496.13	864.97				127.47	39.58	91.96	100.27
320	24615.00	694.71				65.97	42.56	53.70	47.38
321	21248.00	852.37				90.64	43.78	59.01	57.79
322	43163.63	996.28	Travis Place Garage	1010	Travis	52.82	42.81	44.20	44.10
323	31538.63	823.09				319.51	44.99	184.53	145.60
326	41476.63	1021.63				338.37	45.76	205.46	187.03
329	18444.25	607.34	Allen Center One	330	Clay	209.50	43.63	133.54	101.53
330	20838.25	691.81	Two Allen Center	1200	Smith	137.58	46.89	86.29	84.66
331	68242.88	1077.33				645.50	45.53	314.85	188.48
332	65240.00	1071.34				795.67	43.31	293.37	103.72
333	10775.13	455.10				47.49	35.63	44.67	44.69
334	22908.00	618.69				128.58	45.77	101.77	104.27
335	9185.25	496.09				192.32	45.43	84.94	85.45

336	3859.50	259.87	Regency Garage	1315	Louisiana	113.11	43.73	85.17	94.97
338	3300.63	298.33	Foley's	1110	Main	113.24	45.42	102.82	107.61
341	22192.50	675.10				461.75	80.08	449.34	455.81
342	24844.25	951.36				71.16	42.59	54.12	56.83
345	29818.50	759.63				724.59	45.85	662.71	707.82
347	12683.38	504.24	First City Tower	1001	Fannin	85.69	43.24	59.02	59.83
349	64445.50	1032.28				325.91	45.02	167.13	118.02
353	22868.00	660.77	Chevron Tower	1301	McKiney	96.76	43.39	63.00	61.67
354	114795.50	1702.60				282.58	45.32	172.44	137.96
355	63401.88	1007.20				299.50	44.40	191.71	120.04
356	5485.88	270.85	Enron Center North	1400	Smith	60.77	45.44	47.79	46.65
358	424.75	87.25				82.44	44.94	71.57	74.16
359	2474.25	232.15				89.03	44.34	69.70	73.01
360	40933.38	1027.77				190.49	45.12	177.47	181.12
361	56862.38	1245.89				101.12	38.36	85.24	94.56
362	35671.88	1403.52	Continental Center	1600	Smith	367.21	35.74	178.59	108.29
364	44503.00	844.54				441.52	117.71	339.58	334.04
365	23863.13	807.81				73.91	44.73	63.61	63.34
366	451537.00	2945.27		1304	Dallas	162.97	43.13	136.80	142.44
367	31500.25	751.86	Exxon Building	800	Bell	123.04	44.71	89.39	85.00
368	7793.63	374.72	George R. Brown Convention Center	1001	Avenida De Las Americas	85.31	43.03	64.94	59.07
369	9001.13	382.00	HPD Special Operations	1415	Fannin	67.23	44.56	64.47	65.66
370	13581.63	478.04				218.54	75.26	201.20	199.46
372	7984.00	358.49				58.30	42.81	53.78	55.18
373	4069.88	265.29	Houston Press	809	Pease	76.58	43.86	66.08	68.89
375	3303.75	252.13				58.72	43.88	55.57	57.16
376	6817.88	365.60				112.93	43.16	58.36	57.94

377	32020.38	782.92		600	Jefferson	105.33	45.38	96.72	99.84
384	9477.88	389.52				74.21	44.33	70.14	71.85
385	3533.13	315.00				76.21	46.31	57.55	56.34
386	4866.13	280.15				66.45	42.73	56.80	58.43
387	4918.75	295.35	Mickey Leland Federal Building	1919	Smith	77.09	43.77	46.58	44.74
388	4291.75	286.18				68.93	44.38	57.65	56.86
389	5019.63	359.57				70.68	44.36	67.06	68.71
390	6898.13	418.06	Beacons-field Condomi-niums	1700	Main	81.19	43.50	60.01	59.79
391	7028.75	356.99				78.12	44.59	68.29	70.22
393	5851.25	320.21				74.76	44.96	68.42	70.18
394	4438.13	268.54				101.61	43.43	86.99	87.21
395	2576.75	253.68				57.41	45.33	55.31	55.83
396	3720.75	317.83				89.08	44.30	78.71	83.61
397	4129.88	287.21				104.10	43.12	58.87	57.98
398	9319.00	416.45				61.39	43.63	44.79	44.27
401	33307.50	862.13				81.59	41.76	64.69	65.30
403	2547.88	202.51				78.86	43.34	62.52	61.43
404	4670.75	294.81				69.68	44.92	64.53	67.37
405	32434.50	821.62				75.85	43.13	65.61	67.18
409	4805.38	296.25				71.32	44.30	63.38	65.67
410	6328.13	335.15				77.79	44.51	47.16	45.90
411	5073.75	300.00				65.22	43.57	59.53	60.73
414	5929.63	341.85				63.04	44.01	59.01	60.06
415	2489.75	222.49				71.65	43.65	63.82	67.70
416	29859.63	736.11				384.21	43.55	304.32	308.51
417	2554.63	250.96				59.38	44.14	57.03	58.66
418	16279.88	554.71				76.14	43.50	58.71	59.33
419	2273.63	196.26				97.95	42.86	59.70	59.10
422	4963.25	296.44				61.45	48.25	56.64	56.38
423	5494.50	301.54				79.99	44.48	71.56	71.29
425	3844.75	258.81				63.96	44.41	55.77	56.22
426	4652.00	295.27				69.24	43.62	61.23	66.62
428	5080.00	353.24				82.02	43.92	59.22	59.56
430	3041.13	287.29	St. Joseph Hospital	1919	LaBranch	78.24	43.73	60.33	58.36

431	25280.75	747.84				85.51	43.79	69.91	69.39
432	3409.13	235.06				68.80	44.08	63.35	66.64
433	6350.88	374.81				88.86	44.50	61.38	60.17
435	5196.50	293.96				87.34	44.41	57.65	55.58
443	7479.13	369.24				83.23	43.41	57.33	59.09
444	12335.63	566.70				90.26	44.60	61.06	62.46
447	6723.63	346.75				74.14	43.13	64.37	62.22
448	13068.13	720.28				125.44	43.24	84.58	88.09
449	17499.38	581.36	School Of Nursing	1918	Jackson	78.38	44.19	64.46	67.36
451	7817.50	490.30	School Of Nursing	1918	Jackson	62.71	43.31	46.67	44.53
453	700.75	107.77	School Of Nursing	1918	Jackson	58.92	43.06	54.37	56.39
456	15959.75	609.14	St. Joseph Prof.	2000	Crawford	86.77	44.42	74.54	76.68
458	4496.88	300.34				96.80	45.09	62.76	62.40
460	10974.50	445.05				51.64	44.44	45.29	45.02
461	18920.25	709.60				87.80	42.85	49.58	44.06
463	35887.38	1071.52				115.20	0.00	50.00	81.26
464	9870.25	637.25				79.15	46.24	50.81	50.10
465	3303.50	238.12				83.53	47.18	62.32	63.24
466	3268.38	243.68				68.64	48.35	63.90	64.69
467	9871.13	494.34				85.40	46.50	62.13	62.46
468	1488.00	186.88				106.42	46.31	72.03	66.42
469	20090.13	576.83				77.77	46.04	67.06	65.35
473	79997.13	2021.43				99.50	46.13	83.04	85.17
475	9588.63	392.87				81.65	43.10	64.42	63.37
480	72494.50	1406.33				61.18	36.38	55.97	56.93
481	59566.25	992.91				68.43	39.02	53.23	58.83
482	61899.13	1015.17				66.16	37.00	46.76	42.94
483	48625.63	1081.48				78.47	37.87	54.65	53.66
484	12589.00	823.43				92.62	37.35	57.13	56.33
485	23744.13	660.02				72.03	38.70	64.32	68.10
486	14284.25	628.91				96.54	36.96	51.64	51.63
487	37108.50	772.85				80.08	34.82	64.94	68.00
489	112008.13	1348.64				77.26	37.03	65.02	66.46
490	33696.13	755.96				75.24	42.41	66.15	66.28
491	30352.75	761.82				70.32	44.29	66.77	67.07
492	66692.63	1134.91				61.97	33.39	56.24	54.93

493	4028.75	281.33				67.63	34.67	48.05	49.54
494	15541.25	587.05				72.81	33.89	59.07	59.72
497	2251.88	193.12				61.07	36.93	56.02	56.64
500	98402.75	1283.53				73.32	33.18	58.84	60.32
501	12890.13	486.08				52.95	34.19	48.83	48.65
502	44540.50	1106.57				75.03	33.32	52.54	52.00
503	3941.00	269.98				85.79	33.35	47.57	49.90
505	2512.13	218.13				73.53	61.00	71.29	71.69
506	13483.13	810.63				102.85	33.17	61.64	64.12
507	6974.38	402.61				67.89	43.84	59.80	59.07
508	19463.50	580.13	U.S Post Office	401	Franklin	65.50	40.21	55.28	58.06
509	7919.25	368.24				72.95	44.50	66.14	66.76
511	5731.38	563.50				92.00	38.59	72.38	81.18
513	13789.75	537.43				74.46	40.27	54.21	51.28
514	13795.00	497.66				104.29	36.35	89.85	96.75
515	79724.50	1286.39	Harris County Intake Facility	1201	Comerce	100.37	36.69	90.31	90.80
519	227124.38	3011.22				158.54	1.63	62.15	40.55
522	41396.25	825.72				228.96	40.52	202.91	202.96
524	50742.50	901.28				811.54	45.78	395.21	378.18
525	3038.63	254.08	Harris County Criminal Courts	301	San Jacinto	74.19	45.18	56.20	56.11
528	29382.75	854.48				233.55	42.61	117.77	80.39
529	37750.75	1048.48	Harris County Annex Building	402	Caroline	462.69	30.97	266.19	134.77
530	64118.00	1012.96				401.47	47.01	235.72	169.59
531	34906.00	734.43				145.85	48.00	135.01	140.45
532	25371.00	648.52				920.21	165.57	731.62	733.85
533	17599.63	778.13				131.36	49.33	102.43	108.15
535	32074.38	751.49				1049.33	29.92	926.98	1020.88
536	54015.88	929.76	Wells Fargo Bank Plaza	1000	Louisiana	182.01	119.85	157.07	156.44
537	28063.63	1161.53	Doubletree Hotel	400	Dallas	554.84	47.35	515.09	529.10

539	19181.50	599.79				816.55	88.21	753.89	777.45
540	63117.50	1004.28				173.25	21.09	153.84	162.52
541	44057.75	841.54				757.19	46.48	424.16	647.63
542	46352.63	1197.89	Three Allen Center	333	Clay	421.44	45.28	231.83	209.14
543	62726.00	1001.34				248.92	46.38	140.27	99.34
547	46765.50	865.56	Annunciation Church	1618	Texas	565.77	89.39	346.74	375.95
550	65814.50	1026.19				209.26	56.99	186.78	185.09
552	58771.50	1032.71	One City Center	1021	Main	434.78	45.70	218.08	117.73
553	50358.63	1238.62				286.10	35.65	172.17	169.65
554	21378.25	613.03				184.25	41.65	133.70	155.45
555	24124.75	688.51				162.11	45.43	129.86	137.12
556	4095.00	270.75				47.92	46.99	47.43	47.44
557	21357.75	699.88				360.85	45.39	303.31	319.81
558	22917.38	659.40				604.42	32.04	383.97	492.82
559	24532.25	750.72	Wedge International Tower	1415	Louisiana	165.68	42.99	110.50	110.54
560	64666.50	1017.19				141.56	45.29	112.59	114.31
561	31110.00	751.25		1301	Fannin	653.38	44.43	626.04	650.87
562	64487.63	1015.78	Kellogg, Brown & Root Tower	601	Jefferson	187.21	44.39	120.51	107.54
564	4018.13	433.11	HL&P Substation	1501	Polk	67.12	45.38	58.67	60.24
566	31255.25	751.50				222.80	45.90	118.01	79.30
567	15443.50	606.06				65.56	44.19	61.36	61.87
568	5265.00	290.27				66.20	44.38	45.23	45.10
570	14725.63	489.09				79.11	54.98	73.04	73.25
571	4357.88	293.57				155.78	54.41	143.03	145.17
572	12891.63	658.73				86.77	46.23	65.72	63.08
575	22455.63	620.08				85.77	44.14	64.34	65.80
576	18693.38	631.50				257.22	44.59	204.73	233.45
577	11820.50	457.59				103.57	44.61	95.44	97.85
578	4560.25	388.59		1801	Main	67.65	44.80	56.81	58.07
580	25219.88	658.82				102.79	44.17	87.36	89.08
581	30729.75	744.43				92.70	45.65	83.69	84.60
582	35834.38	814.52				74.37	43.83	64.87	66.52
583	10136.88	458.71				114.67	42.63	79.69	71.62

584	9996.50	407.51				274.83	37.72	101.97	91.18
587	6264.63	316.65	Crayon Club	1804	Austin	72.01	43.44	66.79	68.22
590	29515.88	1000.29				84.89	42.99	62.50	61.57
593	7694.25	352.97				60.32	43.88	57.40	58.18
595	24605.38	726.09				73.06	43.79	64.73	65.10
598	25734.38	762.74				85.47	43.69	63.75	64.79
600	2803.00	328.74				68.68	43.83	52.49	53.64
602	7170.75	337.76				75.91	44.70	73.29	74.40
603	14997.13	493.04				274.25	44.54	210.58	255.55
604	16445.25	560.49				85.07	43.79	72.52	75.93
605	16541.25	595.51				72.74	43.86	57.61	60.85
606	7024.88	345.47	St. Josephs Cancer Lab	1703	Pierce	90.07	43.95	80.78	82.50
609	3759.38	284.43				68.00	52.58	64.90	65.20
611	2934.63	216.65				63.95	43.65	57.02	57.52
612	10696.00	427.01				59.19	43.44	55.86	56.96
613	4148.25	281.39	Mecom Building	1500	Gray	64.71	43.36	56.71	58.73
614	4341.25	281.52				66.11	46.13	56.20	56.01
615	12596.00	449.16				88.77	44.27	77.09	78.43
619	23964.25	619.63				68.61	46.04	67.54	68.25
620	6105.38	313.21				83.33	46.70	75.26	78.00
621	17366.13	528.86				112.69	45.26	95.31	101.55
623	75074.38	1466.17				89.42	42.53	76.03	73.00
624	9159.88	417.81				65.18	46.16	57.69	57.83
626	91556.25	2653.29				56.10	34.64	49.91	53.90
627	39804.38	1137.16				88.29	44.40	69.58	71.80
628	10213.38	447.37				75.64	44.85	68.14	72.15
629	9838.75	486.08	Urban League	1300	Main	71.15	43.40	63.42	68.58
630	9019.25	385.97				70.02	46.39	66.21	67.55
631	29293.63	781.58				68.14	39.40	58.61	60.66
632	8038.50	361.52				91.83	41.25	64.30	64.65
634	73300.13	1090.76				63.13	25.48	52.37	58.00
635	112471.00	1455.51				128.53	23.19	106.62	113.76
636	60781.50	989.01				383.69	21.53	228.45	336.24
637	570375.75	3639.19				270.95	17.02	112.84	86.93
638	19152.00	581.89				80.69	44.28	65.67	73.18

639	21041.88	654.00	Howell Building	1111	Fannin	66.39	41.49	58.78	59.73
640	27271.00	600.37	YMCA	1600	Pease	54.84	43.41	45.06	44.75
641	261810.38	1955.71				54.82	30.76	37.37	37.47
642	21945.75	694.11				75.81	43.24	60.74	60.18
643	21967.25	617.27				87.97	42.07	71.22	80.95
644	61410.38	991.62	St. Joseph Hospital	1315	St. Joseph Parkway	134.99	42.88	108.64	113.79
646	6684.00	334.73				76.19	45.08	63.11	63.14
647	62731.13	1002.37				188.19	43.27	113.96	78.40
648	10867.50	424.79	Ampco Building	1311	Preston	85.26	40.14	63.58	61.84
649	56396.13	950.85	Southwest Bell	1200	Clay	219.75	46.26	127.71	105.45
650	26850.88	1171.34				86.46	42.66	62.60	67.75
651	5258.38	296.31				77.76	45.49	61.03	64.92
652	5281.50	323.96	El Paso Eergy	1010	Milam	77.09	46.70	65.02	70.25
653	6845.63	399.41				75.43	50.94	69.83	71.10
654	97230.00	1378.50				111.83	38.59	88.92	93.82
655	20952.75	604.40				141.71	38.92	86.81	71.66
656	56397.50	950.54	First City Tower Garage	1100	San Jacinto St.	655.37	44.63	253.25	161.93
658	61770.25	995.40				340.03	43.23	133.17	59.42

APPENDIX D

The list of geographical urban shapes and textures of downtown Houston

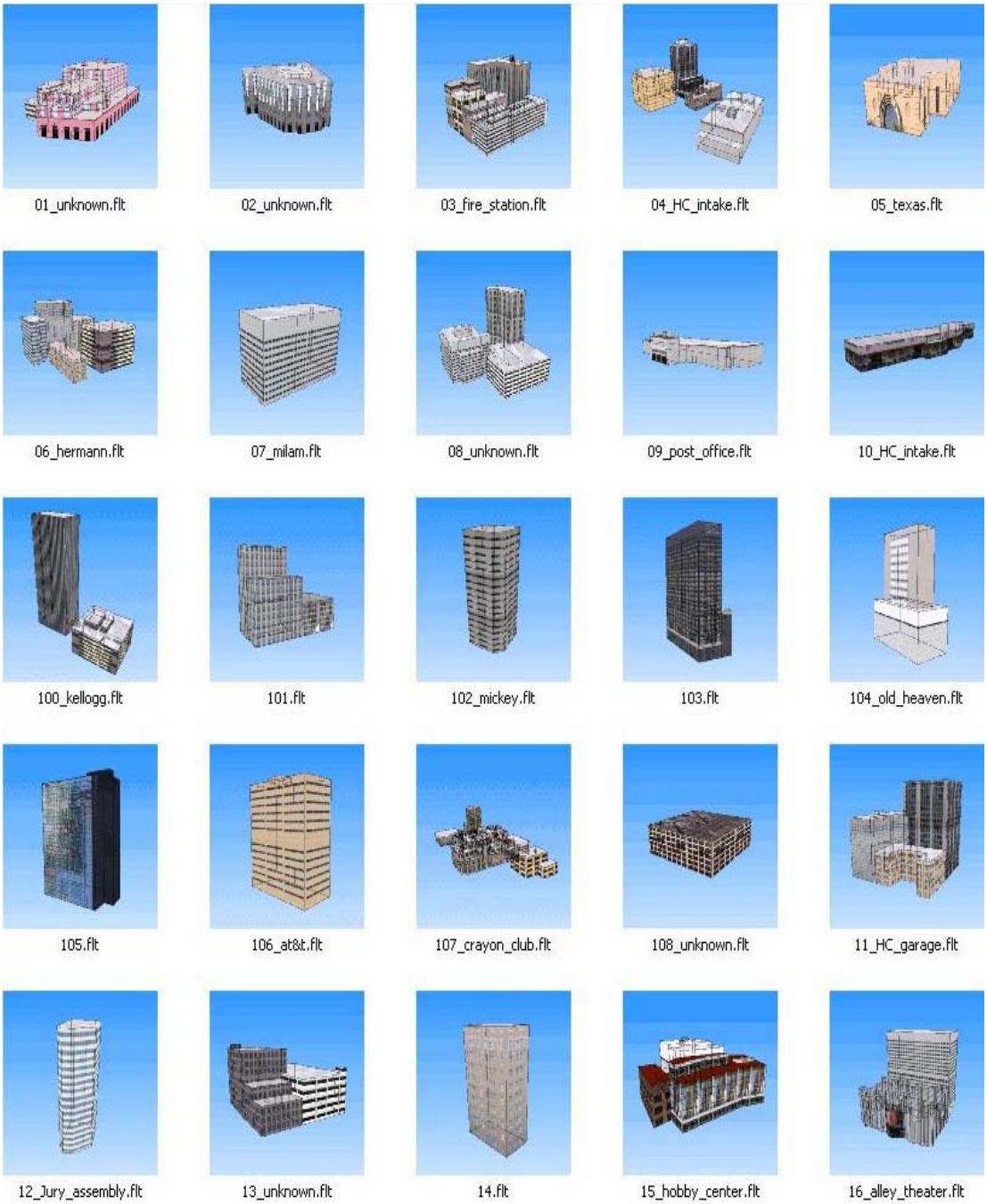


17_Majestic_metro.flt


19_family_center.flt


21_unknown.flt


22_HC_adm.flt


23_unknown.flt


24_houston_chronicle.flt


25_HC_courts.flt


26_unknown.flt


27_bob_casey.flt


28_jones_hall.flt


29_unknown.flt


30.flt


31_HC_criminal_courts.flt

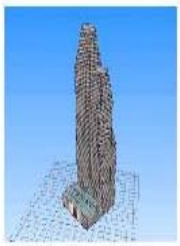
32_bank_america.flt


33_CH_annex.flt


34_chase.flt


35.flt


36_unknown.flt


37_city_hall.flt


38_chase_center.flt


39_unknown.flt


40_christ_church.flt


41_unknown.flt


42_unknown.flt


43_texas_tower.flt


44_library.flt


45_chase_bank.flt


46_convention_center.flt


47_one_shell.flt


48_keystone_loffts.flt


49_unknown.flt


50_cotton_exange.flt


51_exxon_garage.flt


52_operations_center.flt


53_texaco_plaza.flt


54_planet.flt


55_unknown.flt


56_unknown.flt


57_wells_fargo.flt


58_unknown.flt


59_unknown.flt


60_garage.flt


61_unknown.flt


62_unknown.flt


63_unknown.flt


64_el_paso.flt


65_us_customs.flt


66_two_allen.flt


67_unknown.flt


68_interfirst.flt


69_travis_garage.flt


70.flt


71.flt


72_allen1_center.flt


73_milam.flt


74_exxon.flt


75_college.flt


76_allen3_center.flt


77.flt


78_main_garage.flt


79.flt


80.flt


81.flt


82_one_city.flt


83_travis_tower.flt


84_louisina.flt


85_foleys.flt


86_crowne_plaza.flt


87_continental.flt


88.flt


89_first_city.flt


90.flt


91_chevron_tower.flt


92_humble.flt


93.flt


94_park_shops.flt


95.flt


96_enron_center.flt


97_YMCA.flt


98_garage.flt


99_wedge_intl.flt


badguy.flt


hiway02c.flt


signal01.flt


spiderman.flt

stopSign.flt


streetLight1.flt


oakTree.flt


liquidambarTree.flt


big_oak.flt

VITA

Name: Wei-Ming Lin

Address: 153 Chung-hsing St.
Chung-ho, Taipei 235
Taiwan

Email: wimmy@tamu.edu

Education:

2004 M.S. in geography, Texas A&M University
1998 B.A in social work, Fu-Jen Catholic University, Taiwan